Environment Agency

Evidence

Vulnerability of estuaries to sea level rise – stage 1: a review

Report: SC080016/R1

Integrated catchment science programme

Evidence Directorate

The Environment Agency is the leading public body protecting and improving the environment in England and Wales.

It's our job to make sure that air, land and water are looked after by everyone in today's society, so that tomorrow's generations inherit a cleaner, healthier world.

Our work includes tackling flooding and pollution incidents, reducing industry's impacts on the environment, cleaning up rivers, coastal waters and contaminated land, and improving wildlife habitats.

This report is the result of research commissioned and funded by the Environment Agency.

Published by:
Environment Agency, Rio House, Waterside Drive, Aztec West, Almondsbury, Bristol, BS32 4UD
Tel: 01454 624400 Fax: 01454 624409
www.environment-agency.gov.uk

ISBN: 978-1-84911-183-6

Author(s):
Dr. David Prandle

Dissemination Status:
Publicly available
Released to all regions

Keywords:
Estuaries, sea-level, climate change, hydromorphology

Research Contractor:
Dr. David Prandle, Honorary Professor, School of Ocean Sciences, University of Wales Bangor, Menai Bridge, Anglesey, LL59 5AB
Telephone: +44 (0)151 648 1883

Environment Agency's Project Manager:
Dr. Sarah Watkins and Dr. Sara Massey

Project Number:
SC080016

Product Code:
SCHO0310BSAC-E-P

Evidence at the Environment Agency

Evidence underpins the work of the Environment Agency. It provides an up-to-date understanding of the world about us, helps us to develop tools and techniques to monitor and manage our environment as efficiently and effectively as possible. It also helps us to understand how the environment is changing and to identify what the future pressures may be.

The work of the Environment Agency's Evidence Directorate is a key ingredient in the partnership between research, policy and operations that enables the Environment Agency to protect and restore our environment.

The Research & Innovation programme focuses on four main areas of activity:

- **Setting the agenda**, by informing our evidence-based policies, advisory and regulatory roles;
- **Maintaining scientific credibility**, by ensuring that our programmes and projects are fit for purpose and executed according to international standards;
- **Carrying out research**, either by contracting it out to research organisations and consultancies or by doing it ourselves;
- **Delivering information, advice, tools and techniques**, by making appropriate products available to our policy and operations staff.

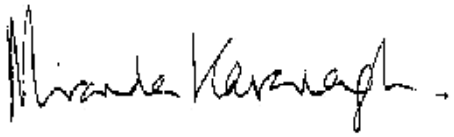

Miranda Kavanagh

Director of Evidence

Executive summary

Sea levels around the UK are predicted to rise at rates not experienced during the present Holocene. The hydro-morphological response of estuaries to rising sea levels and changes in other climatic variables (e.g. increased storminess) will vary markedly between locations. Some deep, narrow systems may undergo little change whilst others (e.g. coastal plain estuaries with extensive inter-tidal areas) may be significantly altered. Changes in estuarine morphology will impact on associated habitats and the determination of ecological status.

Compliance with the Habitats and Water Framework Directive is a priority for the Environment Agency. An understanding of what controls estuarine habitats and the changes that estuaries may undergo in relation to climate change is necessary to ensure that the Environment Agency can manage estuarine systems to achieve, over the longer term, *Good Ecological Status* as required under the Water Framework Directive. A better understanding will also ensure that habitats are maintained in a favourable condition or that compensatory habitats are created if necessary.

It is unrealistic and too costly in terms of time and resource to undertake a detailed assessment / modelling study of every major estuary and embayment in England and Wales. Instead, the aim of the work reported here is to develop an initial screening tool (a set of vulnerability indices) that will provide a rapid indication of estuaries which are likely to be resilient to sea level rise. This tool will be of use to staff implementing the Habitats and Water Framework Directives and the Marine Policy team. It will feed into climate change adaptation strategies and allow the Environment Agency to direct future resources to estuaries where major morphological changes may cause significant change and threaten important habitats.

The work is published in two reports of which this is the first. This report (Stage 1) provides the background for the subsequent development of vulnerability indices (detailed in the Stage 2 report). The Stage 1 report presents reviews of:

- the theoretical understanding of estuarine dynamics, mixing and morphology;
- the availability of UK morphological data;
- the associated coastal ‘forcing’ conditions;
- the likely extent of global climate change.

Estuarine classification systems that enable external forcing factors to be linked to estuarine responses are described in Section 2 and Appendix A; figures, formulae and dimensionless ‘numbers’ are used to illustrate the forms of such linkages. The classifications extend over tidal elevation, storm surges, vertical current structure, salinity intrusion, stratification, seasonal temperature cycles, sediment regimes, morphology, sediment trapping and sorting (in synchronous estuaries) and typological frameworks.

To enable these links between external forcing factors and estuarine responses to be examined more closely (Stage 2 report) details of UK estuarine morphologies and their associated ‘forcing factors’ are presented (Sections 3 and 4, and Appendices B and C). UK estuaries encompass a wide range of variability in ‘forcing factors’, namely tidal range, waves, surges, mean sea level change and river flows.

The limitations to existing predictive capabilities for estuarine responses are suggested together with recommendations to address these limitations.

Contents

1 Introduction

Over the last 100 years sea levels in England and Wales have risen between 10 and 20 cm, while forecasted rises for the next century range between 13 and 76 cm. Globally, air temperatures over the last century rose by 0.5 ^{o}C with forecasts for the next century of up to 4 ^{o}C.

Recognising such changes, this project aims to develop generic classification schemes to indicate the vulnerability/resilience of estuarine morphologies and habitats to the likely effects of global climate change. This report provides the background to this development, reviewing the existing theoretical understanding and observational databases required to construct and assess such classification schemes.

This approach builds on extensive experience in modelling, monitoring and theories of estuarine behaviour developed in the UK's Estuarine Research Programme. These studies show that in the meso- and macro-tidal conditions of UK estuaries, river flow has little influence on tidal dynamics (away from the upper reaches). Hence the major impacts of global climate change on tidal dynamics will be changes in mean sea level (msl). These studies also indicate that estuarine depths and lengths can be related to a combination of the prevailing dynamical and mixing processes - determined by tidal range, river flow and surface sediment. Figure 1.1 illustrates these processes. By encapsulating the results in typological frameworks, the characteristics of any specific estuary can be immediately compared against these theories and against a perspective of other estuaries. Identification of 'anomalous' estuaries can provide insight into 'peculiar' conditions and highlight possible enhanced sensitivity to change.

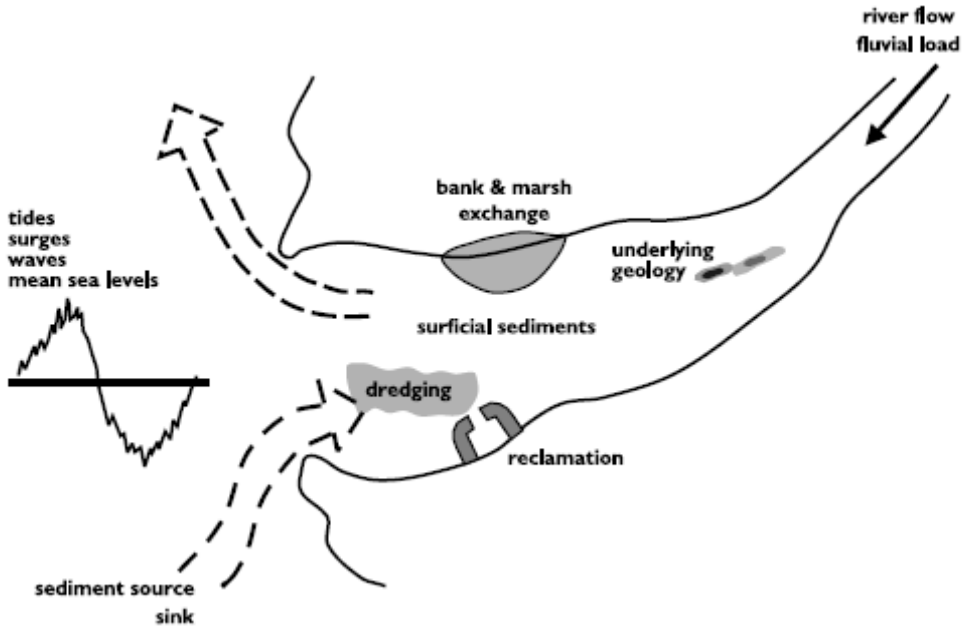

Figure 1.1 Factors influencing estuarine morphology, from Prandle (2004).

Three central questions were posed:

i. What determines existing estuarine morphologies?

   Explaining existing morphologies was seen as pre-requisite to forecasting future changes. Bathymetries reflect a combination of tidal amplitude, Z,

and river flow, Q. Morphological adjustment rates are generally slow and thus existing bathymetries reflect some intermediate adjustment between antecedent formative conditions and a present-day dynamic equilibrium. This adjustment rate depends on both the supply of sediments for deposition and the 'hardness' of the geology for erosion as shown in Figure 1.1.

ii. How have morphologies adjusted to past and on-going changes?

Annual volume changes of UK estuaries are typically of the order of 1 per cent or less. Thus, even where conditions favour net import or export of a certain sediment fraction, limited marine supply or resistance to erosion (fluvial supply is generally much smaller in UK estuaries) can severely delay morphological adjustments (Woodroffe, 2002).

iii. How might future morphologies adjust to accelerating sea level rises?

In addition to the direct dynamical-sedimentary relationships, the response to mean sea level changes includes the problem of how the coastline and estuaries re-adjust within the local coastal and topographical conditions (Pethick, 1984).

To derive a Vulnerability Classification System in Stage 2, the mechanisms synthesised in the Classification Frameworks will be linked with the forcing conditions and tested against the morphological data sets shown in Figures 3.1 to 3.9 (pages 14 and 15).

1.1 Aims and objectives

This study addresses the question 'How will estuarine morphologies and their associated habitats adapt to global climate change?' The challenge is to develop generic frameworks to provide, for any estuary, immediate indications of relative resilience/sensitivity.

The Stage 1 work programme comprised:

- a review of existing classification schemes and identification of underlying parameter groupings;
- quantification of a range of UK forcing conditions;
- details of past and future extent of global climate change;
- a review of the extent and adequacy of existing UK (morphological) data sets.

Related strategic management challenges include:

- sustainable exploitation - balancing commercial and industrial development, dredging, reclamation etc. with improvements to the marine environment;
- satisfying national and international legislation and protocols (Water Framework Directive etc.);
- reducing risks in relation to flooding, navigation and industrial accidents;
- long term planning to accommodate global trends;
- sustainability and diversity of estuarine ecosystems.

The requirement is for a Vulnerability Classification System which combines Theoretical Frameworks and observational data sets to provide a perspective of likely morphological and environmental changes over the next century, across the diverse range of UK estuaries.

1.2 Background

Over millennia, the inter-glacial rise and fall of sea levels effectively determines the morphology of river estuaries. Following the end of the last ice-age, retreating ice cover and the related rise in the mean sea level (transgression) have resulted in receding coastlines and consequent major changes in both the dynamics and morphology of estuaries. Sea levels rose globally by about 150 m between 20,000 and 5000 years before present, followed by a 'still stand', with changes in mean sea levels of less than a few metres. A hinge line at about 55 ^{0}N across the UK separates falling sea levels in the north, from rising sea levels in the south, reflecting the varying rates of isostatic rebound linked to ice thickness (Woodroffe 2002).

Over the Holocene, this rate of rise has been controlled by isostatic rebound, but if sea level rise accelerates with climate change, there could be a switch from a predominately stable system to more actively retreating shorelines. Over shorter time scales (of interest to coastal engineers and coastal planners) some quasi-equilibria develop, encompassing variations in bathymetry over ebb to flood and spring to neap tides, alongside seasonal cycles, random storms and episodic extreme events.

The range of morphological parameters shown in Table 1.1 was derived from the data described in Section 3. The 10th percentile, median and 90th percentile values provide useful indicators of the mean and range of UK estuaries (the 10th percentile is the value below which 10 percent of the data may be found; the median is equivalent to the 50th percentile).

Table 1.1 Range of morphological and 'forcing' conditions in English and Welsh estuaries.

	10 percentile	Median	90 percentile	Units[7]
Volume (HW)[1]	221	1,830	44,100	m ha (m^3)
Surface area (HW)	102	792	8,300	ha (m^2)
C-section area[2]	118	2,800	28,000	m^2
Mean depth	2.2	4.5	13.8	m
Tidal length	3.1	12.7	40.3	km
Breadth	45	580	2,500	m
Side Slope	0.003	0.017	0.184	
Hypsometry[3]	0.29	0.71	0.91	
Tortuosity[4]	2.1	3.0	5.9	
Salt marsh	3	12	36	%
Tide (M2)[5]	1.2	1.5	2.7	m
River flow	13	75	573	(MAX) m^3 s^{-1}
Wave Hs[6]	1.2	1.5	2.1	m
Mean Sea Level rise	1.8	2.3	3.5	mm a^{-1}

Notes:
[1]HW – at high water
[2]C-section area – cross-sectional area
[3]Hypsometry is the cross-sectional transverse profile
[4]Tortuosity is the ratio of shoreline to axial lengths
[5]M2 is the principal lunar semi-diurnal constituent
[6]Hs is significant wave height
[7]1 ha = 10,000 m^2

In global terms, UK estuaries are small (reflecting 'Island' conditions), strongly tidal and almost always vertically 'mixed'. Much of the existing estuarine literature, e.g. Dyer (1997), focuses on large, deep estuaries with relatively low friction effects. Figure A.3 (page 40) shows how to differentiate between such deep estuaries and the shallower frictionally-dominated systems more commonly found in the UK.

1.2.1 Assumptions and approximations

The analytical solutions shown here are invariably derived from linearised approximations to the full dynamical or conservation equations. The existence of one predominant tidal constituent (the principal lunar semi diurnal constituent, M2) in all UK estuaries greatly facilitates such linearisation. Linearisation of the quadratic bed friction formulae has been extensively used and shown to be widely applicable in the strongly tidal estuaries of the UK, e.g. Hunter (1975), Prandle and Rahman (1980).

For examination of vertical current structure and vertical mixing processes, the assumption of vertically and temporally constant coefficients of eddy viscosity and eddy diffusivity proportional to a product of the bed friction coefficient, tidal velocity amplitude and water depth has also been widely adopted, e.g. Bowden (1953), Prandle (1982, 1985). Again, in the shallow, strongly tidal, well-mixed estuaries of the UK, this assumption has been shown to be valid. However, it cannot be expected to reproduce all of the intricate small-scale processes observed and, as such, should be used with caution.

1.2.2 Synchronous estuaries

Since extensive sections (see Section 2.6) of the theoretical results presented in this report were derived for synchronous estuaries, salient features of such estuaries are described here.

A 'synchronous estuary' is one where the sea surface slope due to the axial gradient in phase of tidal elevation significantly exceeds the gradient from changes in tidal amplitude (Dyer 1997). Prandle (2009) shows that the bathymetry for such estuaries is described by breadth and depth variations proportional to $X^{0.8}$, where X is the axial distance from the head of the estuary. From Section A.1, this corresponds to a funnelling factor $\nu = 1.5$. From Figure A.1 (page 37), this value of ν is close to the centre of the range of estuarine morphologies.

The dynamical equation in Section A.3 may be expanded with two terms for the surface gradient. Zx represents the component associated with axial variation in the tidal elevation amplitude, Z, and kZ represents the component associated with phase variation. It can then be shown that, for one predominant tidal constituent, the ratio of these terms is given by:

$$kZ/\,Zx = \tan(90-\delta\theta)$$

where $\delta\theta$ is the phase difference between the actual (observed) value of θ (the phase advance of Z relative to the tidal current amplitude, U) and the value obtained from the synchronous solution in Figure A.3 (page 40). Thus for $\delta\theta < 10$, this ratio exceeds a factor 5 and the synchronous solution is valid. Conversely, for $\delta\theta > 30$, this ratio is less than 2 and the synchronous solution is invalid. Values of θ in UK estuaries are typically in the range $-90 > \theta > 70$, suggesting, from Figure A.3, that the synchronous solution is likely to be valid for meso- and macro-tidal estuaries with depths less than about 20m.

2 Review of existing classification schemes

Estuarine classification systems enable external forcing factors to be linked to estuarine responses. The systems described were selected for their potential use in Stage 2. These linkages are illustrated by figures, formulae and dimensionless numbers.

The classification systems cover:

- tidal elevation;
- storm surges;
- vertical current structure;
- salinity intrusion;
- stratification;
- seasonal temperature cycles;
- sediment regimes;
- morphology;
- sediment trapping and sorting (in synchronous estuaries);
- typological frameworks.

The processes addressed by each of these classification schemes are summarized below (see Appendix 1 for fuller descriptions).

Table 2.1 (overleaf) provides a summary of existing classification schemes with the Figure (in the appendices) which relates to it, the author(s) and underlying parameters used.

2.1 Tidal elevations and Storm surges

As tides and storm surges propagate into estuaries, in some systems they are amplified and in others rapidly diminished. Even within the same estuary, longer-period tidal constituents typically show little amplification, while shorter period higher harmonics are often significantly increased.

Section A.1 indicates how these varying responses are influenced by: shape; length; bed friction and river flow. This theory shows how the impacts of both depth variation X^m and breadth variation X^n (where X is the axial distance from the head) can be represented by a composite funnelling parameter v = (n+1)/(2-m).

Analytical solutions for the first order (linearised) dynamics of estuaries provide a Tidal Response Framework as shown in Figure A.1 (page 37), which explains the above features and illustrates:

i. The restriction of quarter-wavelength resonance to exceptionally long estuaries. The 90^o solid contour shows the lengths (y axis) corresponding to quarter-wavelength resonance. The (y) length of relatively long UK

estuaries such as the Thames (H in Figure A.1) is less than half the resonant length.

ii. For any tidal constituent, the dimensionless estuarine length, y, is inversely proportional to the tidal period, P (values shown are for the predominant lunar semi-diurnal tidal constituent, M2). Thus, y values for diurnal constituents are halved, substantially reducing any amplification within an estuary. By contrast, amplification of quarter-diurnal constituents is significantly increased.

Table 2.1 Estuarine classification schemes.

Classification Scheme	Figure No.[1]	Reference	Parameters
Tidal Response	A.1 (pg 37)	Prandle and Rahman (1980)	D, B, Z, U, f
Current structure			
Tidal	A.5 (pg 43)	Prandle (1982)	D, U, f, dZ/dX
River, wind, density	A.6 (pg 46)	Dyer (1997)	Q, D, τ, f, dp/dX
Saline Mixing	A.7, A.8 (pgs 47, 49)	Ippen (1966)	G, J
Sediment Concentration	A.11 (pg 54)	Prandle (1997)	Ws, E, D
Bathymetric Zone	A.14 (pg 59)	Simpson and Hunter (1974) Prandle (2004)	Ex/L, L_I/L D/U^3, Z, D, Q
Stability	A.16 (pg 61)	Lane and Prandle (2006)	t_{50}, θ, Ws, D
Lengths and Depths	A.17 (pg 63) A.18 (pg 64)	Prandle *et al*. (2005)	Q, Z, D, f tan α
Equilibrium values of Ws, C, and F_T	A.19 (pg 65)	Prandle *et al*. (2005)	Q, Z, D, f, Ws tan α

Notes: [1] In Appendices

B – channel breadth
C – sediment concentration
D – depth
D/U^3 – Simpson-Hunter (1984) mixing parameter
dρ/dX – salinity gradient
dZ/dX – surface gradient
f bed – friction coefficient
Ex/L – tidal excursion : tidal length
F_T – flushing time
G – tidal energy dissipation rate
J – buoyancy input
L_I/L – saline intrusion to tidal length
Q – river flow
t_{50} – half-life in suspension
U – tidal velocity
Uo – river residual velocity
Ws – fall velocity
Z – tidal amplitude
τ – surface wind stress
θ – phase diff btwn U & Z
tan α –lateral slope

2.2 Tidal current amplitudes & vertical current structure

The vertical structure of tidal, wind, density-driven and riverine components of currents can all significantly influence the rates of vertical mixing and the net export/import of contaminants and sediments. Section A.3 shows how current structures vary with depth, friction, latitude and tidal period (Prandle 1982, 1985).

Changes in current speed, direction and phase (timing of peak or slack values) are explained by decomposition of the tidal current ellipse into clockwise and anti-clockwise rotating components. While the main focus is on explaining the amplitude (Figure A.2, page 40) and vertical variations of tidal currents (Figure A.5, page 43), the magnitudes

and vertical structures of wind and density-driven currents are also described (Figure A.6, page 46). A particular emphasis is placed on deriving the scaling factors which encapsulate the influence of the ambient environmental parameters, namely depth, friction factor and Coriolis coefficient (i.e. latitude).

Vertical and horizontal shear in tidal currents generate fine-scale turbulence which determines the overall rate of mixing. The predominance of mixing by vertical stirring driven by tidally-induced turbulence has long been recognised. The roles of tidal straining and resultant convective overturning emphasises the importance of the vertical structure of tidal currents.

Figure A.5 (page 43) shows how, at any point within an estuary, the vertical structure of tidal currents is determined by the Strouhal Number (S_R = UP/D, where U is the tidal current amplitude; P, the tidal period, and D, the water depth). Corresponding scaling parameters for the vertical structure of river, wind and density flows are shown in Table A.2 (page 46).

2.3 Salinity intrusion & stratification

Since settlements were first established along estuaries, people have questioned the extent of salt water intrusion and how this varies over the Spring-Neap tidal cycles and flood-to-drought river flows. Here we show an explicit formula for the length of saline intrusion and indicate how the level of stratification is determined by the ratio of riverine to tidal current amplitudes (U_o/U).

Tidal currents and elevations in estuaries are largely independent of biological, chemical and sedimentary processes, except for parameterisation of the bed stress coefficient. Conversely, all three of these processes are generally highly dependent on tidal motions. Thus Sections A.5, A.6 and A.8 consider how estuarine mixing and sedimentation are influenced by tidal action.

Noting the definition of estuaries as regions where salt and fresh water mix, Appendix A.5 examines the details of this mixing. Saline intrusion undergoes simultaneous adjustments in axial location and mixing length - explaining traditional problems in understanding observed variations over spring-neap and flood-drought conditions. On neap tides, near-bed saline intrusion may enhance stability while, on spring tides, enhanced near-surface advection of sea water can lead to overturning (Prandle, 2009).

2.4 The seasonal temperature cycle

Section A.7 is included for ‘completeness’ – recognising the wider ecological interests in impacts from future changes in air temperatures, winds and cloud covers. In spring, surface heating stabilises the vertical density profile while, in winter, surface cooling can produce overturning (Prandle, 1998).

2.5 Sediment regimes

The predominant influences on sediment regimes in estuaries are tidal and storm currents, enhanced in exposed shallow water by wave stirring. For all but the coarsest grain sediment, several cycles of ebb and flood movement may occur between erosion and subsequent deposition. Hence deposition can occur over a wide region beyond the source. Since time in suspension increases for finer, slowly settling material, such

mechanisms may contribute to a residue of fine materials on tidal flats and to trapping of coarser material in deeper channels.

Suspended sediment concentrations in UK estuaries are invariably several orders of magnitude larger than are found off-shore (Prandle, 1997). Section A.8 seeks to explain how estuarine dynamics re-suspend, trap and sort suspended concentrations. It shows how the half-life of sediments in suspension, t_{50}, is determined by tidal current speed, depth, fall velocity and eddy diffusivity.

Analytical solutions are shown encapsulating and integrating the processes of erosion, suspension and deposition to provide descriptions of the magnitude, time-series and vertical structure of sediment concentrations (see Figure A.11, page 54). These descriptions enable the complete range of sediment regimes to be characterised in terms of variations in sediment type, tidal current speed and water depth. Theories are developed to explain the characteristics seen from tidal analyses of suspended sediment time-series obtained from either model simulations or observations.

2.6 Synchronous estuary: Dynamics, salinity & morphology

Appendices A.1 to A.9, examine how estuarine morphology influences dynamics, mixing and sediment concentrations. Appendix A.10 poses the underlying question as to how estuarine shape, length and depth are determined. This is addressed by introducing the assumption of a 'synchronous' estuary, which then provides explicit formulae for tidal current amplitude and phase, estuarine length and depth.

A 'synchronous estuary' is where the sea surface slope due to the axial gradient in phase of tidal elevation significantly exceeds the gradient from changes in tidal amplitude. The 'synchronous' assumption yields explicit expressions for both the amplitude and phase of tidal currents and the slope of the sea bed. Integration of the latter expression provides an estimate of the shape and length of an estuary. By combining these results with existing expressions for the length of saline intrusion and further assuming that mixing occurs close to the seaward limit, an expression linking depth at the mouth of the estuary with river flow is derived. Hence, a framework for estuarine bathymetry is formulated showing how size and shape are determined by the 'boundary conditions' of tidal amplitude and river flow.

Many earlier texts and much of the literature, (e.g. Prandle and Rahman, 1980; Dyer, 1997), focus on large, deep estuaries with relatively low friction effects. Section A.3.2.1 indicates the differentiation between such deep estuaries and shallower frictionally-dominated systems and the vast difference in their response characteristics are illustrated.

2.7 Sediment trapping & sorting, and typological frameworks

Continuing with this synchronous estuary assumption, in Appendix A.10, the theories and formulae described in Sections A.1, A.3, A.4 and A.8 are integrated into an 'analytical emulator' to show what causes trapping, sorting and high concentrations of suspended sediments and how the balance of ebb and flood sediment fluxes adjusts to maintain bathymetric stability.

This Section indicates how, in 'synchronous' estuaries, bathymetric stability is maintained via a combination of tidal dynamics and 'delayed' settlement of sediments in suspension (Figure A.16, page 61). An analytical emulator integrates explicit formulations for tidal and residual current structures together with sediment erosion, suspension, and deposition (Figure A.15, page 60). The emulator provides estimates of suspended concentrations and net sediment fluxes, and indicates the nature of their functional dependencies. Scaling analyses reveal the relative impacts of terms related to tidal non-linearities, gravitational circulation, and 'delayed' settling.

The emulator is used to derive conditions necessary to maintain zero net flux of sediments, i.e. bathymetric stability. Thus, it is shown how finer sediments are imported and coarser ones are exported, with more imports on spring tides than on neap tides (i.e. selective trapping and sorting and consequent formation of a turbidity maximum). The conditions derived for maintaining stable bathymetry extend earlier concepts of flood and ebb-dominated regimes. Interestingly, these derived conditions correspond with theoretical estimates of maximum sediment suspensions. Moreover, the associated sediment fall velocities are in close agreement with settling rates observed in many estuaries (Manning, 2004). Figure A.16 (page 61) encapsulates these results, illustrating the dependency on delayed settlement (characterised by the half-life in suspension, t_{50}) and the phase difference, θ, between tidal current and elevation. A feedback mechanism between tidal dynamics and net sedimentation/erosion is identified involving an interaction between suspended and deposited sediments.

Importantly, the new dynamical theories for estuarine bathymetry take no account of the sediment regimes in estuaries. Hence the success of these theories provokes a reversal of the customary assumption that bathymetries are determined by their prevailing sediment regimes. Conversely, the suggestion is that the prevailing sediment regimes are in fact the consequence of, rather than the determinant for, estuarine bathymetries.

3 Extent and adequacy of UK (morphological) datasets

Morphological and 'forcing' data for 96 English and Welsh estuaries are shown in Appendix C and Table 3.1. These have all been compiled (mainly by incremental additions to the preceding data set) since 1997 (from earlier observational surveys) and may be regarded as representative descriptions of present day estuarine morphologies in England and Wales.

Table 3.1 Morphological datasets for UK estuaries.

Dataset	Date	Extent	Originator / reference	Application
Monks Wood	1996	25 estuaries SA. CA. INTA, L	NERC institute, Terrestrial Ecology, Yates *et al*. (1996)	Superceded by JNCC
JNCC	1997	163 estuaries CA, ITA, SM, SL, L, T	JNCC Davidson and Buck (1997)	Consistent coverage of estuary-wide parameters
Futurecoast	2002	96 English & Welsh estuaries SA, ITA, SM, SL, CA, W, L, T, V(HW), V(LW), Q, tidal prism	HALCROW Burgess *et al*. (2002)	Development of JNCC dataset
ERP	2003	V, SA & CA all at HW, MW, LW	ABP ABPMer (2003)	Data at three levels useful for hypsometry
FD2107 (part of the ERP – summary of work in FD2119)	2008	Extends Futurecoast by analytical emulator	Hydraulics Research Wallingford (HRW) Manning (2008)	Special applications
Environment Agency	2009	SA, SM	Environment Agency, provided by Niall Phelan	
This project	2009	D_{MEAN}, W, Slope, Hypsometry, Hs, MSL	Prandle (2009)	Additional derived data

Notes: V – volume; SA – surface area; CA –cross-sectional area; INTA – inter-tidal area; SM – salt marsh area, MSL – rate of change in mean sea level; SL – shoreline length; W – width; Q – river flow; LW – low water; Hs – significant wave height; L – tidal length; HW – high water; MW – mean water; D_{MEAN} – mean depth; T – tidal range

Appendix C contains full listings of the Joint Nature Conservation Committee (JNCC), Futurecoast, Estuarine Research Programme (ERP), and Environment Agency data together with further data, which has been derived in the course of this report.

Figures 3.1 to 3.9 (pages 14 and 15) show the distribution of morphological parameters at HW (High Water), MW (Mean Water) and LW (Low Water) for the estuaries shown in Figure A.13 (page 58).

Recognising the difficulties in such basic issues as determining where an estuary starts (at the mouth) or ends (at the head), precise quantification of most parameters is not possible and, therefore reporting values to more than three significant figures can be misrepresentative. For this reason, values in the tables included in Appendix C are rounded down accordingly.

3.1 Monks Wood

This data covers 25 UK estuaries and comprises surface area, cross-sectional area, intertidal area and channel length. This data was reported by Yates *et al*. (1996) and has since been replaced by the data collected by the Joint Nature Conservation Committee (JNCC). For this reason, it is not reported in the appendices, but included in Table 3.1 for completeness.

3.2 Joint Nature Conservation Committee (JNCC)

The JNCC 'Inventory of UK Estuaries' (Davidson and Buck, 1997) forms the core of available morphological data for UK estuaries.

These data, as shown in Table C.1 (page 82), provide values of :

i. Surface Area (ha), **SAHW**, at the High Water limit of Highest Astronomical tides (HWHA)

ii. Intertidal Area (ha), **INTA**, between HWHA and Mean Low Water

iii. Saltmarsh extent (ha), **SAM**

iv. Shoreline length (km), **SHL** (including islands)

v. Tidal length (km), **L,** from the mouth to the upstream tidal limit

vi. Tidal Range (m), **TIDE,** on mean Spring Tide (note: Tidal Range is double Tidal Amplitude).

The mouth was taken as the seaward constriction in Bar-built estuaries and 'Along the Shore' for funnel shaped estuaries and embayments. Minimum criteria were set as tidal length, L>2km, and a minimum inter-tidal breadth of 0.5 km after Davidson and Buck (1997).

The Inventory also includes a classification into nine morphological types. In England and Wales, Ria (3), Coastal Plain (4), Bar-Built (5), Complex (6), and Embayment (9) constitute 96 out of 109 estuaries. Only five of these estuaries are micro-tidal (tidal range, T< 2m) and only 17 meso-tidal (2 < T < 4 m) with the majority being macro-tidal (T>4m).

For overall consistency, the JNCC data are presented in the sequence of 96 estuaries later adopted for Futurecoast studies.

3.3 Futurecoast

The Futurecoast study was commissioned in 2000 by DEFRA and completed in 2002. It aimed to provide predictions of coastal evolution over the next century (Burgess *et al.,* 2002). The project produced a 'toolbox' of supporting information including new observational data sets available in CD format.

Table C2 (page 84) shows:

i. Volume at High Water (ha m), **VOHW**

ii. Volume at Low Water (ha m), **VOLW**

iii. Maximum River Flows (annual daily mean) (m^3 s^{-1}), **QMAX**

iv. Cross Sectional Area (at the mouth) (m^2), **CAHW**

v. Width at the mouth (m), **WIDTH**

From a study of 42 years of river flow data collected by the Centre for Ecology and Hydrology, Prandle (2006) found that mean daily flows are generally close to 1/20 of the maximum values reported here.

3.4 Estuarine Research Programme (ERP)

The Environment Agency/Defra Estuary Research Programme (ERP) conducted some related research between 1997/8 and 2008. This comprised reports into investigated approaches for eco-system impact modelling (FD2108) and hybrid estuary model development (FD2107). A summary of the completed work is provided in the final report, FD2119. All research outputs from the ERP are available on the Estuary guide website (www.estuary-guide.net).

Table C3 (page 86) shows measured data at high water (HW), Mean Sea Level (MW), and low water (LW) for the following:

i. volume (ha m)

ii. surface area (ha)

iii. cross-sectional area (m^2).

These three values enable estimates to be made of the curvature of the lateral slopes (hypsometry).

3.5 Derivations - this project

Recognising the difficulties in such basic issues as determining where an estuary starts (at the mouth) or ends (at the head), precise quantification of most parameters is not possible. Although a high number of significant figures are reported in the JNCC and Futurecoast datasets, the numbers derived here are rounded down to three significant figures for ease of reporting, this has no affect on the degree of accuracy.

Table C.4 (page 88) shows derived values of :

i. Mean depth, **DEPTH**, m.

Mean depth, D_{MEAN}, was calculated as the median value from three estimates, namely:

- 2 * VOHW / SAHW - T/2
- 2 * VOLW / (SAHW – INTA) +T/2
- T/2*(SAHW+SALW)/(SAHW-SALW)

where VOHW is volume at HW (Futurecoast data, Table C.2, page 84)

SAHW is surface area at HW (JNCC data, Table C.1, page 82)

INTA is inter-tidal area (JNCC data, Table C.1, page 82)

And T is the tidal range (JNCC data, Table C.1, page 82)

ii. Mean width, **BREADTH** (at the mouth), m

The mean width (at the mouth) is estimated from:

$$BREADTH = 2 * CAHW / (D_{MEAN} \times (1+ T / 2D_{MEAN}))$$

where the depth at the mouth is estimated as 1.8 x D_{MEAN} based on a power law depth variation, X^n , with an average value of power n = 0.8. The $(1 + T / 2D_{MEAN})$ term is an adjustment for a value of CAHW at MWL, where CAHW is cross-sectional area at HW (Table C2, page 84)

iii. Mean lateral slope, **SLOPE**, (non-dimensional)

Slope is estimated from the mean depth and breadth at the mouth calculated above

$$SLOPE = 2 * D_{MEAN} / BREADTH$$

iv. Curvature of the lateral slopes, $\mathbf{AZ^2/BZ}$ (non-dimensional)

ERP surface area data, Table C.3 (page 86), is fitted to the expression

$$SA(Z) = aZ^2 + bZ + SA_{MWL}$$

where the height, Z, is measured relative to mean water level (MWL) and the mean depth is when SA(Z) = 0 enables the curvature to be calculated from the above equation as aZ^2 / bZ (i.e. the ratio of the increase in breadth (between MW and HW) associated with the quadratic and linear terms):

$$SA_{HW} - 2 * SA_{MW} + SA_{LW} / (SA_{HW} – SA_{LW})$$

v. Significant wave height, **HS**, (extracted from MET data), m. The values of significant wave height were extracted from a chart based on UK Meteorological Office data.

vi. Changes in mean sea level **msl**, (extracted from Shennan and Horton, 2002), mm decade^{-1}.

The values of mean sea level variation were extracted from Figure B.5 (page 73) after Shennan and Horton (2002).

Figures 3.1 to 3.9 (overleaf) show the distribution of morphological parameters at HW (High Water), MW (Mean Water) and LW (Low Water) for the estuaries shown in Figure A.13 (page 58), the data are shown in Appendices C.1 to C.4.

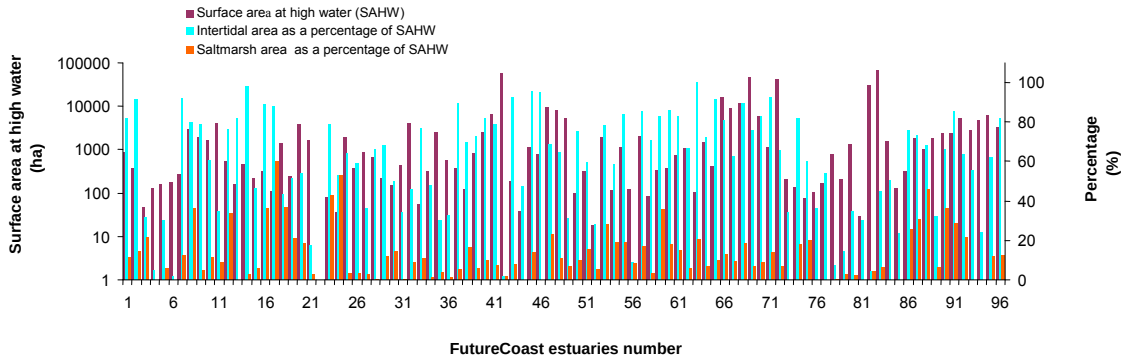

Figure 3.1 Surface area at high water, percentage of intertidal and saltmarsh area (JNCC dataset).

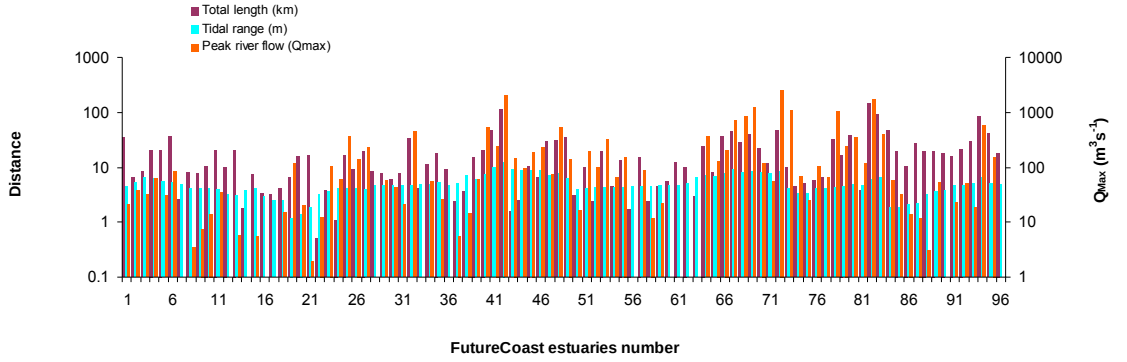

Figure 3.2 Tidal lengths and ranges (from JNCC) and maximum river flows (from Futurecoast).

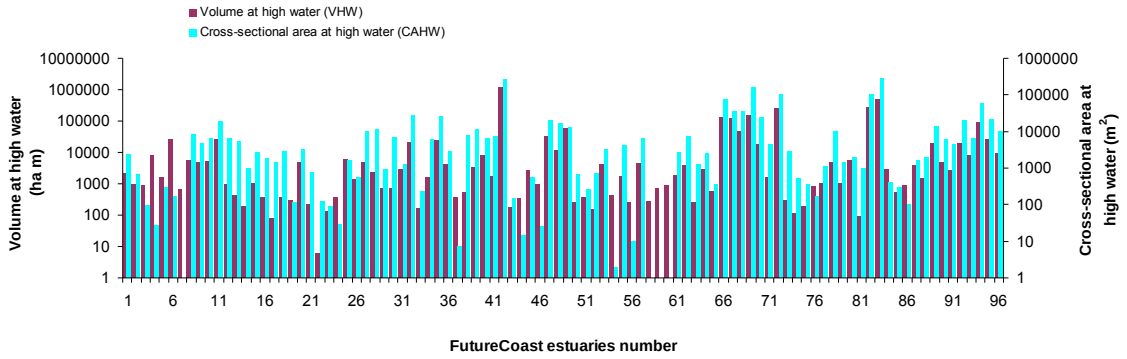

Figure 3.3 Volumes and cross-sectional areas at high water (from Futurecoast).

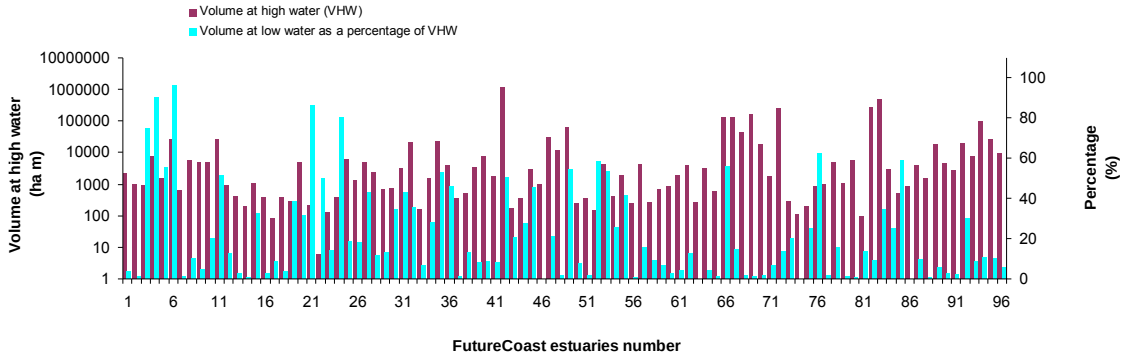

Figure 3.4 Volumes at high water and low water (from Futurecoast). Low water values are as a percentage of volume at high water.

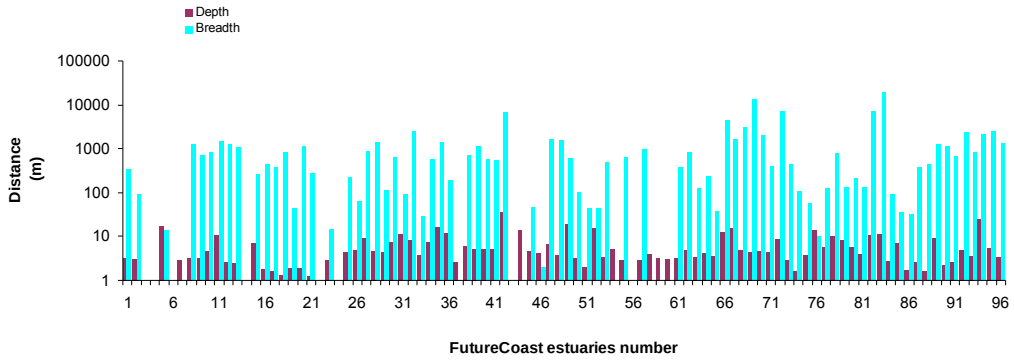

Figure 3.5 Depths and breadths derived from Futurecoast data (Derived data).

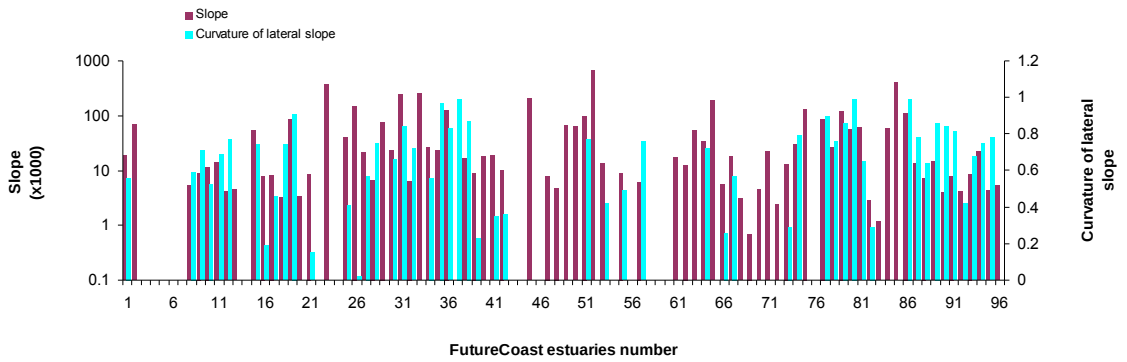

Figure 3.6 Slope derived from depth and breadth in derived data, and curvature of lateral slope derived from ERP data (derived data).

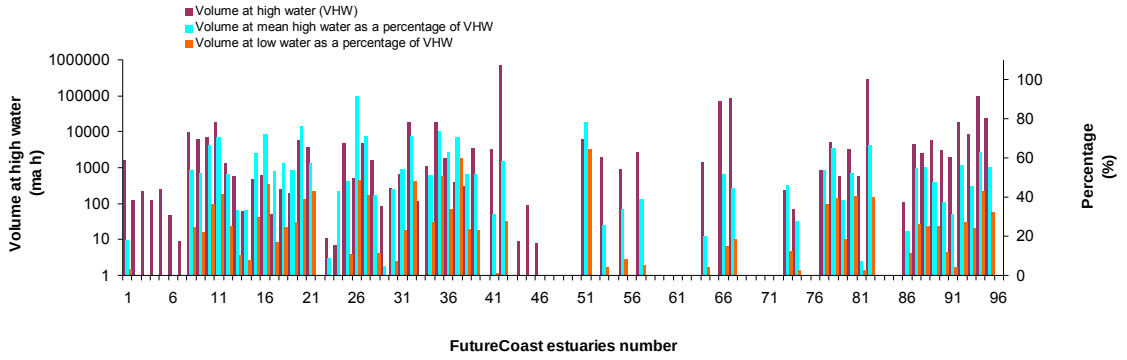

Figure 3.7 Volume at high water, mean sea level and low water as a percentage of volume at high water (ERP data).

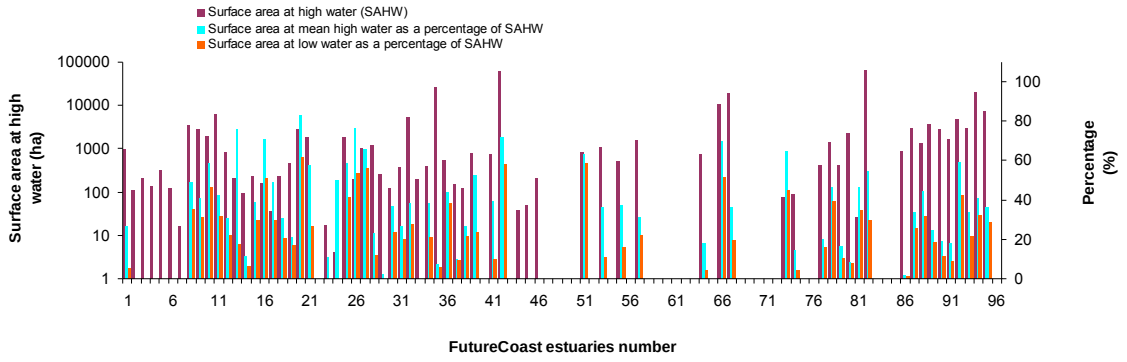

Figure 3.8 Surface areas at high water; surface areas at mean sea level and low water as a percentage of surface area at high water (ERP data).

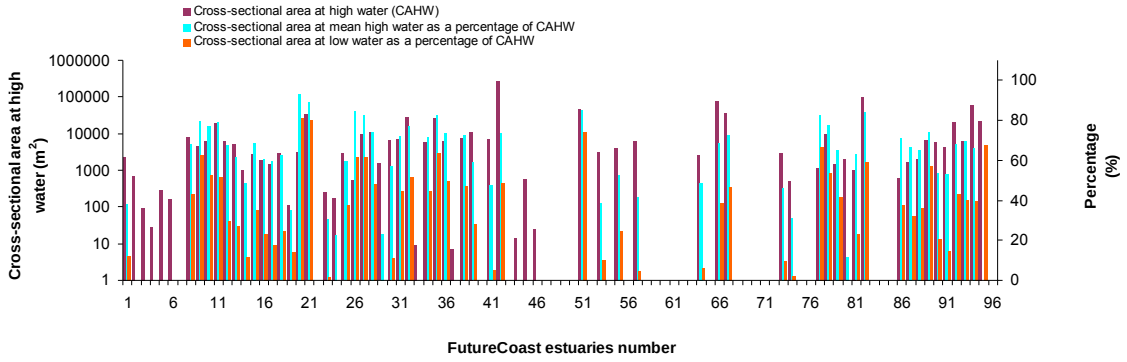

Figure 3.9 Cross-sectional area at high water; cross-sectional area at mean sea level and low water as a percentage of cross-sectional area at high water (ERP data).

Figures 3.1 to 3.9 are a quick and useful way of viewing the estuarine data sets tabulated in Appendix C, thus enabling gaps and general trends in these data to be readily seen.

4 UK coastal 'forcing' conditions

UK estuaries encompass a wide range of variability in the 'determining' parameters, namely:

i. tidal range – micro to macro

ii. waves/surges – severe westerly exposure to 'protected' bays; open-coast to 'resonant' seas

iii. mean sea level change (relative) – falling north to rising south with Holocene variations

iv. river flows – post-glaciation meltwater through to highly regulated systems.

The descriptions of controlling processes in Appendix 1 determined a set of salient parameters. Appendix 2 describes the nature, variability and sensitivities of tides, surges, waves, mean sea level, river flows, temperature, salinity and sediment supply.

The range of morphological 'forcing' conditions in English and Welsh estuaries provided in Table 1.1 (page 3) in Section 1.2 are discussed below.

4.1 Tides

Tidal systems on Earth are driven by the gravitational attraction of the moon and the sun. The integration of tidal potential over the spatial extent of the deep oceans means that tidal energy in shelf seas propagates from adjacent oceans.

The ratio of the mass of the sun to the mass of the moon is given as $M_s/M_m = 26.4 \times 10^6$,while the corresponding ratio of distances (distance to the Sun (d_s)/distance to the moon (d_m)) is ≈ 390. Thus the relative impact of sun:moon is given as

$$(M_s/M_m) / (d_s/d_m)^3 \approx 0.46$$

The 'equilibrium' magnitudes of the principal constituents relative to the principal lunar semi-diurnal constituent (M2) are:

- Principal solar semi-diurnal constituent (S2) - 0.46;
- Lunar ellipse constituent (N2) - 0.19;
- Principal lunar diurnal constituent (O1) - 0.42;
- Principal solar diurnal constituent (P1) - 0.19; and
- Principal lunar and Solar diurnal constituent (K1) - 0.58.

The period of the principal solar semi-diurnal constituent (S2) is 12.00 hours. The moon rotates in 27.3 days, extending the period of the principal lunar semi-diurnal constituent (M2) to 12.42 hours. The ubiquitous 15 day Spring-Neap variations in tides follows from successive intervals of coincidence (Springs) and opposition (Neaps) of the phases of M2 and S2. The two constituents are in phase when the sun and moon are aligned with the earth, i.e. both at full moon and new moon.

The morphology of shelf seas can selectively amplify tides for different constituents. Figure B.2 (page 69) indicates the amplification of ocean values of the M2 tide within

the seas of North West Europe. In general, the observed amplitudes of semi-diurnal constituents relative to diurnal are significantly larger than indicated from the ratios of their equilibrium magnitudes shown above, see Pugh (1996) for further details of tidal responses in coastal seas.

4.2 Surges

Like tides, surges propagate as shallow water waves, raising sea levels along coasts to the right of propagation as shown in Figure B.4 (page 71). Flooding often involves not only large but 'peculiar' surges. Rapid increases of sea level on time scales of hours can cause severe flooding in low lying coastal regions and dramatic loss of life. Rapid decreases in sea level can cause problems in the safe navigation of large vessels in shallow water.

Storm surge generation is via the two forces of wind stress and the horizontal gradient of atmospheric pressure at the sea surface. The wind effect depends on water depth and increases in importance as the depth decreases, whereas the pressure effect is independent of depth. The most important mechanism for surge generation is wind stress acting over shallow water. Surges are, therefore, large and dangerous where storms impact on large areas of shallow continental shelves (Heaps, 1967 and 1973).

4.3 Surface waves

In contrast to tides and surges, surface wind waves have wavelengths which, except on beaches, are small in comparison with the water depth. They are generated by winds, which produce waves with a spectrum of frequencies and magnitudes depending on the distance over which the wind acts, known as 'fetch'.

Ocean-generated waves travel very large distances and are known as 'swell'. In shoaling water, the wave orbital velocities reach the seabed and their propagation slows, causing refraction and dissipation of energy by bottom friction. Wave energy is also dissipated in deep water by white capping and ultimately by breaking at the shore. Wave conditions at the coast, therefore, depend on fetch, wind duration, exposure to incoming swell, and (local) bathymetry.

Around the UK, west and north-facing coasts are exposed to swell and have long fetch, thus they are characterized by large and long period waves. The Irish Sea is relatively enclosed, meaning that the fetch is are relatively short and so waves are not so large and have shorter periods. Very shallow water dissipates wave energy and so reduces extreme wave heights (Ippen, 1966).

4.4 Mean sea level

Over the Holocene, the rate of rise shown in Figure B.5 (page 73) has been controlled by isostatic rebound, i.e. the rise of land masses that were depressed by the huge weight of ice sheets during the last glacial period. If sea level rise accelerates with climate change, there could be a switch from a predominantly stable shoreline to much more active regression.

Global air and sea surface temperature warming in the 21st century will lead to rising sea levels as a result of thermal expansion, changes in ocean density and dynamics, and melting of glaciers, ice caps and ice sheets. Figure B.6 (page 74) shows the projected global average sea level rise and its components in 2090 –

2099 (relative to 1980 – 1999) for the six scenarios in the most recent Intergovernmental Panel on Climate Change (IPCC) report (Meehl *et al.*, 2007). Possible problems related to this sea level rise include sea water intrusion into hitherto freshwater areas and increased risk of flooding events, as shown in Figure A.3 (Figure 40).

Over 80 per cent of British monthly mean sea level variance can be related to seasonal changes, the static pressure effect and the influence of winds over the continental shelf. This complicates the calculation of the longer-term background global change. In the future, the expansion of the climate data set by means of remote sensing of oceans, atmosphere, and ice caps, and by further in-situ measurements of the deep ocean, will result in more sophisticated modelling of climatic trends and improved forecasts of long-term sea-level variations.

4.5 River flows

The mean discharge of the world's largest river, the Amazon, is 200,000 $m^3 s^{-1}$, representing 20 per cent of net global freshwater flow. Moreover, the cumulative discharge of the next nine largest rivers amounts to a similar total (Schubel and Hirschberg 1982). Outside of these ten largest rivers, Q < 15,000 $m^3 s^{-1}$. Table 1.1 (page 3) shows annual daily maxima for UK estuaries typically ranging from 10 to 600 $m^3 s^{-1}$. From a study of 42 years of river flow data collected by the Centre for Ecology and Hydrology (CEH, 2009), Prandle (2006) found that mean flows are generally close to 1/20 of the maximum values given in Table 1.1. Hence, mean flows in UK estuaries typically range from 0.5 to 30 $m^3 s^{-1}$. Thus, estimates of the minimum flows for continuous estuarine functioning, described in Appendix A.5, of approximately 1$m^3 s^{-1}$ correspond reasonably with the minimum mean flow for UK estuaries.

4.6 Temperature

An important characteristic of temperatures in shelf seas is pronounced seasonality, particularly through its influence on density. From spring to autumn, thermal stratification develops readily in deeper water where tidal mixing is weak. Such stratification exists between March and October and affects the biology and chemistry of the water column by limiting the vertical exchange of nutrients, suspended sediments and, therefore, light.

In UK shelf seas, the sea surface temperature closely follows the air temperature, with a mean temperature of 1-2 °C above that in air (Prandle, 1998). The amplitudes of their seasonal variabilities are nearly the same in shallow water, but the sea surface amplitude is somewhat reduced in deeper water. Any increase in wind speed forces the sea surface temperature to converge even more closely towards the ambient air temperature. Beneath the surface, increasing depths both delay and attenuate seasonal variability (compared to that at the surface). This process is reinforced by thermal stratification in deeper waters. Anomalies in observed sea surface temperatures can generally be directly related to concurrent air temperature anomalies with an indirect influence of anomalous wind conditions.

The mean values of both air and water temperatures are overwhelmingly determined by (the cosine of) latitude, with little influence from water depth or tidal current amplitude. By contrast, corresponding seasonal amplitudes vary directly with latitude alongside an exponential function of depth with much larger values in shallow, weakly-mixed waters. Stratification insulates the sea from both solar heating and surface heat exchanges, which lowers both the mean and variability of deeper water temperatures.

4.7 Salinity

In strongly tidal estuaries, saline intrusion has little impact on tidal propagation (Prandle 2009). Conversely, the nature of saline intrusion is overwhelmingly determined by the combination of tidal motions alongside the flow of river water. The pattern of intrusion may be altered by 'interventions' such as dredging, barrier construction or flow regulation alongside impacts from changes in mean sea level or river flows linked to global climate change. The extent of saline intrusion in estuaries will have an impact on sensitive marine and freshwater habitats.

Spatial and temporal variations in the patterns of intrusion are generated by:

- the flood to ebb tidal cycle
- the neap-spring cycle
- the hydrological cycle
- storm events.

Close to shore salinity often predominates over temperature in determining coastal stratification levels. Seasonal variations at the coast (due to river flow variations) generally decrease offshore with little variability found at distances greater than 50 km offshore.

4.8 Sediment supply

The predominant influences on sediment regimes in estuaries are tidal and storm currents, enhanced in exposed shallow water by wave stirring. For all but the coarsest grain sediment, several cycles of ebb and flood movement may occur between erosion and subsequent deposition. Hence, deposition can occur over a wide region beyond the source. Since time in suspension increases for finer, slowly settling material, such mechanisms may contribute to a residue of fine materials on tidal flats and to the trapping of coarser material in deeper channels.

Understanding and predicting concentrations of Suspended Particulate Matter (SPM) in estuaries are important because of their impact on:

i. light occlusion and, thereby, primary production;

ii. pathways for adsorbed contaminants and

iii. rates of accretion (deposition) and erosion, and associated bathymetric change.

In the absence of significant residual currents, the erosional time series for a semi-diurnal lunar constituent (M2), semi-diurnal solar constituent (S2) dominated tidal current regime will show pronounced SPM components at quarter-diurnal, spring-neap and time-averaged constituents.

5 Global Climate Change

As discussed in Section 4.4, the impacts of global climate change will include a rise in mean sea level. The impacts of global climate change on flooding are discussed in two DEFRA / Environment Agency publications (DEFRA 2003, 2004) whilst the most up-to-date details of projected future impacts can be found in the IPCC Fourth Assessment Report (Solomon *et al.*, 2007) and in the UK Climate Projections (UKCP, 2009).

Following the end of the last ice-age, retreating ice cover and the related rise in the mean sea level have resulted in receding coastlines (transgression) and consequent major changes in both the dynamics and morphology of estuaries. Sea levels rose globally by about 150 m between 20,000 and 5,000 BP, followed by a 'still stand' with changes in mean sea level of less than a few metres. A hinge line at approximately 55ºN across the UK separates 'falling' sea level to the north, from rising in the south. This is a reflection of the varying rates of isostatic rebound linked to ice thickness described in Sections 1.2 and 4.4.

Large post-glacial melt-water flows gouged deep channels with the rate of subsequent in-filling dependent on localised sediment supply. De-forestation and subsequent changes in land-use have substantially changed the patterns of river flows and both the quantity, and nature of, fluvial sediments.

Over shorter time scales, of interest to coastal planners, some quasi-equilibria develop encompassing variations over ebb to flood and spring to neap tides alongside seasonal cycles, storms and episodic extreme events. Thus present day morphologies reflect adjustments to these longer-term, larger-scale effects together with more recent, localised impacts from isostatic re-bound, urban development and engineering interventions. Woodroffe (2002) provides good background information on adjustments of coastlines to mean sea level changes.

As shown in Figure 5.1 (overleaf) sea levels in England and Wales have risen between 10 and 20 cm over the last century, while projected rises for 2095 range between 13 and 76 cm (UKCP, 2009). Globally, air temperatures have risen by nearly 0.8 ^{o}C since the late 19th century with forecasts for an increase over the next century of up to 4 ^{o}C.

Many morphological changes seen over the last century were related to human interventions, the responses to which often manifest themselves in unforeseen ways at remote sites at much later times. By contrast, the challenge for the next century is likely to be from impacts global climate change, although the responses are still uncertain.

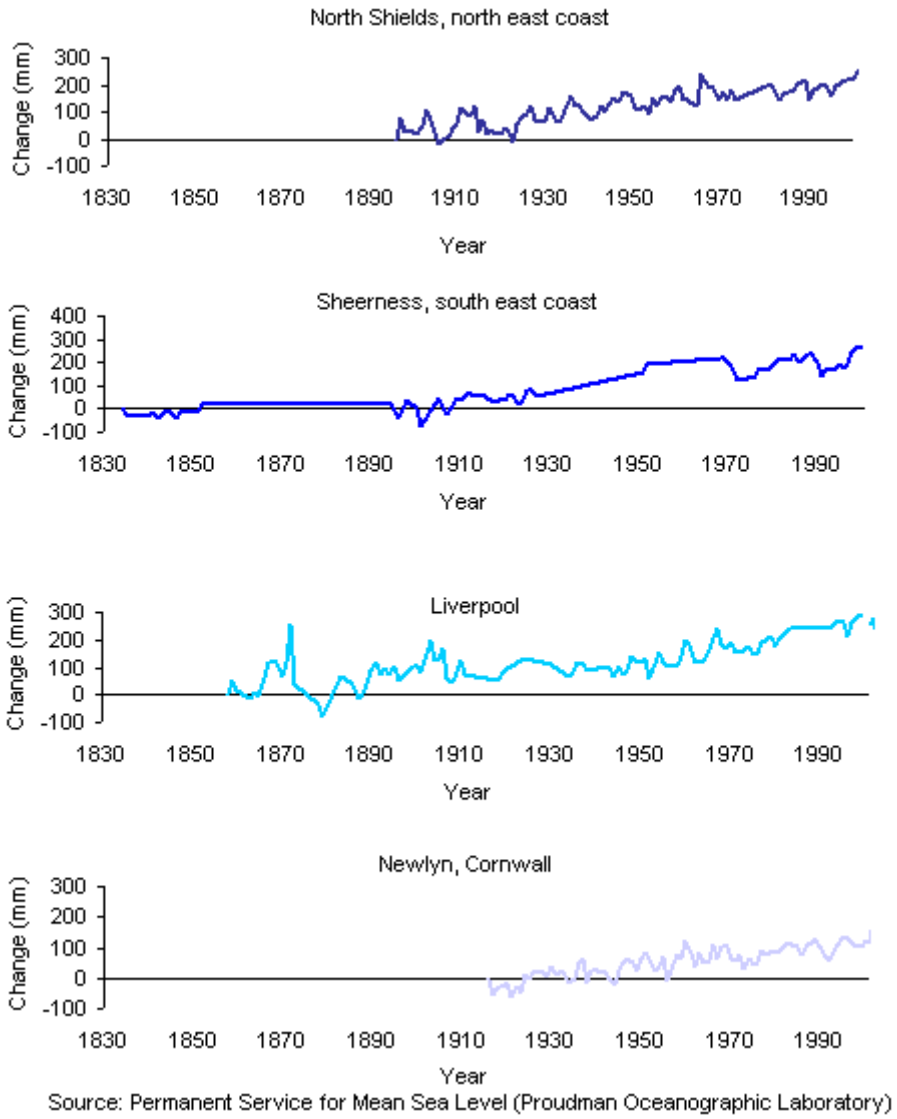

Figure 5.1 Sea level change in England and Wales 1830 to 2006 (Environment Agency, 2008).

6 Discussion

To address the impacts of global climate change, there is a need for improved scientific understanding within numerical models able to predict effects within estuaries. Continued development of theoretical frameworks is necessary to interpret ensemble modelling simulations and to reconcile disparate findings from the diverse range of estuarine types.

6.1 Gaps in the knowledge

This review has identified areas where the knowledge is either restricted to larger, commercially used estuaries, or is lacking, as is the case of models capable of accurately predicting sedimentary processes and impacts that sea level rise would have on sensitive coastal habitats. The following sections summarise where there is a need for further research.

6.1.1 Modelling

A likely response to identification of significant vulnerability of certain estuaries is the commissioning of detailed numerical model studies. The associated data requirements for setting-up, forcing, calibrating, validating and establishing confidence in such models will be more extensive than those described in Sections 3 and 4.

Tidal predictions for sea levels at the mouth of estuaries have been available for more than a century. One-dimensional models (1-D), available since the 1960s, can provide accurate simulations of the propagation of tidal heights and phases. However, tidal currents vary over much shorter spatial scales reflecting localised changes in bathymetry, creating small-scale variability in both the vertical and horizontal dimensions. This calls for models in two and three dimensions. The full influence of turbulence on the dynamics of currents and waves and their interaction with near-bed processes remains to be clearly understood. Broadly, first-order dynamics are now well understood and can be accurately modelled. Hence, research focuses on 'second-order' effects, namely higher-order (and residual) tides; vertical, lateral and high frequency variability in currents, salinity and sediment distributions.

Models can accurately predict the immediate impact of changes in bathymetry (following dredging or reclamation), river flow or bed roughness (linked to surface sediments or flora and fauna) on tidal elevations and currents. Likewise, such models can provide estimates of the variations in salinity distributions (ebb to flood, spring to neap tides, flood to drought river flows), though with a reduced level of accuracy. The further step of predicting longer-term sediment redistributions remains problematic (Lane and Prandle 2006).

Against a background of subtly changing chemical and biological mediation of estuarine environments, specific difficulties arise in prescribing:

- available sources of sediment
- rates of erosion and deposition
- the dynamics of suspension
- interactions between mixed sediment types.

The ‘decay-time’ for tidal, surge, wave and associated turbulent energy in estuaries is usually measured in hours. By contrast, the flushing time for river inputs generally extends over days. Hence, while simulation of the former is relatively independent of initial conditions, simulation of the latter is complicated by ‘historical’ chronology with associated accumulation of errors.

6.1.2 Monitoring

As a long-established maritime nation, coastal conditions around the UK are well recorded over the last century. There are generally good long-term observations of tides, surges, waves, mean sea level and river flows. Less detailed data exists for temperature and salinity and there is often little information on sediment supply. The excellent availability of data for estuaries with major ports, e.g. Mersey, Thames, Humber and Southampton Water, contrasts with sparse data for most UK estuaries. The descriptions of the gross estuarine bathymetric parameters of volume, surface area, cross-sectional areas, depths, lengths and breadths, as described in Section 3, are adequate for an initial assessment of the theories outlined in Section 2. While tides, surges and waves are generally the major sources of energy input into estuaries, pronounced seasonal cycles often occur in temperature, light, waves, river flows, stratification, nutrient supply, oxygen and plankton. These seasonal cycles, together with extreme episodic, events may prove extremely significant for estuarine ecology.

Hence, further developments of theories are likely to require more information on:

i. axial, vertical and transverse variations;

ii. tidal changes (spring-neap), seasonal cycles and episodic events;

iii. inter-annual and longer-term variability.

Confidence in future forecasts can only be satisfied by proven capability to reproduce historic trends, therefore there is a need to assemble appropriate long-term recordings of key parameters. Such data sets may be compiled from combinations of remote sensing, moorings and coastal stations. A monitoring strategy for studying bathymetric changes, which would be capable of better resolving processes operating in estuaries would comprise of:

- shore-based tide gauges throughout the length of the estuary, supplemented by water level recorders in the deeper channels;
- regular bathymetric surveys, e.g., 10-year intervals with more frequent re-surveying in regions of the estuary where bathymetry changes more rapidly;
- a network of moored platforms with instruments for measuring currents, waves, sediment concentrations, temperature and salinity.

6.2 Towards a method of assessing the vulnerability of estuaries to sea level rise

The Stage 2 report uses the synthesised classification schemes, forcing conditions and morphological data sets described here to derive a vulnerability classification system. This involves establishing links, based on the theories from Section 2, between the forcing parameters (Section 4) and the observed morphologies (Section 3).

The classification schemes were shown to explain both amplitude and phase variations of elevations and currents (cross-sectionally averaged) for the primary tidal constituents.

Qualitative descriptions of vertical current structure have been derived for:

- oscillatory tidal components
- residual components associated with river flow, wind forcing and both well-mixed and fully stratified density gradients.

Table 6.1 summarises the theoretical results described in Section 2 and Appendix A. The 'dynamical' relationships in Table 6.1 (current amplitude to the ratio of friction to inertia) were derived solely from a combination of tidal forcing and bathymetry. The mixing of river and sea water is introduced for the results from Stratification limit to salinity intrusion. By combining all of the results, the formula for Bathymetric Zone was formulated, showing how size and shape are determined by the boundary conditions of tidal amplitude and river flow.

The result for Flushing Time (F_T) being proportional to the saline intrusion divided by the river flow velocity is of direct concern for Water Framework Directive interests, since this parameter directly determines the concentrations of dissolved pollutants in estuaries.

Further application of theories for synchronous estuaries enables these frameworks to be extended to illustrate conditions corresponding to stable bathymetry and sedimentary regimes shown by the last two equations in Table 6.1.

Table 6.1 Functional relationships related to classification schemes.

Classification scheme	Functional relationship
Current amplitude (shallow water)	$U \propto Z^{½} D^{¼} f^{-½}$
Current amplitude (deep water)	$U \propto Z D^{-1/2}$
Estuarine tidal length	$L \propto D_0^{5/4} / Z^{½} f^{½}$
Depth at the mouth	$D_0 \propto (\tan\alpha\ Q)^{0.4}$
Depth variation	$D(x) \propto D_0 x^{0.8}$
Ratio of friction : inertia	$F/\omega \propto 10 Z / D$
Stratification limit[1]	$Z \sim 1m$
Salinity intrusion	$L_I \propto D_0^2 / f\ U_0\ U$
Bathymetric zone	$L_I < L$, $E_X < L < 1$, and $D/U^3 < 50\ m^{-2}\ s^3$
Flushing time	$F_T \propto L_I / U_0$
Suspended sediment concentration	$C \propto f\ U$
Equilibrium sediment fall velocity	$W_s \propto f\ U$

Notes: [1]This is taken to be when the tidal elevation amplitude, Z , is approx. 1m

C – suspended sediment concentration
D – depth
D_0 – depth at mouth
$D_{(X)}$ – depth variation
E_X – tidal excursion
f – bed friction coefficient
F – linearised bed friction coefficient
F_T – flushing time
L – tidal length
L_I – salinity intrusion
U – tidal current amplitude
U_0 – river flow velocity
W_s – sediment fall velocity
Z – tidal elevation amplitude
ω - tidal frequency ($P/2\pi$, where P is the tidal period)

In Stage 2 of this project, four indices of vulnerability are derived, indicating the likely impacts of global climate change in tidally-dominated UK estuaries on:

i. Mass Flow;

ii. Energetics;

iii. Vertical Mixing and

iv. Salinity Intrusion.

7 References

ABPmer, 2003 Estuaries database 2003 Posford-Haskoning: ABPmer, CD-ROM (Estuaries Research Programme Phase 1 Uptake Project FD2110)

ABRAHAM, C., 1988. Turbulence and mixing in stratified tidal flows, pp.149-180 In: (Editors. J. Dronkers & W. van Leussen), *Physical processes in estuaries,* Berlin: Springer Verlag, 560pp.

BAGNOLD, P. A., 1963. Mechanics of marine sedimentation. In: *The Sea: Ideas and Observations on Progress in the Study of the Seas,* M. N. Hill, (Editor) vol. 3, *The Earth Beneath the Sea: History,* pp. 507-582, John Wiley, Hoboken, N. J.

BALLS, P.W., 1994. Nutrient inputs to estuaries from nine Scottish East Coast Rivers: Influence of estuarine processes on inputs to the North Sea. *Estuarine, Coastal & Shelf Science*, 39, 329-352.

BOWDEN, K. F. 1953. note on wind drift in a channel in the presence of tidal currents. *Proceedings of the Royal Society of London,* A219, 426-446.

BURGESS, K.A., BALSON, P., DYER, K.R., ORFORD, J. AND TOWNEND, I.H., 2002. Futurecoast the integration of knowledge to assess future coastal evolution at a national scale. *In: 28th International Conference on Coastal Engineering. American Society of Civil Engineering*, *Cardiff, UK, Vol. 3*. pp. 3221-3233.

CENTRE FOR ECOLOGY AND HYDROLOGY. 2009. River Flow Data – Time Series Downloads. Available from: http://www.ceh.ac.uk/data/nrfa/river_flow_data.html

CHURCH, J.A., GREGORY, J.M., HUYBRECHTS, P., KUHN, M., LAMBECK, K., NHUAN, M.T., QIN, D. AND WOODWORTH, P.L. 2001. Changes in sea level. pp.639-693 in, Climate Change 2001: The Scientific Basis. Contribution of Working Group I to the Third Assessment Report of the Intergovernmental Panel on Climate Change. (eds. J.T. Houghton, Y. Ding, D.J. Griggs, M. Noguer, P.J. van der Linden, X. Dai, K. Maskell and C.A. Johnson).Cambridge: Cambridge University Press. 881pp.

DAVIDSON, N.C. AND BUCK, A.L., 1997. *An inventory of UK estuaries. In: Introduction and Methodology,* Vol. 1 (of 7). Joint Nature Conservation Committee (http://www.jncc.gov.uk), Peterborough, UK, 46 pp.

DEFRA/ENVIRONMENT AGENCY, 2003. *Climate Change Scenarios UKCIP02: Implementation for Flood and Coastal Defence.* R&D Technical Summary W5B-029/TS.

DEFRA/ENVIRONMENT AGENCY, 2004. *Impact of Climate Change on Flood Flows in River Catchments.* Technical Summary W5-032/TS.

DYER, K.R., 1997. *Estuaries: A Physical Introduction (2nd Ed.)* John Wiley, Hoboken, N. J., 195pp.

ENVIRONMENT AGENCY 2008. Sea level change in England, 1830 to 2006. Available from: http://www.environment-agency.gov.uk/research/library/data/58624.aspx

FLATHER, R.A., 1976. A tidal model of the north west European Continental Shelf *Memoire Societe Royale Science Liege, Ser* 6,10,141-164.

HEAPS, N.S., 1967 Storm Surges. *Oceanography and Marine Biology Annual Review,* Barnes, H. (Editor).London: Allen & Unwin, 5,11-47.

HEAPS, N.S., 1983. Storm surges,1967-1982.*Geophysical Journal Royal Astronomical Society*, 74, 331-376.

HUNTER, J. R. 1975. A note on quadratic friction in the presence of tides. *Estuarine, Coastal and Shelf Science* 3(4), 473-475.

IACMST (Inter Agency Committee on Marine Science and Technology) 2005. *Charting Progress - an integrated assessment of the state of UK seas. Part 2 – Marine Processes and Climate*. 138pp. Available from: http://www.defra.gov.uk/marine/pdf/science/stateofsea/chartprogress-2.pdf

IPPEN, A.T. (Editor) 1966 *Estuary and Coastline Hydrodynamics.* McGraw-Hill, New York. 744pp.

LANE, A. AND PRANDLE, D. 2006. Random-walk particle modelling for estimating bathymetric evolution of an estuary. *Estuarine, Coastal & Shelf Sciences*, 68, 175-187.

MANNING, A.J., 2004., Observations of the properties of flocculated cohesive sediments in three western European estuaries. In: Ciavola, P. and Collins, M.B. (Editors), "*Sediment Transport in European Estuaries"*, *Journal of Coastal Research*, SI 41, 70-81.

MANNING, A.J. 2008. Enhanced UK Estuaries database: explanatory notes and metadata (project FD2107) Report TR 167, H R Wallingford 20pp

MEEHL, G.A., STOCKER, T.F., COLLINS, W.D., FRIEDLINGSTEIN, P, GAYE, A.T., GREGORY, J.M., KITOH, KNUTTI, R., MURPHY, J.M., NODA, A., RAPER, S.C.B., WATTERSON, I.G., WEAVER, A.J. AND ZHAO, Z.-C. 2007: Global Climate Projections. In: *Climate Change 2007: The Physical Science Basis. Contribution of Working Group I to the Fourth Assessment Report of the Intergovernmental Panel on Climate Change* [Solomon, S., D. Qin, M. Manning, Z. Chen, M. Marquis, K.B. Averyt, M. Tignor and H.L. Miller (eds.)]. Cambridge University Press, Cambridge, United Kingdom and New York, NY, USA.

O'BRIEN, M.P., 1969. Equilibrium flow area of inlets and sandy coasts. *Journal Waterways and Coastal Engineering. Division. ASCE,* 95, 43-52.

PETHICK, J.S., 1984. *An Introduction to Coastal Geomorphology*. Arnold. London. 260 pp.

POSTMA, H., 1967. Sediment transport and sedimentation in the estuarine environment." *Estuaries,* (G. H. Lauff, Editor). American Association for the Advancement of Science., Washington, D.C., 158- 180.

PRANDLE, D. AND RAHMAN, M. 1980. Tidal response in estuaries. *Journal of Physical Oceanography,* 10(10), 1552-1573.

PRANDLE, D. 1982. The vertical structure of tidal currents and other oscillatory flows. *Continental Shelf Research,* 1, 191-207.

PRANDLE, D. 1985. On salinity regimes and the vertical structure of residual flows in narrow tidal estuaries. *Estuarine Coastal and Shelf Sciences,* 20, 615-633.

PRANDLE, D. 1997. The dynamics of suspended sediments in tidal waters. *Journal of Coastal Research,* (Special Issue No 25): 75-86.

PRANDLE, D. 1998. Global expressions for seasonal temperatures of the sea surface and ambient air: the influence of tidal currents and water depth. *Oceanologica Acta*, 21(3): 419-428.

PRANDLE. D. 2003. Relationships between tidal dynamics and bathymetry in strongly convergent estuaries, *Journal of Physical Oceanography,* 33(12), 2738-2750.

PRANDLE, D. 2004. How tides and river flow determine estuarine bathymetry. *Progress in Oceanography.* 61, 1-26.

PRANDLE, D., LANE, A., AND MANNING, A.J. 2005. Estuaries are not so unique. *Geophysical Research Letters*, 32, L23614, doi:10.1029/2005GLO24797.

PRANDLE, D. 2006. Dynamical controls on estuarine bathymetry: assessment against UK data base. *Estuarine Coastal & Shelf Sciences,* 68(1-2), 282-288.

PRANDLE, D. 2009. *Estuaries: dynamics, mixing, sedimentation & morphology.*235pp Cambridge University Press, Cambridge, UK

PRITCHARD, D. W., 1955. Estuarine circulation patterns. *Proceedings of the American Society of Civil Engineers* 81,717/1-717/11.

PUGH, D.T. 1996. *Tides, Surges and Mean Sea-Level*, Chichester: John Wiley

RIGTER, B. P. 1973. Minimum length of salt intrusion in estuaries. *Proceedings of the American Society of Civil Engineers, Journal of the Hydraulics Division* 99**,** (HY9), 1475-1496.

ROMANO, C., WIDDOWS, J., BRIMLEY, M.D. AND STAFF, F.J., 2003. Impact of Enteromorpha on near-bed currents and sediment dynamics: flume studies. *Marine Ecology Progress Series,* 256, 63-74.

ROSSITER, J R, 1962. Tides and storm surges. *Proc. Roy. Soc. London* (A265), 328-330.

SCHUBEL, J. R., AND HIRSCHBERG, D. J. 1982. The Chang Jiang (Yangtze) Estuary: Establishing its place in the community of estuaries. In V. S. Kennedy (Ed.), *Estuarine comparisons,* pp. 649-654. New York: Academic Press.

SHENNAN, I. AND HORTON, B., 2002. Holocene land- and sea-level changes in Great Britain. *Journal of Quaternary Science* 17, 511-526.

SIMPSON, J. H. AND HUNTER, J. R., 1974. Fronts in the Irish Sea. *Nature* 250, 404-406.

SIMPSON, J.H. AND BOWERS, D.G., 1981. Models of stratification and frontal movement in shelf seas. *Deep-Sea Research* 28, 727-738.

SIMPSON, J.H., BROWN, J., MATTHEWS, J. AND ALLEN, G., 1990. Tidal straining, density currents and stirring in the control of estuarine stratification. *Estuaries* 13 (2), 125-132.

SOLOMON, S.D., QIN, D., MANNING, M., CHEN, Z., MARQUIS, M., AVERYT, K.B., TIGNOR, M. AND MILLER, H.L. (Eds.) 2007. Contribution of Working Group I to the Fourth Assessment Report of the Intergovernmental Panel on Climate Change. Cambridge University Press, Cambridge, United Kingdom and New York, NY, USA. 996pp.

SOULSBY, R.L., 1997. *Dynamics of Marine Sands: a Manual for Practical Applications*. Telford, London, 249 pp.

UKCP. 2009. UK Climate Projections. Available from: http://ukclimateprojections.defra.gov.uk/

UNCLES,R.J., STEPHENS, J. A. AND SMITH, R.E., 2002. The dependence of estuarine turbidity on tidal intrusion length, tidal range and residence time. *Continental Shelf Research*, 22, 1835-1856.

VAN RIJN, L.C., 1993. *Principles of Sediment Transport in Rivers, Estuaries and Coastal Seas*. Aqua Publications, Amsterdam, the Netherlands.

WINTERWERP , J. C. AND VAN KESTEREN, W. G. M., 2004. *Introduction to the physics of cohesive sediments in the marine environment.* Developments in Sedimentology (56), Elsevier :Amsterdam, pp 466.

WOODWORTH, P.L., TSIMPLIS, M.N., FLATHER, R.A. AND SHENNAN, I., 1999. A review of the trends observed in British Isles mean sea level data measured by tide gauges. *Geophysical Journal International,* 136(3), 651–670.

WOODROFFE, C. D. 2002 *Coasts: form, process and evolution.* 623pp Cambridge University Press, Cambridge, UK.

YATES, M. G., CLARKE, R.T., SWEETMAN, R.D., EASTWOOD, J.A., LE DURRELL, S. E. A. V. dit, WEST, J.R., GOSS-CUSTARD, J.D., CLARK, N. A., HOLLOWAY, S.J. AND REHFISH, M.M. 1996. Estuary sediments and shorebirds. 1. Determinants of the intertidal sediments and estuaries. A report by the Institute of Terrestrial Ecology under contract to ETSU (ETSU Project T/04/00201/REP). Monks Wood, UK, 90pp.

List of abbreviations

Symbols used

A	cross-sectional area
B	channel breadth
C	sediment concentration in suspension
D	water depth
D_o	depth at the mouth
$D_{(X)}$	depth variation
E	eddy viscosity
E_X	tidal excursion length
F	linearised bed friction coefficient
F_R	flow ratio ($U_0\pi/U$)
F_T	flushing time
G	tidal energy dissipation rate
H	total water depth (D +z)
Hs	significant wave height
HW	high water
INTA	inter-tidal area
J	buoyancy input
K_Z	eddy diffusivity
K1	principal lunar and solar diurnal constituent
L	estuarine tidal length
L_I	salinity intrusion length
LW	low water
M2	principal lunar semi-diurnal tidal constituent
MW	mean water
N2	lunar ellipse constituent
O1	principal lunar diurnal constituent
P	tidal period
P1	principal solar diurnal constituent
Q	river flow
Ri	Richardson Number
R_1	amplitude of the anti-clockwise current component

R_2	amplitude of the clockwise current component
S	surface area
SL	shoreline length
SM	salt marsh area
S_R	Strouhal Number (UP/D)
S_T	Stratification Number
S_T'	modified Stratification Number
S_X	axial density gradient
S2	principal solar semi-diurnal tidal constituent
T	tidal range
Ta	air temperature at the sea surface
Ts	surface water temperature
U	tidal current amplitude
Uo	velocity component of river flow
V	volume
W	width
Ws	sediment fall velocity
X	axial distance from the head of the estuary
Z	tidal elevation amplitude
f	bed friction coefficient (~ 0.0025)
g	gravitational constant
k	wave number ($2\pi/\lambda$)
m	power of axial depth variations (x^m)
n	power of axial breadth variation (x^n)
t	time
t_{50}	half-life of sediments in suspension
tan α	side slope gradient (B/2D)
x	axial distance (dimensionless)
z	water level
α	exponential settling rate $e^{-\alpha t}$
θ	phase advance of tidal amplitude (Z) relative to tidal current amplitude (U)
λ	wavelength
ν	funnelling parameter (n+1)/(2-m)
π	3.141592

ρ	water density
$\Delta\rho$	excess density of sea water
$\partial\rho/\partial x$	axial density gradient
τ	surface wind stress
ω	tidal frequency ($P/2\pi$)
Ω	Coriolis coefficient

ACRONYMS

ABP	Associated British Ports
ABS	Acoustic Back Scatter
DEFRA	Department for Environment, Food and Rural Affairs
EA	Environment Agency
ERP	DEFRA's Estuarine Research Programme
JNCC	Joint Nature Conservation Committee
LIDAR	Light detection and ranging
MSL	Mean Sea Level
OBS	Optical Back Scatter
PSMSL	Permanent Service Mean sea Level
SAR	Synthetic aperture radar
SPM	Suspended particulate matter
WFD	Water Framework Directive

Glossary

Analytical emulator	functional synthesis of dynamical processes
Bathymetric stability	near equilibrium between dynamics, morphology & sediments
Zone	likely parameter ranges for morphology of tidal estuaries
Circulation	longer-term (tidally averaged) flow paths
Currents	tidal, salinity and wind driven
Episodic events	storm surges, waves
Eustatic	global change in volume of sea water
Flushing time	time to reduce initial estuary-wide concentrations by half
Friction	bed friction coefficient
Gravitational circulation	circulation by vertical density differences
Higher harmonics	tidal constituents generated by non-linearities
Holocene	last 10000 yrs since the end of last ‘ice-age’-
Hypsometry	cross-sectional transverse profile
Inertia	acceleration term in momentum equation
Inter-tidal	between low water, LW, and high water, HW
Isostatic	movement of Earth’s crust
Mixing	dilution of river water into sea (and other contaminants)
Monitoring	long-term systematic observational programme
Morphology	geometrical form of estuary
Phase difference	time-lag measured as a fraction of (tidal) cycle
Residuals	generally used to indicate any non-tidal component
Regime formula	relationship between estuary morphology and ‘forcing’
Remote sensing	satellite, aircraft, coastal radar measurements
Richardson No.	ratio of buoyancy to turbulent mixing
Secular	long-term (> decade)
Steric	global change in sea level due to thermal expansion
Strouhal Number	indicator of tidal current structure UP/D
Stratification Number	ratio of turbulent mixing to riverine buoyancy
Salinity intrusion	landward extent of sea water within estuaries
Seasonal cycles	annual variations in temperature, rainfall

Significant wave height, Hs	4 x variance in wave heights
Simpson-Hunter mixing parameter	D/U^3
Straining	circulation from vertical structure of tidal currents
Stratification	degree of vertical mixing of salt and river water
Surge	meteorologically generated sea-surface disturbance
Synchronous estuary	little axial amplification of tidal constituents
Tides-amphidrome	spatial pattern of tidal heights and phase

Tidal Constituents:

	Period	
M2	12.42h	principal lunar semi-diurnal
S2	12.00h	principal solar semi-diurnal
N2	12.66h	lunar ellipse
O1	25.82h	principal lunar diurnal
P1	24.07h	principal solar diurnal
K1	23.93h	principal Lunar and Solar diurnal
M4	6.21h	quarter-diurnal higher harmonic of M_2
MS4	6.10h	quarter-diurnal higher harmonic of M_2 and S_2
MSf	14 day	interaction of M_2 and S_2
S_a	365 day	solar annual
SS_a	183 day	solar semi-annual
Z0	infinite	residual, time-averaged component

Tidal ranges	Tidal amplitudes
micro < 2 m,	micro < 1 m
meso 2 – 4 m	meso 1 – 2 m
macro > 4 m	macro > 2 m

Theoretical Frameworks	generic response diagram illustrating parameter dependencies
Tortuosity	ratio of shoreline to axial lengths
Transgression	coastal ‘retreat’

Appendix A Estuarine Classification Schemes

The following estuarine response characteristics link ‘external forcing’ to impacts within estuaries. The figures, formulae and dimensionless parameter groupings illustrate the likely forms for such links. The classifications extend over:

- tidal elevation
- storm surges
- vertical current structure
- salinity intrusion
- stratification
- seasonal temperature cycles
- sediment regimes
- morphology
- sediment trapping and sorting (in synchronous estuaries)
- typological frameworks.

Appendix A.1 Tidal elevations

The theoretical results shown here assume that tidal propagation in estuaries can be represented by linearised shallow-water wave equations reduced to a one-dimensional cross-sectionally averaged form. Axial variations in breadths (n) and depths (m) are described by X^n and X^m, where X is the axial distance from the head (the synchronous approximation described subsequently is equivalent to m = n = 0.8). Figure A.1 (overleaf) represents a generalised response diagram (Prandle and Rahman, 1980), showing amplitude and phase variations along any such estuary as a function of the funnelling parameter $\nu = (n+1)/(2-m)$. Maximum amplification of tides within an estuary occurs for $\nu = 1$. Nodal lengths, similar to those associated with 'quarter wave-length amplification' in a frictionless prismatic channel, are indicated by the thick line corresponding to a phase difference of 90^o.

These responses vary according to the value of the linearised friction factor, reflecting how bathymetry and friction together determine the nature of tidal propagation in estuaries. Moreover, through the adoption of dimensionless parameters, the framework can explain the tidal response at any axial position, for all tidal constituents, along any funnel-shaped estuary.

To convert to a dimensionless format we adopt λ as a unit of horizontal dimension; H_L, as a unit of vertical dimension and P, the tidal period, as a unit of time, with

$$\lambda = (g\, H_L)^{½}\, P$$

corresponding to the tidal wavelength for H_L constant (g is gravity).

Axial distance from the head, X, is converted to a dimensionless form by

$$y = \frac{4\pi}{2-m} x^{\frac{2-m}{2}}$$

where $x=X/\lambda$.

In an analysis of UK estuaries, Prandle (2006) provided the following estimates of the 'funnelling factor', ν :

- All - 1.85 ;
- Ria -1.72;
- Coastal plain - 2.07, and
- Barb-built - 2.25.

Maximum tidal amplification occurs for $\nu = 1$ with considerable reduction of this peak for $\nu > 2$. Thus tidal elevations and currents are likely to be more spatially homogeneous in Bar Built estuaries, reflecting conditions closer to equilibrium.

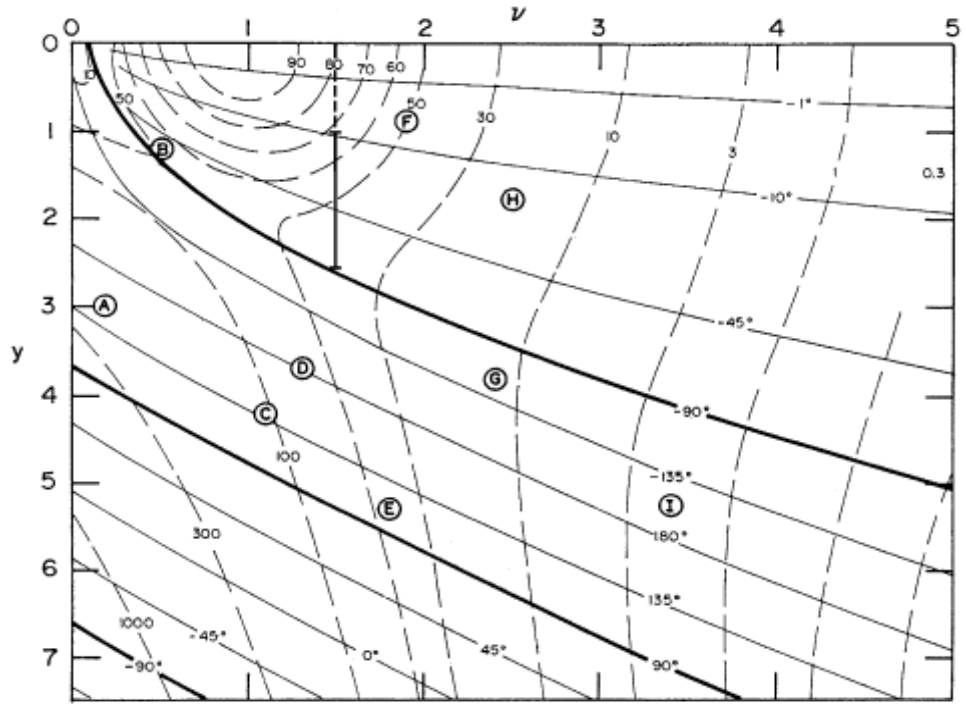

Figure A.1 Semi-diurnal tidal elevation responses for s=2π (=F in Appendix A1.3), from Prandle and Rahman (1980).

Notes: ν represents the degree of bathymetric funnelling and *y,* distance from the mouth (*y* = 0). Dashed contours indicate relative amplitudes, continuous contours relative phases. Vertical line at ν = 1.5 shows typical lengths of synchronous estuaries. Lengths, y, (for M2) and shapes, ν, for estuaries: A - Fraser, B - Rotterdam Waterway, C - Hudson, D - Potomac, E - Delaware, F - Miramichi, G - Bay of Fundy, H - Thames, I - Bristol Channel and J - St. Lawrence.

The sensitivity to bed friction is shown in Section A.3 (tidal current amplitudes) for solutions for synchronous estuaries.

This response diagram reproduces a number of features commonly encountered, namely:

i. quarter-wavelength resonance found in sufficiently long estuaries where the mouth lies close to the amplitude nodes described above,

ii. the dimensionless estuarine length, $y_{M,}$ (the value of y at the mouth), is inversely proportional to the tidal period (P), thus doubling P halves y_M. Hence, for a diurnal tidal constituent, the y_M values for estuaries A to I, are halved and we expect a relatively small amplification of such constituents. For MSf, a 14-day constituent (interaction of the principal Lunar and Solar semi-diurnal constituents, M2 and S2), the reduction in the y_M values would indicate little amplification or phase difference along any estuary,

iii. for quarter-diurnals, (higher harmonics of M2 and, M2 and S2) the values of y_M are doubled. Thus, we expect higher amplification and larger phase differences compared with values for semi-diurnal constituents. However, it is important to distinguish between the response to external forcing represented by the present analysis and the internal generation of higher harmonics by nonlinear processes, such as quadratic friction and shallow water and convective terms, within an estuary.

Appendix A.2 Storm surges

The response to storm surges can be seen from Figure A.1 by approximating the time-sequence by A(1 –cos ωt), i.e. a 'bell curve' of maximum amplitude of 2A and duration 2π/ω.

A.2.1 Resonant amplifications

The estuarine length, L_M, for maximum amplification is approximated by:

$$L_M = (2\text{-}m)(0.75\nu + 1.25)\, g^{½}\, D_0^{½}\, P/(4\,\pi)$$

(Using the same notation as defined above for Section A.1), Substituting m = 0.8 and ν = 2.0 gives, for the M_2 frequency, $L_M = 37\, D_0^{1/2}$ (km) or 117 km for D_0 = 10 m.

This indicates that only the longest of UK estuaries, such as the Bristol Channel, are likely to exhibit significant amplification for tides or surges close to semi-diurnal frequencies. Significant amplification of storm surges within estuaries may occur for surges of duration less than 12 hours. Such surges are commonly associated with secondary depressions that can accompany larger cyclonic systems (depressions).

Appendix A.3 Tidal current amplitudes

A convenient summary of tidal current responses is obtained by using solutions for synchronous estuaries, i.e. where the surface slope due to the gradient in phase of tidal elevations significantly exceeds the gradient from changes in tidal amplitude, Z.

Omitting the advective term from the momentum equation, we can describe tidal propagation in an estuary by:

$$\frac{\partial U}{\partial t} + g\frac{\partial z}{\partial X} + f\frac{U|U|}{H} = 0$$

$$B\frac{\partial z}{\partial t} + \frac{\partial}{\partial X} A\,U = 0$$

where U is velocity in the X-direction; z is water level; D is water depth; H is the total water depth (H = D +z); f is the bed friction coefficient (≈ 0.0025); B is the channel breadth; A is the cross-sectional area; g is the gravitational acceleration, and t is time.

The component of f U|U|/H at the predominant tidal frequency, M_2 may be approximated by

$$\frac{8}{3\pi}\frac{25}{16} f\frac{|U^*|U}{D} = FU$$

with $F = 1.33fU^*/D$, where 8/3π derives from the linearisation of the quadratic velocity term.

Appendix A.3.1 Synchronous solutions

$$\tan\theta = -\frac{F}{\omega} = \frac{SL}{0.5\,D\,k}$$

where SL = ∂D/∂X

$$U = Z\,g\,k\,/\,(\omega^2 + F^2)^{1/2}$$

$$k = \frac{\omega}{(0.5Dg)^{1/2}}$$

where θ is the phase lag of tidal currents relative to tidal elevation (ω = 2π/ P) and k is the speed of phase propagation for both U and Z.

A particular advantage of the above solutions is that they enable the values of a wide range of estuarine parameters to be calculated and illustrated as direct functions of depth, D and tidal amplitude, Z . The ranges selected in Figure A.2 are Z = 0 to 4 m and D = 0 to 40 m.

Figure A.2 (overleaf) shows that current amplitudes extend to 1.5 ms^{-1}. Maximum values of U occur at approximately D_0 = 5 + 10 Z (m).

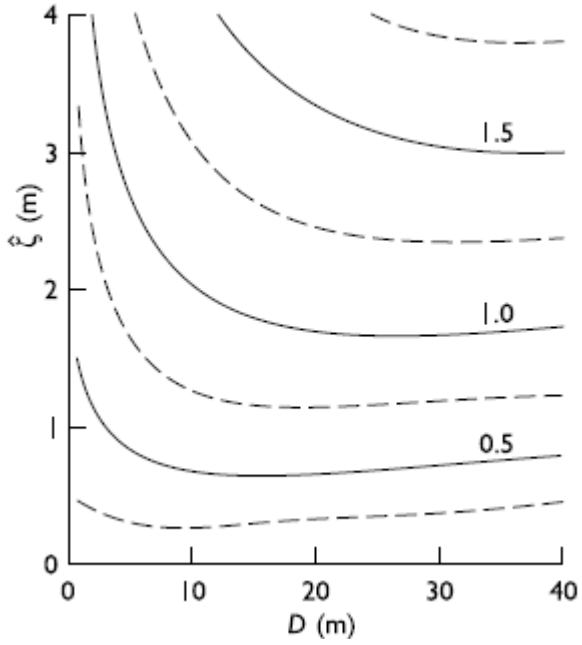

Figure A.2 Tidal Current Amplitude, U (m s^{-1}) as a function of depth, D and tidal amplitude, Z (shown on the y-axis as ς). Bed friction coefficient, f = 0.0025, from Prandle (2004).

Appendix A.3.2 Ratio of friction to inertia

Figure A.3 illustrates the ratio of the linearised bed friction to inertial terms (F/ ω_1).

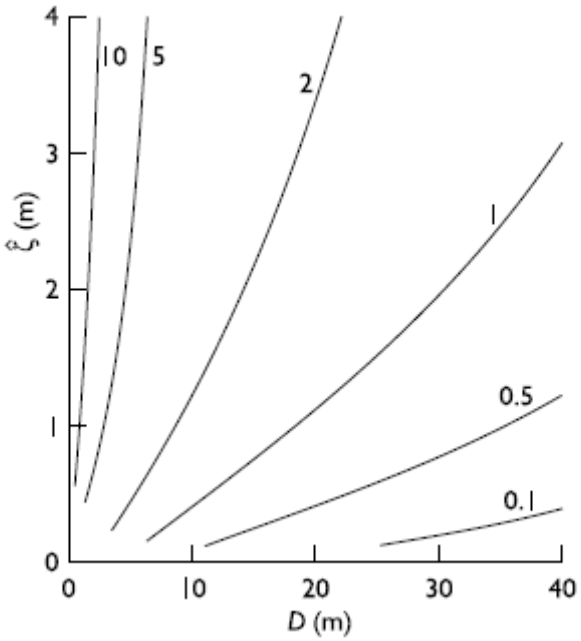

Figure A.3 Ratio of the linearised friction term, F, to the inertial term, ω_1, as a function of depth, D, and tidal amplitude, Z (given as ς on the y-axis in the Figure), from Prandle (2004).

Note: contour values also indicate tan $\theta = -F/\omega_1$

For $F >> \omega_1$, $U^* \propto \varsigma^{*\,½} D^{¼} f^{-1/2}$

For $F << \omega_1$, $U^* \propto \varsigma^{*} D^{-½}$

F/ ω_1 is approximately equal to unity for Z = D/10.

For values of Z >> D/10, tidal dynamics become frictionally dominated and currents change by a factor of two as f varies over the range 0.001 to 0.004.

For Z << D/10 friction becomes insignificant.

Table A.1 indicates the sensitivity to bed friction of currents amplitude, bed slope and estuarine length.

The synchronous solution corresponds to m = n = 0.8, this corresponds to $\nu = 1.5$ in Figure A.1 (page 37), i.e., close to the centre of values encountered..

Table A.1 Parameter sensitivity for modified friction f' = εf.

	F/ω >> 1 or Z >> D/10	**F/ω << 1 or Z << D/10**
Current amplitude, U	$\varepsilon^{-1/2}$	1
Seabed slope, SL	$\varepsilon^{½}$	ε
Estuarine length, L	$\varepsilon^{-1/2}$	ε^{-1}

A.3.2.1 Depth profile, D, and estuarine length, L

Substituting X = 0 and D = D_0 at the mouth, estuarine lengths are given by:

$$L = \frac{D_0^{5/4}}{Z^{1/2}} \frac{4}{5} \frac{(2g)^{1/4}}{(1.33 f \omega)^{1/2}} \sim 2460 \frac{D_0^{5/4}}{Z^{1/2}} \quad \text{for} \quad f = 0.0025$$

(units are in metres, m; subscripts 0 denote values at the mouth).

The dependency on $D_0^{5/4} / Z^{1/2}$ shown in Figure A.4 (overleaf) indicates estuarine lengths are significantly more sensitive to depth than to tidal amplitude. This expression for estuarine length was compared with data from some 50 estuaries from around the coasts of the UK and the eastern USA by Prandle (2003).

Overall, the theoretical values show broad agreement with the observed values. For the UK estuaries, estimates of mud content were available, enabling some of the discrepancies between observed and estimated values of estuarine length, L, to be reconciled by introducing an expression for the bed friction coefficient, f based on relative mud content.

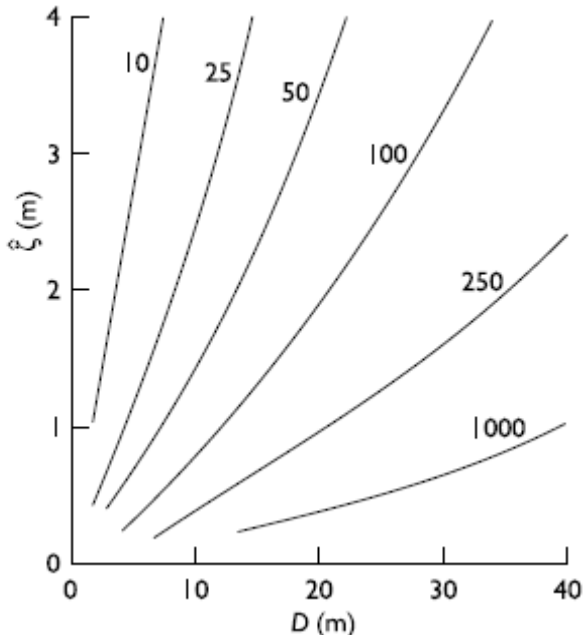

Figure A.4 Estuarine length, L (km) as a function of depth, D_0, and tidal amplitude, Z, with bed friction coefficient, f = 0.0025, from Prandle (2004).

Appendix A.4 Vertical current structure

Solutions are first shown for the simplest case of unidirectional flow. These solutions are extended to indicate two-dimensional flow introducing the effects of rotation (Coriolis force). The sensitivity of these solutions to bed friction factor, eddy viscosity, tidal period and latitude is then described. Further solutions are shown for current components associated with wind, river flow and well-mixed density gradients.

A.4.1 Unidirectional tidal flow (no rotation)

Here, and elsewhere throughout this report, analytical solutions are obtained by introducing the assumption of a vertically and temporally constant eddy viscosity coefficient, E (E = K = f U D, where K is the related eddy diffusivity coefficient; f the bed friction coefficient; U the tidal current amplitude and D water depth). Prandle (1982, 1985 and 1997) found that these approximations were valid in shallow, strongly tidal estuaries i.e. for most UK estuaries.

For this assumption vertical structure of tidal currents is determined by two parameters

$$\text{(i)} \qquad J = \frac{3\pi\ (E\omega)^{1/2}}{8 f U}$$

where J is dimensionless and reflects the effect of the quadratic bottom stress through the bed-stress coefficient, f and the depth-averaged velocity amplitude, U.

And $$\text{(ii)} \qquad Y = (\omega/E)^{1/2} D$$

where Y may be interpreted as a depth parameter converted to a dimensionless form by Ekman scaling.

Adopting the above approximation for E, the characteristics of vertical structure of tidal currents can be reduced to dependency on

$$Y = \frac{8}{3\pi} J$$

Introducing the Strouhal Number, $S_R = U P / D$

we see $Y \approx J \approx 50 / S_R^{1/2}$ for f = 0.0025. Figure A.5 shows how the amplitude and phase of tidal currents vary as a function of S_R. The amplitude structure increases asymptotically with increasing S_R up to a value $S_R \sim 350$. Accompanying phase variations are at a maximum for this value of S_R but decrease for both smaller and larger values. In meso- and macro-tidal estuaries, the Strouhal Number will be well in excess of 1000, indicating an amplitude structure close to the 'asymptotic' solution for large S_R, but with a phase structure that reduces with increasing values of S_R.

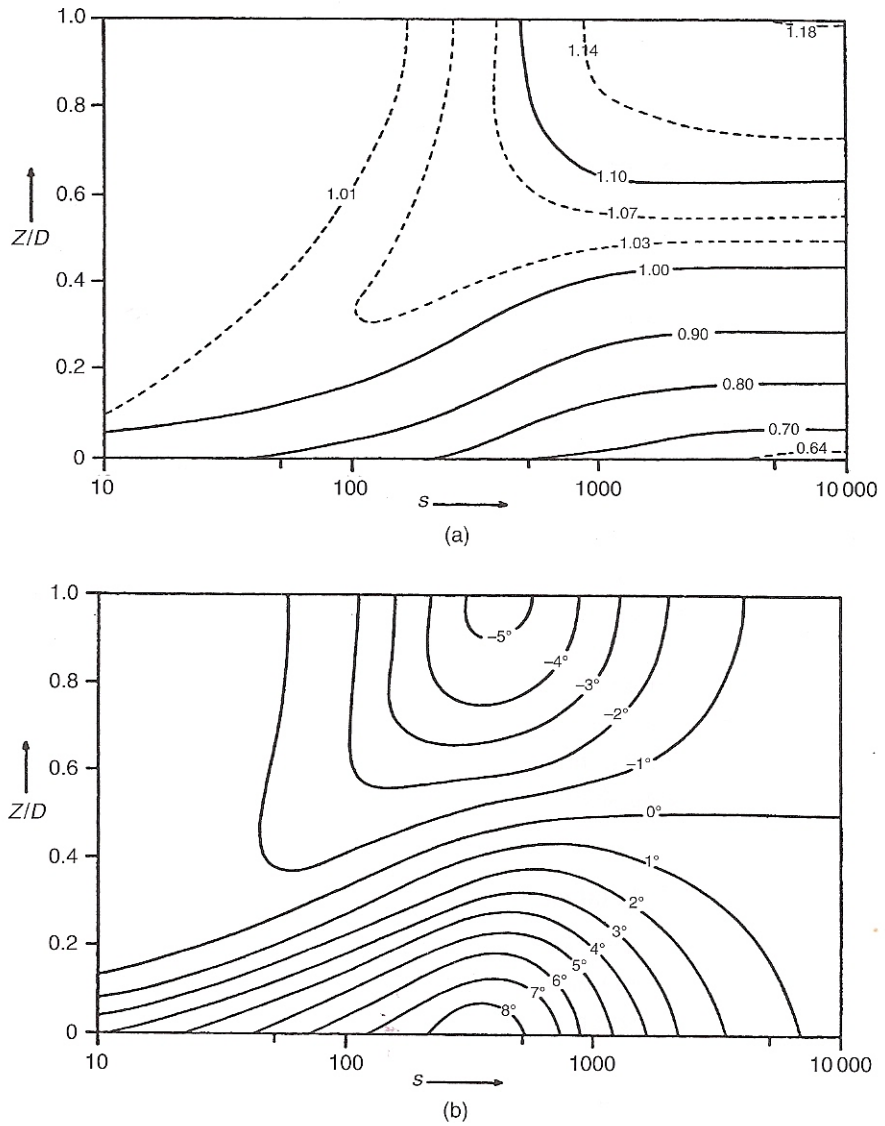

Figure A.5 Tidal current profile as a function of the Strouhal Number, SR = U P/D after Prandle (1982). s on x-axis represents the Strouhal Number, SR, from Prandle (1982).

Notes: Top: vertical variation in amplitude (as a ratio of depth-mean value) $U(z)/U_{mean}$. Bottom: vertical variation in phase structure relative to depth-mean value $\theta(z) - \theta_{mean}$

A.4.2 Effects of rotation (Coriolis force)

In wide and deep estuaries the Coriolis force may significantly influence tidal currents with rotary ellipse patterns replacing unidirectional flows. Decomposing such ellipses into anti-clockwise and clockwise components, the current structure for the a-c and c-w components can be estimated from Figure A.5 by calculating their respective Strouhal numbers as follows:

$$S_1 = 2\pi |R_1| / (D (\Omega + \omega))$$

and $$S_2 = 2\pi |R_2| / (D (\omega - \Omega))$$

where $\Omega = 1.45\ 10^{-4}$ sin (latitude); Ω is the Coriolis parameter; R_1 and R_2 are amplitudes of the anti-clockwise and clockwise current components.

Thus, for semi-diurnal constituents in latitudes less than 70^0, vertical structure will be greater for the clockwise component than for the anticlockwise component. The more pronounced current structure for the clockwise component means that the tidal current ellipse becomes more positively eccentric towards the bed (positive eccentricity indicates that $|R_1| > |R_2|$). It can be similarly deduced that the direction of the major axis of the ellipse will veer in a clockwise sense towards the bed.

At mid-latitudes, for the other major tidal frequency bands, i.e. diurnal, quarter diurnal, etc., the ratio $(\Omega + \omega) : | \Omega - \omega |$ is smaller than for the semi-diurnal band. Hence, the difference between the velocity structures for the two rotational components should be less than that for the principal semi-diurnal lunar constituent, M2.

A.4.3 Sensitivity to friction factor, f; eddy viscosity, E; tidal period, P and latitude

In the vicinity of the bed, reducing the eddy viscosity, E, enhances vertical current structure; decreases amplitude; increases eccentricity (in a positive anti-clockwise sense) and advances phase. These trends are similar to those shown for increasing bottom friction but in the latter case, there is an additional reduction in the overall current amplitudes.

Enhanced (linearised) frictional coefficients, F, apply for secondary constituents factored by $3/2\ R_P / R_S$, where R_S is the current amplitude for this secondary constituent and R_P is the amplitude for the predominant constituent. There is also enhanced influence of the friction term at latitudes close to the inertial frequency, i.e. for the principal semi-diurnal lunar constituent, M_2, $\sin^{-1}(24/2 / 12.42) \sim 75^0$.

A.4.4 Wind driven currents

The vertical variation of wind-driven currents can be described in the form of an Ekman spiral:

$$R(z) = \frac{\tau_w}{\rho E b e^{bH}} \{ e^{bz} + \frac{Eb}{F} - 1 \}$$

where $b^2 = i (\Omega/E)$ and Ω is the Coriolis coefficient.

In deeper water ($bD >> 1$, i.e. $D >> (E/\Omega)^{1/2}$) the first term predominates and

$$R_{z=H} = \frac{-\tau_w i^{1/2}}{\rho(\Omega E)^{1/2}}$$

i.e. a surface current of magnitude dependent on latitude and veering at 45° clockwise to the wind stress.

In shallow water, the second term predominates and

$$R = \frac{\tau_w e^{-bD}}{\rho F}$$

i.e. a current of magnitude dependent on the bed friction coefficient and aligned with the wind.

Steady-state surface currents are typically 1 or 2 per cent of wind speed, increasing in deeper water both in magnitude and veering toward the theoretical deep water values of 45° to the right of the wind. The observed veering ranges from 3^0 to 35^0 (clockwise).

A.4.5 River flow and well-mixed density gradient components

Analytical solutions provide estimates for residual flow components associated with:

i. a river flow, Q,

ii. a wind stress, τ_w and

iii. a well-mixed longitudinal density gradient, $\partial\rho/\partial x$.

The relative magnitudes of each of these components are defined in terms of dimensionless parameters and the residual current profiles (a), (b) and (c) are shown in Figure A.6 (overleaf).

The eddy viscosity coefficient E is assumed to be constant and given by

$$E = f\, U^* H$$

where U* is the depth-mean tidal current amplitude and H is total water depth (friction factor, f ≈ 0.0025).

Introducing, in well-mixed estuaries, the assumption of a (temporally and vertically) constant relative axial density gradient, S_x ($S_x = (1/\rho)(\partial\rho/\partial x)$), with density linearly proportional to salinity.

Figure A.6 (overleaf) shows the residual current profiles pertaining to river flow, wind forcing and mixed saline intrusion. Table A.2 (overleaf) summarises these results showing corresponding values at the surface and bed along with related gradients in surface elevation.

To interpret the magnitudes of these residual flow components, we introduce the depth-averaged equation of motion for steady state residual flows:

$$\frac{\partial\zeta}{\partial x} + \frac{H}{2\rho}\frac{\partial\rho}{\partial x} - \frac{\tau_W}{\rho g H} + \frac{4}{\pi}\frac{f\, U^* U_0}{gH} = 0$$

Then introducing the dimensionless parameters (shown in Figure A.6, overleaf):

$$S = H\frac{\partial\rho}{\rho\partial X}, \qquad W = \frac{\tau_W}{\rho g H}, \qquad F = \frac{f\, U^* U_0}{gH}$$

The forcing terms associated with density, wind and bed friction are in the ratio:

$$\frac{S}{2} : W : \frac{4}{\pi}F$$

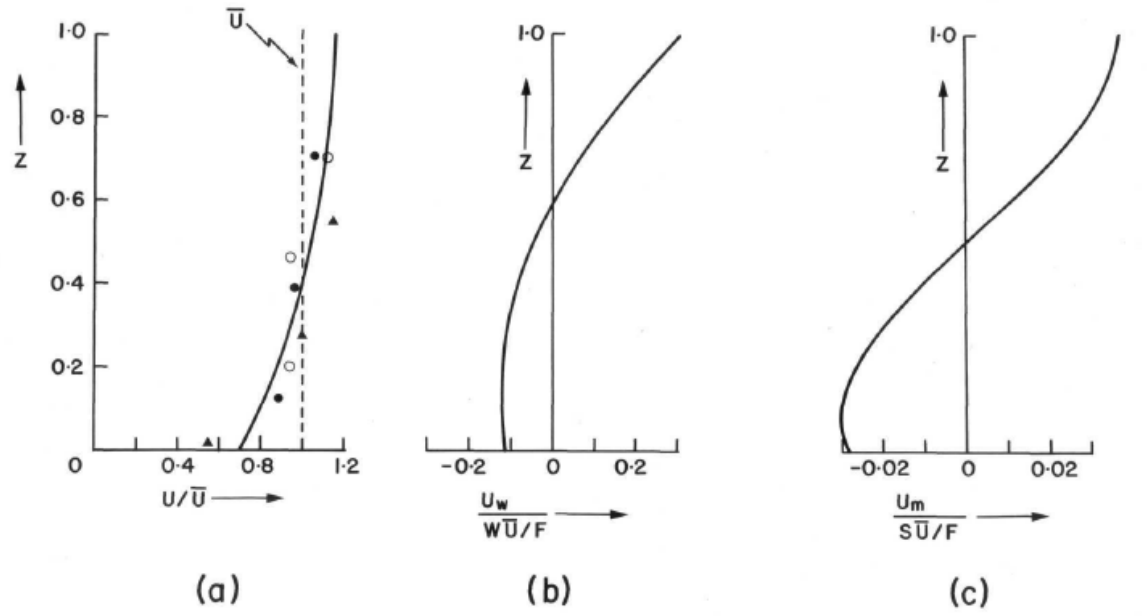

Figure A.6 Vertical structure for riverine (a), wind-driven (b) and density induced residual currents (c) after Prandle (1985).

From Table A.2, the density forcing term, S/2 is balanced by a surface gradient, 0.46 S with the remaining component driving a residual circulation of 0.036 SU_0/F (seawards) at the surface and 0.029 SU_0/F (landwards) at the bed. Similarly the wind stress term, W is counteracted by a surface gradient 1.15 W, with the 'excess' balance driving a circulation of 0.31 WU_0/F at the surface and 0.12 WU_0/F at the bed.

Clearly wind forcing is more effective in producing a residual circulation than longitudinal density gradients and both 'forcings' influence elevations to a greater extent than currents. Thus, for steady-state conditions, both wind and density forcing are mainly balanced by surface gradients, with only a small fraction of the forcing effective in maintaining a vertical circulation.

Table A.2 Residual surface gradients and current components at the surface and bed, after Prandle (1985).

	Surface gradient	Surface velocity	Bed velocity
(a) River flow, $Q=U_0D$	-0.89 F	1.14 U_0	0.70 U_0
(b) Wind stress, τ_W, no net flow	1.15 W	0.31 (W/F) U_0	-0.12 (W/F) U_0
(c) Mixed density gradient	-0.46 S	0.036 (S/F) U_0	-0.026 (S/F) U_0
(d) Stratified 'wedge' lower-layer depth, dH	-1.56 $F/(1-d)^2$	1.26 $U_0/(1-d)^2$	-0.18 $U_0/(1-d)^2$

Appendix A.5 Salinity intrusion

This section describes the lengths of saline intrusion, together with the amount of time taken for the estuary to be flushed, and the axial location of saline intrusion.

A.5.1 Length of saline intrusion and flushing times

Prandle (1985) derived the following approximation for the length of saline intrusion in

i. a well-mixed prismatic channel

$$L_I = \frac{0.005\, D_0^{\,2}}{f\, U\, U_0}$$

ii. a stratified saline wedge

$$L_I = \frac{0.07 D_0^{\,2}}{f\, U U_0}$$

based on the equations shown in A4.5 and assuming the excess density of seawater $\Delta\rho/\rho \sim 0.027$ and an axial salinity gradient $S_x = 0.027 / L_I$

Using the assumption that the riverine component of velocity in the saline intrusion region is approximately 1 cm s^{-1}, Figure A.7 illustrates typical values of the lengths of saline intrusion.

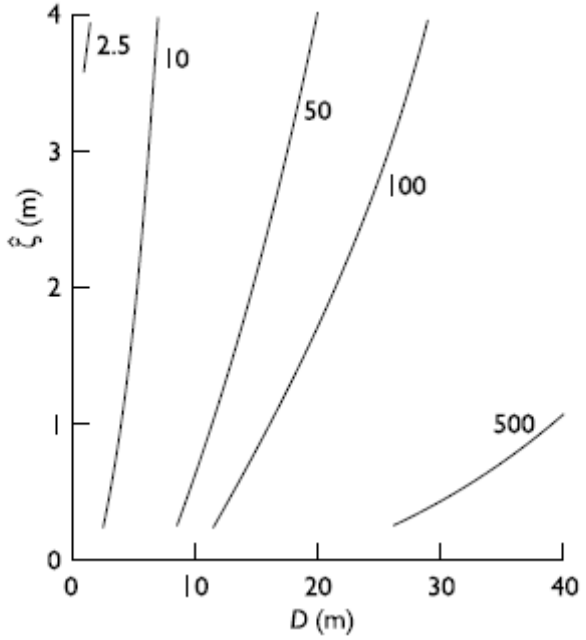

Figure A.7 Saline intrusion length, L_I (km) after Prandle (2004). Values scale by $0.01/U_0$ (m s^{-1}). ς, on the y-axis, represents tidal amplitude, Z.

A.5.2 Axial location of saline intrusion

An additional factor, which must be incorporated in funnel-shaped estuaries, is axial migration of the intrusion. This introduces a complex inter-dependency between the

length and location of the intrusion. Analysis of observations suggests that this axial migration adjusts to enable mixing to occur as far seawards as is consistent with containing the mixing within the estuary.

Prandle (2004) derived the solution for the proportional length, x_i, of the centre of intrusion from the mouth:

$$x_i^2 = \frac{333 \tan\alpha \, Q}{D_0^{5/2}}$$

corresponding to $l_i = L_I/L = 2/3x_i$

assuming $Q = U_0 D_i^2 / \tan\alpha$ where $\tan\alpha$ is the side slope of the triangular cross-section.

For a synchronous estuary, depths and breadths vary with axial length raised to a power of 0.8, hence depth, D_i at x_i is $D_0 x_i^{0.8}$ (D_0 depth at the mouth, x=1), giving a residual velocity U_0 at the centre of the intrusion:

$$U_0 = D_i^{1/2} / 333 \quad m\,s^{-1}$$

This expression yields values of U_0 = 0.006 m s^{-1} for D = 4 m, 0.012 m s^{-1} for D = 16 m.

An interesting feature of the results for the axial location of saline intrusion and the expression for residual river flow current is their independence of both tidal amplitude and bed friction coefficient (although there is an implicit requirement that tidal amplitude is sufficient to maintain partially mixed conditions).

Uncles *et al*. (2002) illustrate the dependency between saline intrusion, tidal range and flushing times.

Appendix A.6 Stratification

Reviewing indicators for estuarine stratification, Prandle (2009) emphasised that the ratio between the velocity component of the river flow, U_0, and the tidal current amplitude, U, (U_0/U) is the common key indicator of stratification. Calculations of values of this ratio, corresponding to the boundary between 'mixed' and 'stratified' conditions were obtained from:

i. a Flow Ratio, $F_R = U_0 \pi / U = 0.1$;

ii. a Richardson No., Ri = 0.25;

iii. a balance between gain in potential energy and tidal dissipation and

iv. observations of stratification.

All four approaches indicate values of U_0 close to 1 cm s^{-1} in the intrusion zone of 'mixed' estuaries (Figure A.8, overleaf). This indicator confirms that stratification generally increases with larger river flow, narrower breadths and weaker tidal currents. However, the apparent indication that stratification increases with shallower water is counteracted by reduced tidal current shear nearer the surface in deep water and the related reduced role of tidal straining (Figure A.5, page 43).

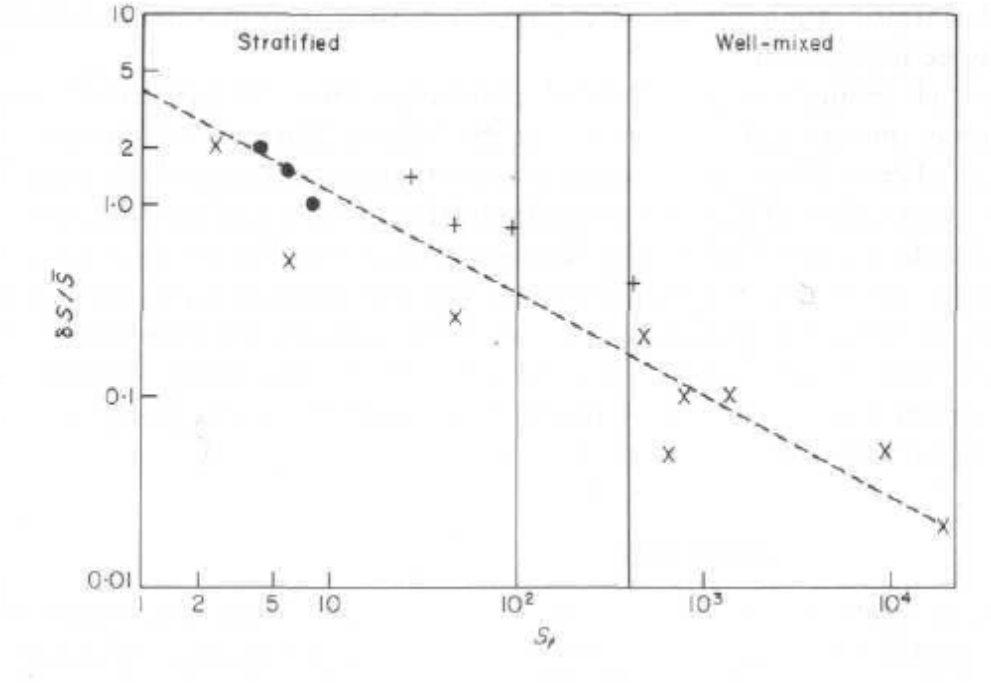

Figure A.8 Stratification δs/s versus stratification number, $S_T = 0.017\ \varepsilon\ (U/U_0)^2$.

Notes: • - Rigter (1973) flume tests
+ - Waterways Experimental Station, Vicksbury, Mississippi (WES) flume tests
x - observations from Prandle (1985).
δs/s salinity difference between bed and surface as a fraction of depth-mean value, other terms are defined in Section A6.1, after Prandle (2009)

A.6.1 Stratification number

Ippen (1966) demonstrated that vertical mixing could be related to the balance between turbulence associated with the rate of dissipation of tidal energy by bed stress ($G= \varepsilon(4/3\pi)f\rho U^3L_I$) and the energy required to increase the potential energy level by vertical mixing ($J= ½\ \Delta\rho\ g\ D^2U_0$).

The effectiveness of mixing, ε, is defined by Simpson and Bowers (1981) as the ratio of work done by mixing to that by tidal friction at the bed. Values of ε range from less than 0.001 in well-mixed conditions, up to 0.015 in more stratified conditions, with a typical value of 0.004 (less than 1 per cent of the energy involved in tidal dissipation is effective in promoting vertical mixing). Thus, a modified Stratification Number is defined as:

$$S_T' = S_T\varepsilon = \frac{\varepsilon G}{J} = 0.85\frac{\varepsilon f UL_I}{\frac{\Delta\rho}{\rho}gD^2U_0} = 0.017\varepsilon\left(\frac{U}{U_0}\right)^2$$

Thus the Stratification Number extends the concept of the Simpson-Hunter criterion (D/U^3), shown in Figure A.9 (overleaf), to balance net mixing of fresh water input over the saline intrusion length. Prandle (1985) showed that estuaries change from mixed to stratified as the Stratification Number decreases from above 400 to below 100 as shown in Figure A.8. Adopting the limit S_T=250, then for ε = 0.004, the boundary corresponds to S_T' = 1, δs/s = 0.25 and U_0 < 0.01 U.

A.6.2 Stratification levels in Synchronous Estuaries

The Simpson and Hunter (1974) stratification criterion, $D/U^3 > 50\ m^{-2}\ s^3$, for stratification to persist is shown in Figure A.9. This indicates that estuaries with tidal elevation amplitudes Z > 1 m will generally be mixed.

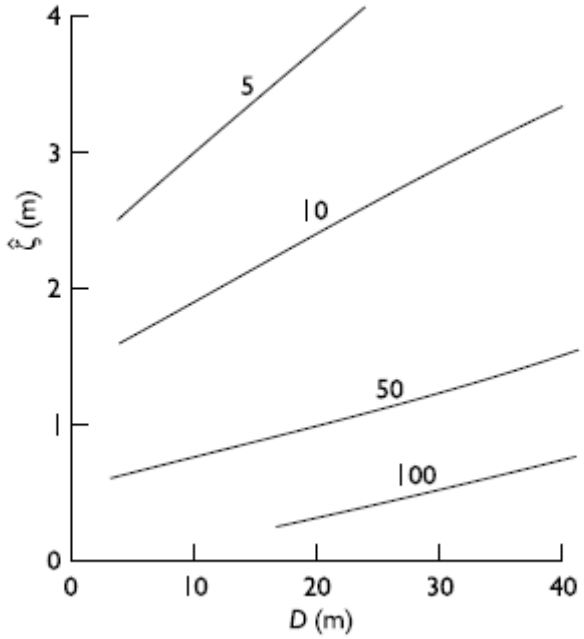

Figure A.9 Simpson-Hunter stratification parameter D/U^3 ($m^{-2}\ s^3$). ς on the y-axis represents tidal elevation, Z, after Prandle (2004).

A.6.3 Estuarine flushing times

For a prismatic channel, the estuarine flushing time, T_F, can be approximated by the time taken to replace half of the fresh water in the intrusion zone by river flow, i.e.

$$T_F = \frac{0.5(L_I / 2)}{U_0}$$

Balls (1994) indicates observed values of flushing times in UK estuaries. For typical values of T_F = 2 to 10 days and intrusion lengths, L_I = 12.5 to 100 km this equation requires U_0 varying from 1.5 to 3cm s^{-1}.

Appendix A.7 The seasonal temperature cycle

A generalised theory, outlined by Prandle (1998), describes the annual temperature cycle in estuaries and adjacent seas. A sinusoidal approximation to the annual solar heating component, S, is assumed and the surface loss term is expressed as a constant, k, times the temperature difference between air and sea (T_a - T_s). For vertically-mixed conditions, analytical solutions show that in shallow water the water temperature follows closely that of the ambient air temperature with limited separate effect of solar heating. Conversely, in deep water, the water surface temperature variations will be reduced relative to those of the ambient air. Providing such deep

water remains mixed vertically, the seasonal variation will be inversely proportional to depth and maximum temperatures will occur up to three months after the maximum of solar heating, i.e. as late as September in the northern hemisphere. The annual mean water temperature will exceed the annual mean air temperature by the annual mean of the solar heating component, S, divided by the surface exchange coefficient, k. A numerical model was used to derive generalised expressions for the mean and amplitude of both air and water surface temperatures, as functions of latitude, depth and tidal current speed.

Water density can be approximated by:

$$\rho = 1000 + 0.7S - 0.2\,T \ (\text{Kg m}^{-3})$$

where S is salinity in ‰ and T is temperature in ^{0}C. Thus stratification at the demarcation limit, $\delta S \sim 0.25$ ‰ (Section A.6.1) is equivalent to a surface-to-bed temperature difference of 0.875 ^{0}C.

Density stratification associated with heat exchange at the water surface may be significant when the (bed) frictional boundary layer does not extend through the whole depth. This is generally confined to the deepest, micro-tidal estuaries and, hence is generally a second-order effect in UK estuaries.

Seasonal temperatures vary with:

i. the level of solar heating (i.e. latitude);

ii. ambient air temperature;

iii. wind speed (strongly controlling the rate of air-sea heat exchange);

iv. water depth; and

v. the degree of vertical stirring.

The fundamental simplifications introduced are:

i. approximation of the annual solar heat input by a mean value plus a sinusoidal term: $S_0 - S^* \cos \omega t$;

ii. representation of the heat losses by a term $k(T_s - T_a)$ where T_s is the water surface temperature, T_a the air temperature and k a constant 'exchange' coefficient;

iii. assumption of a localised equilibrium i.e. neglect of horizontal components of advection and dispersion;

iv. representation of vertical mixing processes by an eddy dispersion coefficient encompassing the effects of vertical mixing processes by both vertical advection and dispersion.

Mean sea-surface temperature :

$$\bar{T}s = \bar{T}a + \frac{S_0}{k}$$

and for the seasonal cycle,

$$\hat{T}s \cos(\omega t - g_s - B) = \frac{S^* \cos \omega t + k\hat{T}a \cos(\omega t - g_a)}{(k^2 + \alpha^2 D^2 \omega^2)^{1/2}}$$

where B = arctan ($-\alpha D\omega$, k), and α is the thermal capacity of water.

Figure A.10 shows the values of $\hat{T}_s / \hat{T}_a$ for a range of values of $\hat{T}_a$ and D. These results correspond to solar heat input $S_0 = S^* = 100$ W m^{-2} and k = 50 W m^{-2} $^oC^{-1}$ with phase lag of air temperatures relative to solar heating $g_a = 30°$. These results are essentially similar for $0° < g_a < 90°$ and for either S* or k changed by a factor of 2.

As shown in Figure A.10, four quadrants can be distinguished, differentiating shallow and deep water and small and large $\hat{T}_a$.

In Q1, D « k/aω and $\hat{T}_a$ >> S*/k, thus $\hat{T}_s \rightarrow \hat{T}_a$ and $g_s \rightarrow g_a$.

In Q2, D » k/aω and $\hat{T}_a$ >> S*/k, thus $\hat{T}_s \rightarrow \hat{T}_a$ k/Dαω and $g_s \rightarrow g_a + 90°$.

In Q3, D « k/aω and $\hat{T}_a$ << S*k, thus $\hat{T}_s \rightarrow$ S*/k and $g_s \rightarrow 0^0$.

In Q4, D » k/aω and $\hat{T}_a$ << S*/k, thus $\hat{T}_s \rightarrow$ S*/Dαω and $g_s \rightarrow 90^0$.

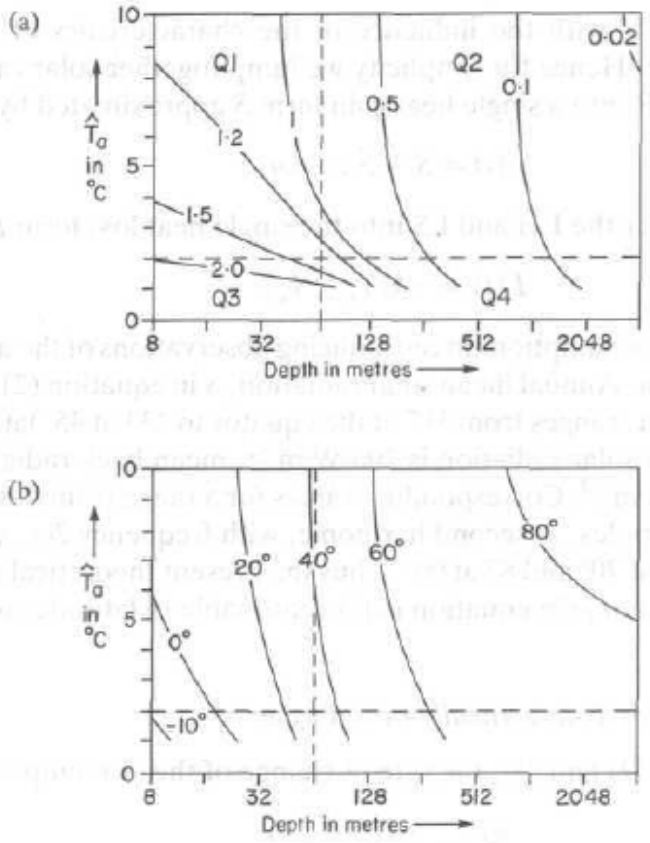

Figure A.10 The annual temperature cycle in well-mixed waters as a function of seasonal amplitude of air temperature and water depth, after Prandle (2009).

(a) Ratio of seasonal amplitudes of sea to air temperatures, $\hat{T}_s/\hat{T}_a$, with quadrants 1-4 marked.
(b) Phase lag in days between peaks of air and sea temperatures

Results correspond to $S_0 = S^* = 100W\ m^{-2}, k = 50W\ m^{-2}\ ^oC^{-1}, g_a = 30^o$

A.7.1 Global expressions for mean and seasonal cycles of sea surface and ambient air

Prandle (1998) formulated a coupled air-sea thermal exchange model to reproduce the annual temperature cycle of the sea surface and ambient air yielding the following expressions:

$$\overline{T}_s = 40\cos\lambda - 12.5$$

$$\overline{T}_a = 35\cos\lambda - 10.0$$

$$\hat{T}_s = 0.080\,\lambda / (1 - \exp(-D/50)) \quad \text{for } U < 0.2\ \text{m s}^{-1}$$

$$\hat{T}_s = 0.064\,\lambda / (1 - \exp(-D/50)) \quad \text{for } U > 0.2\ \text{m s}^{-1}$$

$$\hat{T}_a = 0.086\,\lambda / (1 - \exp(-D/50)) \quad \text{for } U < 0.2\ \text{m s}^{-1}$$

$$\hat{T}_a = 0.067\,\lambda / (1 - \exp(-D/50)) \quad \text{for } U > 0.2\ \text{m s}^{-1}$$

Where temperatures are in degrees Centigrade, depths, D, in metres, U is the tidal current amplitude. $\overline{T}_s$ is the mean sea surface temperature, $\overline{T}_a$ is the mean air temperature, $\hat{T}_s$ is the seasonal amplitude of sea surface temperature, and $\hat{T}_a$ is the seasonal amplitude of air temperature.

Appendix A.8 Sediment regimes

The predominant influences on sediment regimes in estuaries are tidal and storm currents, enhanced in exposed shallow water by wave stirring. For all but the coarsest grain sediment, several cycles of ebb and flood movement may occur between erosion and subsequent deposition. Hence, deposition can occur over a wide region beyond the source. Since time in suspension increases for finer, slower settling material, such mechanisms may contribute to a residue of fine materials on tidal flats and to trapping of coarser material in deeper channels.

Bed roughness strongly influences erosion and deposition rates and is largely determined by the composition (fine to coarse) and form (ripples, waves) of the bed. Sediment processes are complicated by the continuous dynamical feedback between this roughness and the overlying vertical structure of tidal currents and waves and their associated turbulence regimes. Bed roughness can change significantly over both the ebb to flood and neap to spring tidal cycles. Associated erosion and deposition rates may then vary considerably over these cycles and dramatically over seasons, or in the course of a major event.

Conventionally, erosion is assumed to occur when the bed shear forces exceed the resistance of the bed sediment, characterised by a 'critical shear stress for erosion'. In nature, this threshold depends on particle size distribution and both chemical and biological modulation, including effects of bioturbation and biological binding. Bioturbation of the top metre or so of surface sediment may significantly reduce erosion thresholds. Conversely, (surface) biological binding can have the opposite effect, especially in inter-tidal zones (Romano *et al.,* 2003). Erosion depends, not only on the prevailing physical, chemical and biological composition, but on corresponding conditions at (and since) the time of deposition.

Subsequent settlement of particles depends on their size, density and the ambient regime of turbulence and chemical forces in the surrounding water. Sedimentation is usually assumed to occur when quiescent dynamical conditions are below some

threshold for erosion at a rate equal to the product of the near-bed concentration and the settling velocity (Van Rijn, 1993).

Suspended sediments exhibit extreme variability, with particle diameters ranging from fine to coarse; from clay <4 μm, silt < 60 μm, sand < 1000 μm to gravels. In higher concentrations, silt and clay tend to flocculate into multiple assemblages, which can both settle more rapidly and inhibit the upward flux of turbulent energy from the sea bed. Moreover, once deposited, consolidation of cohesive material can radically change re-erosion rates. Only a few percent of mud content may strongly influence a seemingly cohesionless sandy bed (Winterwerp and van Kesteren, 2004).

A.8.1 Scaling parameters

By assuming that eddy diffusivity, K_z, and eddy viscosity, E can be approximated by

$$K_z = E = fUD,$$

where f is the bed friction coefficient, U the tidal current amplitude, and D depth, analytical solutions indicate how the essential scaling of sediment motion is synthesised in the dimensionless parameter

$$E/W_S D$$

where W_S is the sediment fall-velocity. Turbulent diffusion, parameterized by the coefficient, E, promotes the suspension of particles by random vertical oscillations, whereas the fall velocity, W_S, represents steady advective settlement. The time taken for a particle to mix vertically by dispersion is D^2/E whereas settlement by vertical advection occurs within D/ W_S. Thus the ratio of E: W_S D reflects the relative times of deposition by advective settlement to diffusive vertical excursions. The significance of this parameter is illustrated by the simulated time-series of suspended sediment shown in Figure A11 after Prandle (1997).

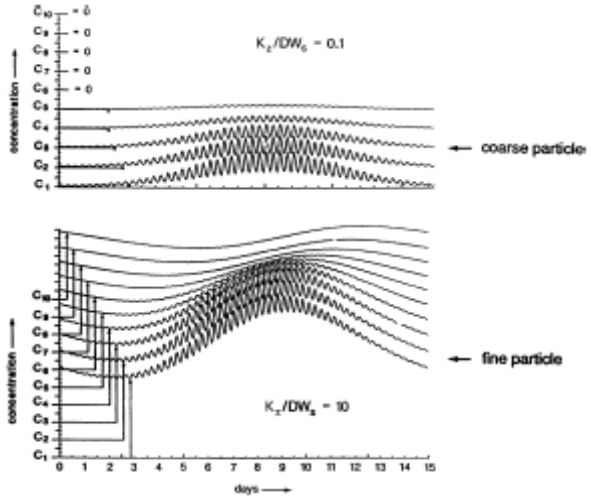

Figure A.11 Model simulations of suspended particulate matter (SPM) over a spring-neap tidal cycle, after Prandle (2009).

Notes: C1, C2….C10 are concentrations at fractional heights z½ = 0.15 to 0.95 after Prandle (2009). Top: Kz /DWS = 0.1; Bottom: Kz /DWs = 10

A.8.2 Deposition

The rate of deposition is expressed by a suspended sediment concentration, $C\, e^{-\alpha t}$, where $\alpha = 0.693/t_{50}$ represents the exponential settling rate in terms of a half-life in suspension t_{50}.

$$\text{For } E << W_S D \qquad \alpha = 0.7\, W_S^2 / E$$

deposition is by advective settlement. Fractional rate of deposition is determined by $(l/2)[(W_S^2 t)/E]^{1/2}$, that is, 10 per cent after $0.04E/W_S^2$, 50 per cent after E/W_S^2 and 90 per cent after $3.2E/W^2$.

$$\text{For } E >> W_S D \qquad \alpha = 0.1E/D^2$$

Deposition is independent of Ws but dependent on both the magnitude of the vertical dispersion coefficient and on the precise near-bed conditions.

As E approximates W_S, D, the mean time in suspension approaches a maximum and hence, both mean concentration and net transport will increase. This condition occurs for $W_S \sim 1 mms^{-1}$, i.e. particle diameter, d ~ 30µm.

A.8.3 Vertical profile of suspended sediments

A continuous functional description of the vertical profiles of suspended sediment concentrations was calculated by numerical fitting of a profile $e^{-\beta z}$, (where z is the fractional height above the bed), the following expression for β was derived:

$$\beta = [\, 0.91 \log_{10} (6.3\, E / W_S\, D)\,]^{-1.7} - 1$$

Complete vertical mixing is achieved for $E/W_sD > 2$, and "bed load" only occurs for $K/W_sD < 0.1$. Approximating settling velocities by:

- sand, $W_S = 10^{-2}$ m s^{-1}, concentrated near the bed;
- silt $W_S = 10^{-4}$ m s^{-1}, shows significant vertical structure, and
- clay by $W_S = 10^{-6}$ m s^{-1}, well mixed vertically.

A.8.4 Suspended Particulate Matter (SPM) time series for continuous tidal cycles

By integrating the analytical solutions for Suspended Particulate Matter (SPM) concentrations over successive tidal cycles, the spectra of suspended sediments is calculated. This is proportional to the ratio of the exponential settlement rate, α, to the frequency of the erosional tidal currents, ω.

The concentration, C(t), associated with erosion varying sinusoidally at a rate of cos ωt subject to an exponential decay rate, αC, involves integration over all preceding time, t', from ∞ to t, that is

$$C(t) = \int_{-\infty}^{t} \cos\omega t' e^{-\alpha(t-t')}\, dt' = \frac{\alpha\cos\omega t + \omega\sin\omega t}{\alpha^2 + \omega^2}$$

Hence the concentration, C_ω, for any erosional constituent, ω, is given by:

$$C_\omega = \frac{\gamma f \rho [U^N]_\omega}{D(\omega^2 + \alpha^2)^{1/2}}$$

where $[U^N]_\omega$ is the erosional amplitude at frequency ω.

Thus, erosion generated at each tidal constituents is modulated by an exponential decay rate that involves an amplitude reduction by $(\alpha^2 + \omega^2)^{-1/2}$ and a phase-lag of arctan (ω/α).

For $\alpha > 10\omega$, the suspended sediment tidal amplitude is proportional to $1/\alpha$ with zero phase lag of SPM relative to current. Whereas for $\omega >$ l0 α, the amplitude is proportional to tidal period $(1/\omega)$ with a 90° phase lag.

For sand $10^{-2} > \alpha > 10^{-3}$ s^{-1} and 1m < t_{50} < 10m, hence the former condition applies and the amplitude response at all tidal frequencies is much reduced.

For silt and clay $10^{-4} > \alpha > 10^{-6}$ s^{-1} and 2h< t_{50} < 200h. Since the major tidal constituents lie in the range $\omega \geq 10^{-4}$ s^{-1}, the cyclical amplitude response is relatively independent of α but proportional to tidal period, resulting in an enhancement of longer period constituents. Wherever there is a plentiful supply of erodible sediment of a wide size distribution, the resulting suspended sediment time series away from the immediate near-bed area is likely to be dominated by silt-clay.

In the absence of significant residual currents, the erosional time series for a semi diurnal lunar constituent (M2), a semi-diurnal solar constituent (S2) dominated tidal regime will show pronounced components at the quarter diurnal constituents, M4 and MS4, the 14 day lunar and solar interaction, MSf, and the infinite residual time-averaged component, Z0 frequencies.

Appendix A.9 Morphology

Pethick (1984) provides a useful introduction to coastal morphology.

A.9.1 Estuarine depths as a function of river flow

Prandle (2004) showed that the best agreement between observations and theory for the landward limits of saline intrusion occurred when the landward limit of saline intrusion was at a minimum. Adopting this latter result as a criterion to determine the position, x_i where the saline intrusion will be centred, requires

$$x_i^2 = 333\frac{Q\tan\alpha}{D_0^{5/2}}$$

where $Q = U_0 D_i^2 / \tan\alpha$; tan α is the side slope of the triangular cross-section.

Noting that, for a synchronous estuary, the depth, D_i, at x_i is $D_o\, x_i^{0.8}$, we obtain:

$$U_o = D_i^{½} / 333 \text{ m s}^{-1}$$

For depths ranging from a few metres to tens of metres, it yields values of U_0 close to 1 cm s^{-1}, as commonly observed. This result can be extended to provide an expression for the depth at the mouth:

$$D_0 = 12.8\,(Q\tan\alpha)^{0.4}$$

The estuarine length, L, is then given by

$$L = 2980\left(\frac{Q\tan\alpha}{f\,Z}\right)^{1/2}$$

The results for U_0 and D_0 are independent of both the friction coefficient, f, and the tidal amplitude, Z. O'Brien (1969) noted that the minimum flow area of tidal inlets was

effectively independent of the type of bed material. However, the two expressions for estuarine length are dependent on the inverse square root of both f and Z.

A.9.2 Observed vs. computed estuarine bathymetries

Examination of a range of UK estuaries indicated that in general, 0.02 > tan α > 0.002, hence

$$2.68\ Q^{0.4} > D_0 > 1.07\ Q^{0.4}$$

Figure A.12 (overleaf) shows results from both UK estuaries and a wider area (Prandle, 2004). For the steeper side slope, values for D_0 are: 2.7 m for Q = 1 $m^3\ s^{-1}$; 6.7 m for Q = 10 $m^3\ s^{-1}$; 16.9 m for Q = 100 $m^3\ s^{-1}$ and 42.4 for Q = 1000 $m^3\ s^{-1}$. Comparable figures for the smaller side slope are depths of 1.1, 2.7, 6.7 and 16.9 m. Figure A.12 shows that this envelope encompasses almost all of the observed estuarine co-ordinates of (Q,D).

Prandle (2004) suggested an Estuarine Morphological Zone bounded by tidal dynamics, salinity intrusion lengths and stratification

i. $L_l/L < 1$,

ii. $Ex/L < 1$ and

iii. $D/U^{*3} < 50 m^{-2} s^3$

where the tidal excursion

$$E_x = (2/\pi)\ U^*\ P$$

Figure A.14 (page 59) illustrates this Zone alongside the distribution of UK estuaries shown in Figure A.13 (overleaf).

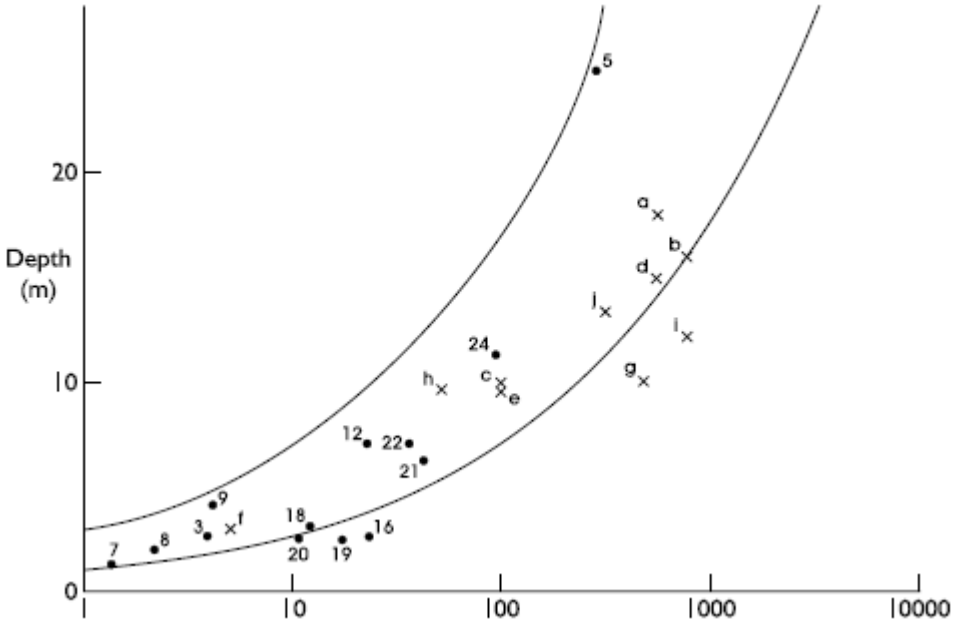

Figure A.12 Depth at the mouth as a function of river flow, Q ($m^3\ s^{-1}$).
Note: UK estuaries are labelled by numbers, others by letters, see Prandle (2004)

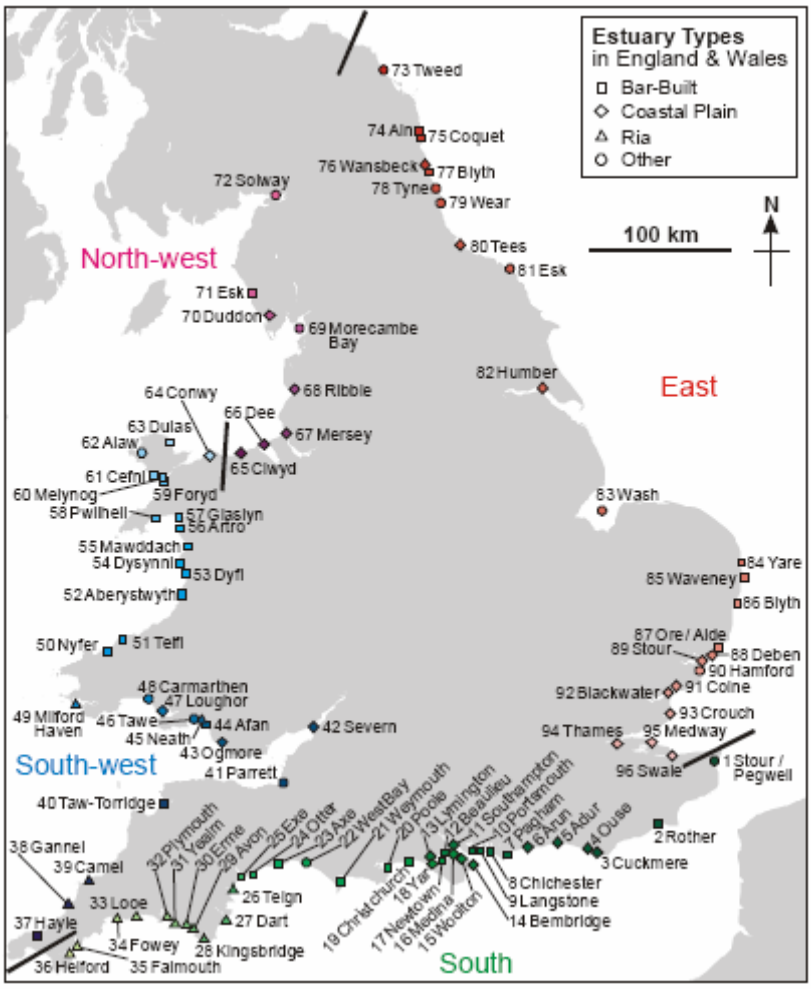

Figure A.13 Estuaries of England and Wales morphological types after Davidson and Buck (1997). Numbers correspond to the Futurecoast data set.

Appendix A.10Synchronous estuaries: sediment trapping and sorting

The ‘synchronous estuary’ solutions for tidal dynamics and salinity intrusion are extended to include erosion, suspension and deposition of sediments. Integrating all of these processes into an analytical emulator, as described by Prandle (2009), yields explicit expressions for concentrations and cross-sectional fluxes of sediments. This allows conditions consistent with zero net flux of sediments to be identified alongside their sensitivity to tidal range, particle size, bed friction coefficient and bathymetry. It is shown how the exchange of sediments switches from export towards import as the ratio of tidal amplitude to depth increases and as sediment size decreases. Thus, quantitative explanations are provided for the trapping, sorting and high concentrations of sediments in estuaries.

Suspended concentrations of fine sediments in tidal estuaries typically range from 100 to more than 1000 mg/l, whereas concentrations in shelf seas are invariably less than 10 mg/l. Moreover, observational and numerical modelling studies indicate only a small fraction of the net tidal flux of sediments is permanently deposited. By introducing a ‘synchronous estuary’ assumption, Section A.9 shows how estuarine

bathymetries are determined by the tidal elevation amplitude, Z, and river flow, Q, alongside the bed friction coefficient, f (a proxy representation of the alluvium).

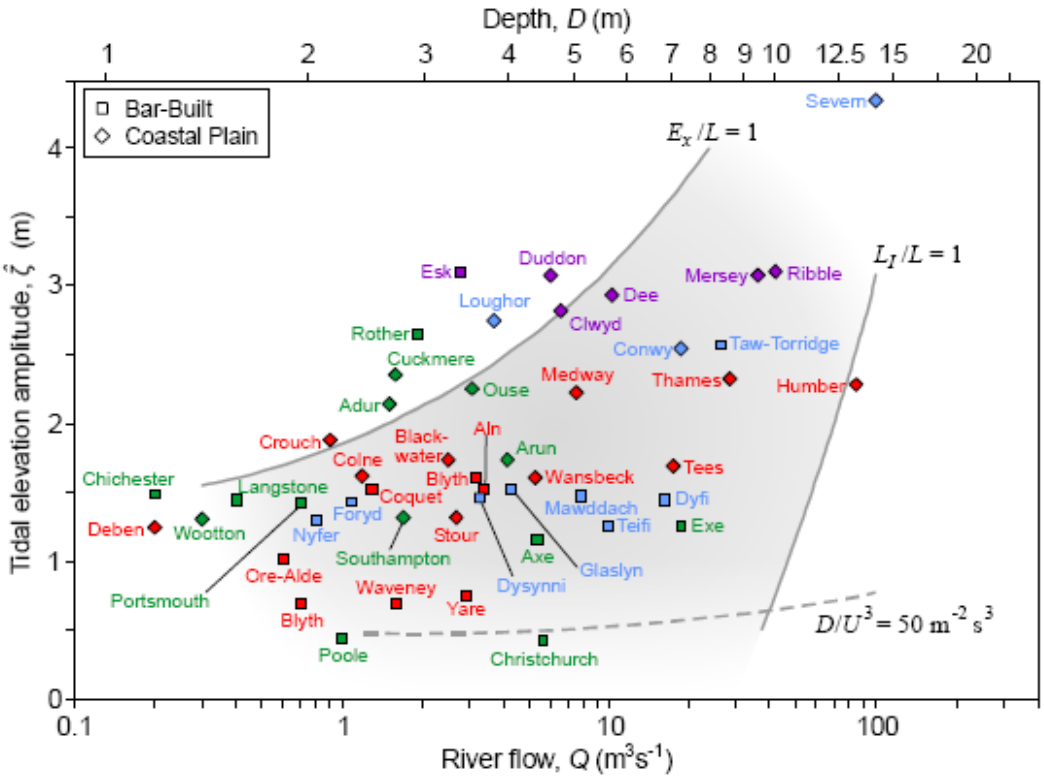

Figure A.14 Bathymetric zone after Prandle (2009).
Notes: Bounded by E_x <L, L_I < L and D/U^{*3} < 50 $m^2\ s^{-3}$
ς on the y-axis represents the tidal elevation amplitude, Z

A 10.1 Formulation of an Analytical Emulator

Postma (1967) first described the mechanisms responsible for estuarine trapping of fine sediments, namely gravitational circulation, non-linearities in the tidal dynamics, and delays between re-suspension and settlement. Postma noted that while estuaries may contain both coarse and fine material, it is the characteristics of the latter which generally predominate in determining bathymetry in conjunction with tidal amplitude, river flows, and sediment supplies. Delayed settlement is introduced by the adoption of exponential settling rates, with associated half-lives, t_{50}, as described in Section A.8.2.

Figure A.15 (overleaf) indicates how these processes are integrated within the emulator. The emulator is applicable within strongly tidal (hence mixed) funnel-shaped estuaries and incorporates processes that are pronounced in shallow estuaries with triangular cross sections. It provides clear illustrations of parameter dependencies and enables conditions of zero net sediment flux to be determined.

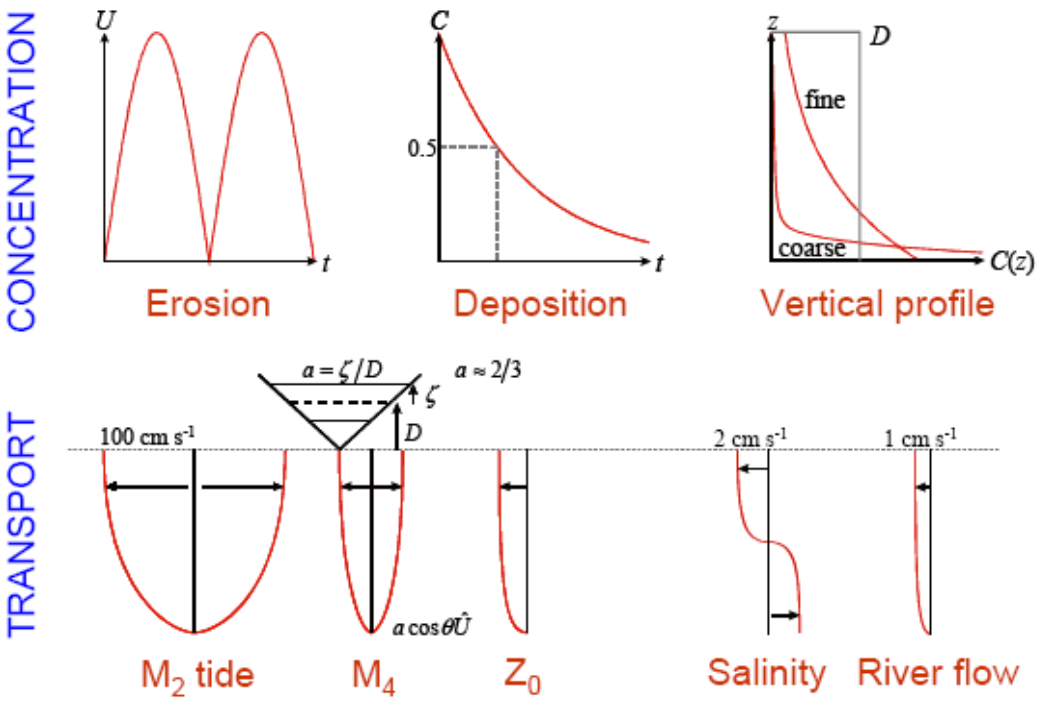

Figure A.15 Schematic of dynamical and sedimentary components integrated into the analytical emulator, after Prandle (2009).

A.10.2 Import or export of sediments

Separate components from tidal non-linearities, involving cos θ and sin θ (where θ is the phase difference between tidal elevation amplitude, Z and current elevation amplitude, U) determine the balance between import and export of sediments. Combinations of θ and t_{50} corresponding to zero net flux of sediments can be determined. It is found that for zero net flux, $W_s \sim f U$, where W_s is the sediment fall velocity; f the bed friction coefficient, and U the current elevation amplitude. This latter relationship coincides with values of $K_Z / W_S D$ (the basic scaling parameter characterising suspended sediments, with D being the depth) in the range 0.1 to 2, i.e. close to conditions corresponding to maximum suspended sediment concentrations.

Figure A.16 (overleaf), after Lane and Prandle (2006) illustrates how the balance between net import or export varies for depths from 4 to 16 m; fall velocities of 0.0001, 0.001 and 0.01 m s^{-1} and tidal amplitudes from 1 to 4 m (representative of neap to spring tidal variations). Proceeding upstream from deep to shallow water, the balance between import of fine sediments and export of coarser ones becomes finer, i.e. selective 'sorting' and trapping. Likewise, more imports, extending to a coarser fraction, occur on spring than on neap tides.

However, as more fine sediments are trapped, the effective value of the bed friction coefficient, f, decreases, resulting in a tendency to increase estuarine length. The consequently more energetic dynamics will tend to increase depths and introduce coarser sediments. Hence some equilibrium will prevail, governed by the balance between the type and quantity of (marine) sediment supply.

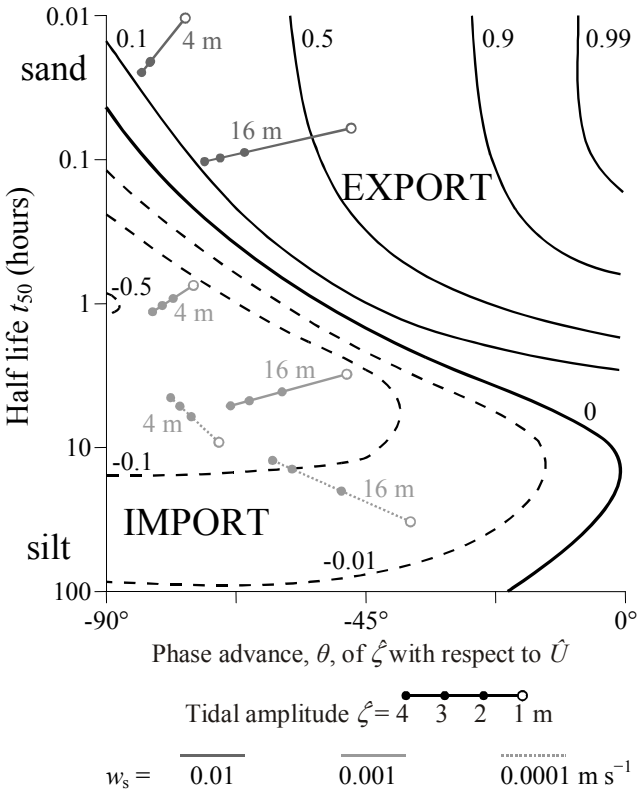

Figure A.16 Spring-neap variability in import vs. export of sediments as a f (t50,θ) after Lane and Prandle (2006).

Notes: Variability over elevation amplitude Z = 1, 2,3 and 4 m, fall velocities W_s = 0.0001, 0.001 and 0.01 m s^{-1} for depths, D= 4 and 16 m. Horizontal axis, ς, corresponds to the amplitude of tidal elevation Z.

A.10.3 Stable morphology

Within regions where tidal influences predominate, the ratio of sediment import (IM) to export (EX) is given by:

$$\frac{IM}{EX} = \frac{r}{3}\tan\theta = 0.37\left(\frac{f\,U}{W_S}\right)^2$$

where r = ω/α, with α, the exponential deposition rate; θ, the phase difference between tidal elevation, Z and tidal current, U; f, the bed friction coefficient and W_s, the sediment fall velocity.

Zero net flux then corresponds to:

$$W_S = 0.61\,f\,U \sim 0.0015\,U$$

The distribution for mean sediment concentration, $\overline{C}$, may be approximated by inserting this value of Ws

$$\overline{C} = \gamma\,\rho\,f\,U^2/D\alpha = \gamma\,\rho\,U\,(1+a^2)$$

A.10.4 Link to tidal energetics

Having shown that the balance of import to export of sediments depends directly on the phase lag,θ, between tidal elevation and current, we note the direct correspondence with net tidal energy dissipation (which is proportional to U cos θ). Thus we identify a relationship between the whole estuary tidal energy balance and localized cross-sectional sediment flux balance. Such relationships have been suggested previously by Bagnold (1963), and minimizing net tidal energy dissipation can be used as a stability condition in morphological models as per Pethick (1984).

Appendix A.11 Typological frameworks

A.11.1 Morphological types

Davidson and Buck (1997) provide the following descriptions of the three most common estuarine types in England and Wales:

- **Ria** estuaries have some features superficially in common with fjords and fjards, although they have not been shaped by glacial processes. Ria estuaries are drowned river valleys formed by tectonic subsidence of the land, a rise in sea level, or a combination of both. Sedimentation has not kept pace with inundation and the estuarine topography still resembles a river valley. Ria estuaries are relatively deep, with narrow well-defined channels that are substantially marine-influenced. They have no entrance sill or ice-scoured rock-bar and are shallower than fjords. The substratum is predominantly rocky but the sheltered parts of bays and inlets contain soft sediments. Elsewhere, secondary sedimentation masks the bedrock.

- **Coastal plain** estuaries were formed during the Holocene transgression by the flooding of pre-existing valleys in both glaciated and un-glaciated areas. Maximum depths in these inlets are generally less than 30 m and the central channel is often sinuous. The channels have a triangular cross-section, similar to that of terrestrial valleys and the cross-section usually has a large width-depth ratio. In outline coastal plain estuaries are often funnel-shaped, widening towards the mouth, which may be modified by spits. Unlike rias, coastal plain estuaries have extensive mudflats, sand flats and salt marshes. These estuaries are usually floored by varying thicknesses of recent sediments, often muddy in the upper reaches and becoming increasingly sandy towards the mouth. Coastal plain estuaries are generally restricted to temperate latitudes, where the amount of river-borne sediment is relatively small. River flow in large coastal plain estuaries is small in comparison with tidal prism volume, so salinity in much of the estuary is little reduced from that of sea water.

- **Bar built** estuaries also occur in part drowned river valleys that were incised during ice ages and subsequently inundated. They are distinguished by recent sedimentation that has kept pace with the inundation, such that they are sediment-filled and have developed a characteristic bar (or spit) across their mouths. The bar, or spit, usually forms where waves break on the beach. For a bar or spit to develop, tidal range must be small and large volumes of sediment available; consequently bar built estuaries are mostly associated with depositional coasts. Sediment sources vary, with some estuaries bars or spits developed from material carried down the coast by longshore drift, whilst others develop as shingle storm beaches made up chiefly of reworked offshore glacial deposits. Bar built estuaries are only a few metres deep

and often have extensive lagoons and shallow waterways just inside their mouths. Many naturally formed coastal lagoons have developed from an extreme form of bar built estuary in which the bar or spit has entirely, or almost entirely, closed off a bay or inlet.

Figures A.17 and A.18 (overleaf) taken from Prandle (2009) show observed lengths, L, and depths at the mouth, D_0, from 50 UK estuaries plotted as functions of (river flow, Q and tidal elevation amplitude, Z, i.e. the mean river flow and the M2 tidal amplitude at the mouth, where M2 is the semi-diurnal lunar constituent). The estuaries are restricted to those classified as either Bar-Built or Coastal Plain after Davidson and Buck (1997). Corresponding theoretical values, as per Prandle *et al*. (2005) for lengths, L and depths at the mouth, D_0 are shown for comparison.

Overall the observed values of depths and lengths are broadly consistent with the new dynamical theories. The smaller depths in Bar-Built estuaries are clearly demonstrated. By identifying estuaries where depths diverge significantly from the theory, estimates can be made of the much larger flows existent in their post-glaciation formation. Regional discrepancies can also be used for inferring coasts with scarce or plentiful supplies of sediment for infilling.

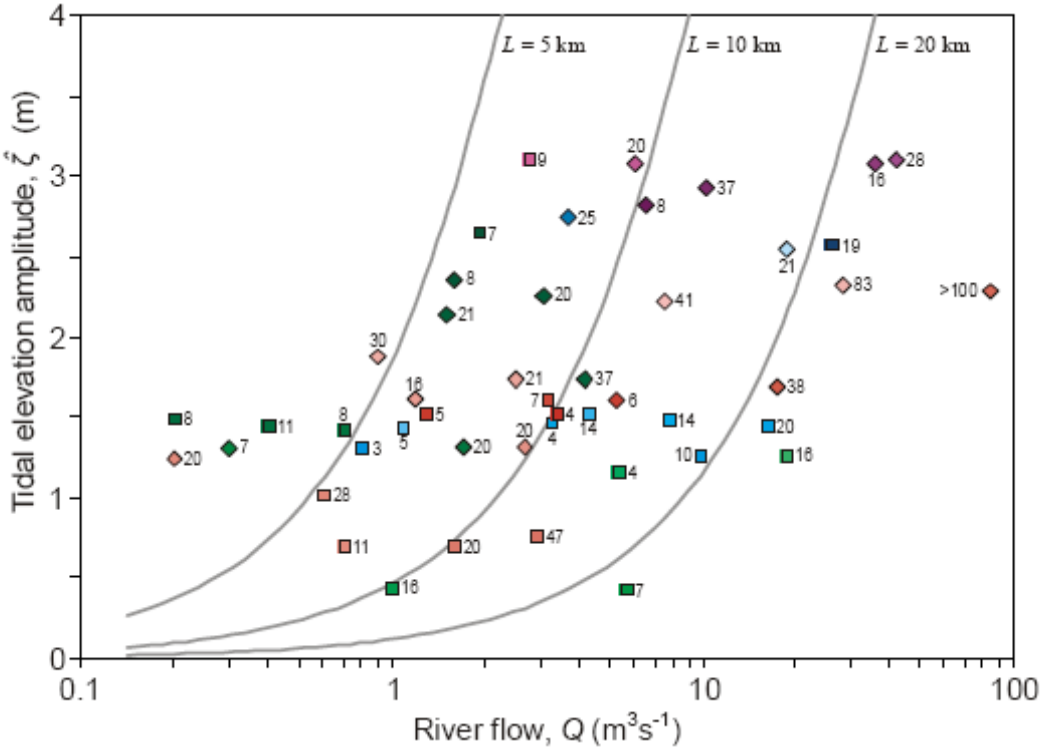

Figure A.17 Observed vs. theoretical estuarine lengths, L (km) as a function of river flow, Q and tidal elevation amplitude, Z, modified from Prandle *et al*. (2005) by permission of American Geophysical Union.

Notes: Contours show theoretical values for estuarine length, L
Observed data from estuaries shown in Figure A.13 (page 58)
Vertical axis, ς, corresponds to the amplitude of tidal elevation, Z.

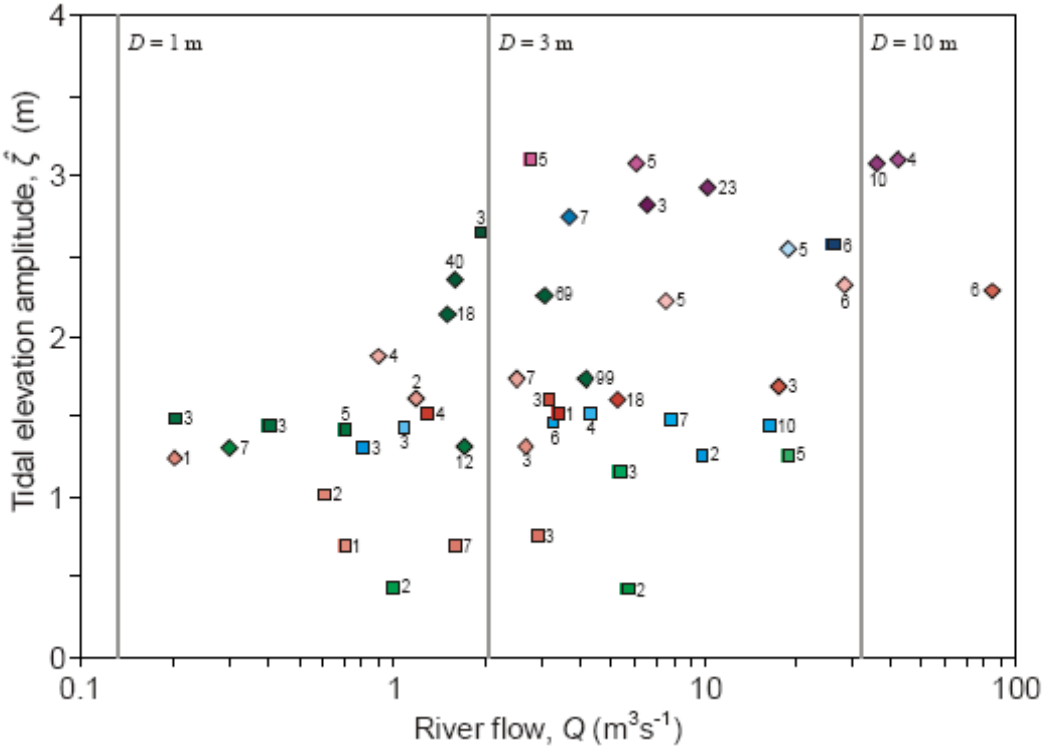

Figure A.18 Observed vs. theoretical estuarine depths at the mouth, D_0, as a function of river flow, Q, and tidal elevation amplitude, Z, modified from Prandle *et al*. (2005) by permission of American Geophysical Union.

Notes: Top axis shows theoretical values for D_M for side slope tan α=0.013
Observed data from estuaries shown in Figure A.13 (page 58).
Vertical axis, ς, corresponds to the amplitude of tidal elevation Z

Figure A.19 (overleaf), after Prandle *et al*. (2005) indicates typical values of:

i. values of effective fall velocities for morphological equilibria

ii. depth and time-averaged suspended sediment concentrations

iii. flushing times.

The observed results from Manning (2004) shown in Figure A.19 are representative of observed settlement of fine sediments in a wide range of European estuaries. These studies indicated that settling was primarily via the formation of micro and macro-flocs, close to the range suggested by the present theory.

The curves for sediment fall velocity, W_s, and suspended sediment concentration, C, align directly with those for tidal current amplitude, U (Figure A.2, page 40). This typology illustrates why many estuaries show high levels of fine suspended sediments. The results for sediment fall velocity, W_S, suggest a narrow range, typically between 1 and 3 mm s^{-1}.

Likewise, prevailing observed suspended sediment concentrations are in good agreement with theoretical values (Manning, 2004). Figure A.19 also shows loci of representative flushing times, T_F. For river-borne dissolved or suspended sediments, the indicated values generally lie between 2 and 10 days (for residual current U_0 = 1 cm s^{-1}). These values are consistent with the ranges indicated from observations by Balls, (1994) and Dyer (1997). Flushing times greater than the principal semi-diurnal tidal period, M2 (12.42h) provide valuable longer-term persistence of marine-derived

nutrients, while flushing times less than the 15-day spring-neap cycle yield effective flushing of contaminants. Hence, there might be some ecological advantage to the bathymetric envelope defined by these two flushing times.

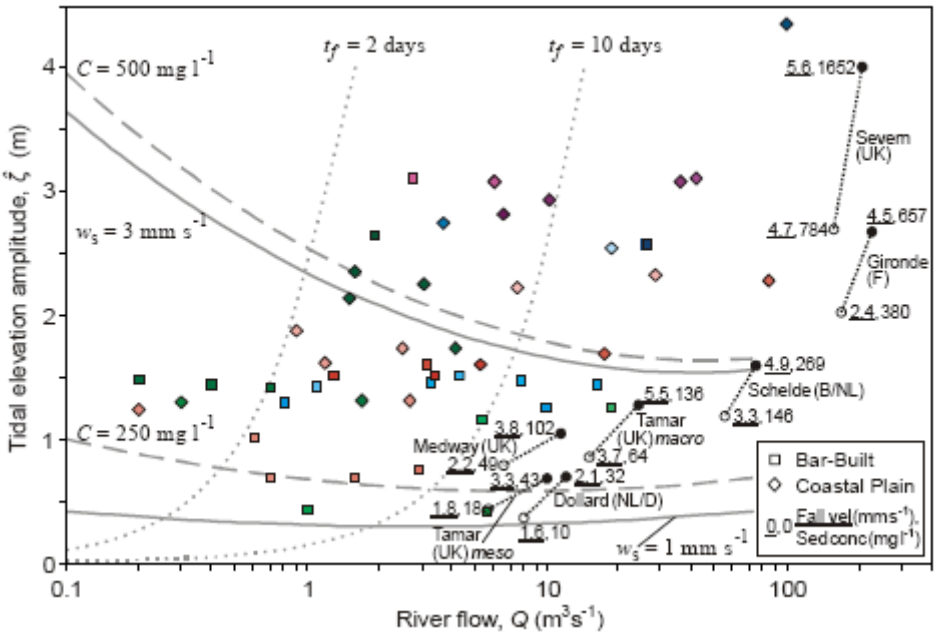

Figure A.19'Equilibrium' values of sediment concentrations, fall velocities and estuarine flushing times (Prandle *et al*. 2005, reproduced by permission of American Geophysical Union).

Notes: Observed vs. equilibrium theory for: sediment concentrations, C (dashed contours) and fall velocities, Ws (full contours).
Observed values for Ws and C in the Dollard, Gironde, Medway, Schelde, Severn and Tamar estuaries.
• spring tides; ° neap tides. Flushing times (t_f) from 2 to 10 days (dotted contours)
Vertical axis, ς, corresponds to the amplitude of tidal elevation Z.

Appendix B UK coastal forcing conditions

The descriptions of controlling processes in Appendix A determined a set of salient parameters of interest, namely: tides; surges; waves; mean sea level; temperature; salinity and sediment supply. Here we describe the nature, variability and sensitivities of these parameters.

Gravitational attraction and the related astronomical orbits of the Sun – moon – earth system determine ocean tidal amplitudes over millennia. Minor variations may occur at the coast associated with changes in water depth, bed roughness and stratification levels etc.

Solar radiation, modulated by atmospheric conditions, effectively determines most of the other parameters. Wind forcing directly determines waves and storm surges (with some influence of pressure gradients in deeper water) and strongly influences sea surface temperatures. Precipitation largely determines river flows and associated coastal variations in salinity. However, in all of these cases, complex relationships exist between the original atmospheric impact and the subsequent influence on each parameter.

Globally, mean sea levels are determined by air/water temperatures, leading to ice release and expanding ocean volumes. Rates of relative land movements, isostatic rebound and consolidation can produce local effects substantially in excess of these global changes.

Coastal gauges can directly measure tides, surges, waves, (relative) mean sea level, temperature, salinity, turbidity and river flows. Remote sensing by satellites, aircraft and coastal radars can provide expanded spatial patterns including coastal bathymetry. Off-shore moorings and ships' (ferries) surveys provide direct in-situ data.

However, monitoring parameters invariably involves some compromises in accuracy, resolution, representativeness etc. Some assimilation of observations within numerical model simulations is widely used for temporal and spatial interpolation/extrapolation of parameter distributions (Prandle, 2009).

Appendix B.1 Tides

Much of the theory presented here focuses on strongly-tidal estuaries where tidal current amplitude can be used as a basis for parameterising the linearised bed-friction coefficient, F; eddy viscosity, E, and diffusivity, K, together with related half-lives of sediments in suspension, t_{50}. Figure B.1 (overleaf) shows tidal elevations in the Mersey, illustrating the predominance of the semi-diurnal lunar constituent, M2.

Newton's gravitational theory showed that the attractive force between bodies is proportional to the product of their mass divided by the square of their distance apart. This means that only the tidal effects of the sun and moon need be considered. Mathematically it is convenient to regard the sun as rotating around a 'fixed' earth, thus enabling the same theory to be applied to the attraction from both the sun and moon.

Appendix B.1.1 Non-rotating earth

Integrating the tangential force, with the constant of integration determined from satisfying mass conservation, indicates a surface displacement,η:

$$\eta = \frac{a}{4}\frac{M}{E}\left(\frac{a}{d}\right)^3 (3\cos 2\theta + 1)$$

where M/E is the ratio of the mass of the moon to that of the Earth, i.e. 1/81, and a/d is the ratio of the radius of the earth to their distance apart, i.e. 1/60. The longitude, θ, is measured relative to their alignment along the ecliptic plane of the moon's orbit. The radial force component is negligible compared with gravity, g.

This corresponds to bulges on the sides of the earth nearest and furthest from the moon of about 35 cm, with depressions at the poles of about 17 cm.

Appendix B.1.2 Rotating earth

Taking account of the Earth's rotation, cos θ = cos ϕ x cos λ, where ϕ is latitude and λ the angular displacement, changes the surface displacement, η, to:

$$\eta = \frac{a}{2}\frac{M}{E}\left(\frac{a}{d}\right)^3 (3\cos^2\phi\cos^2\lambda - 1)$$

Thus, we note the generation of two tides per day (semi-diurnal) with maximum amplitude at the equator, ϕ=0, and zero at the poles ϕ = 90^o. The period of the principal solar semi-diurnal constituent, S2 is 12.00 h. The moon rotates in 27.3 days, extending the period of the principal lunar semi-diurnal constituent, M2, to 12.42 h. The ubiquitous spring-neap variations in tides follows from successive intervals of coincidence and opposition of the phases of M2 and S2. The two constituents are in phase when the sun and moon are aligned with the earth, i.e. both at full moon and new moon.

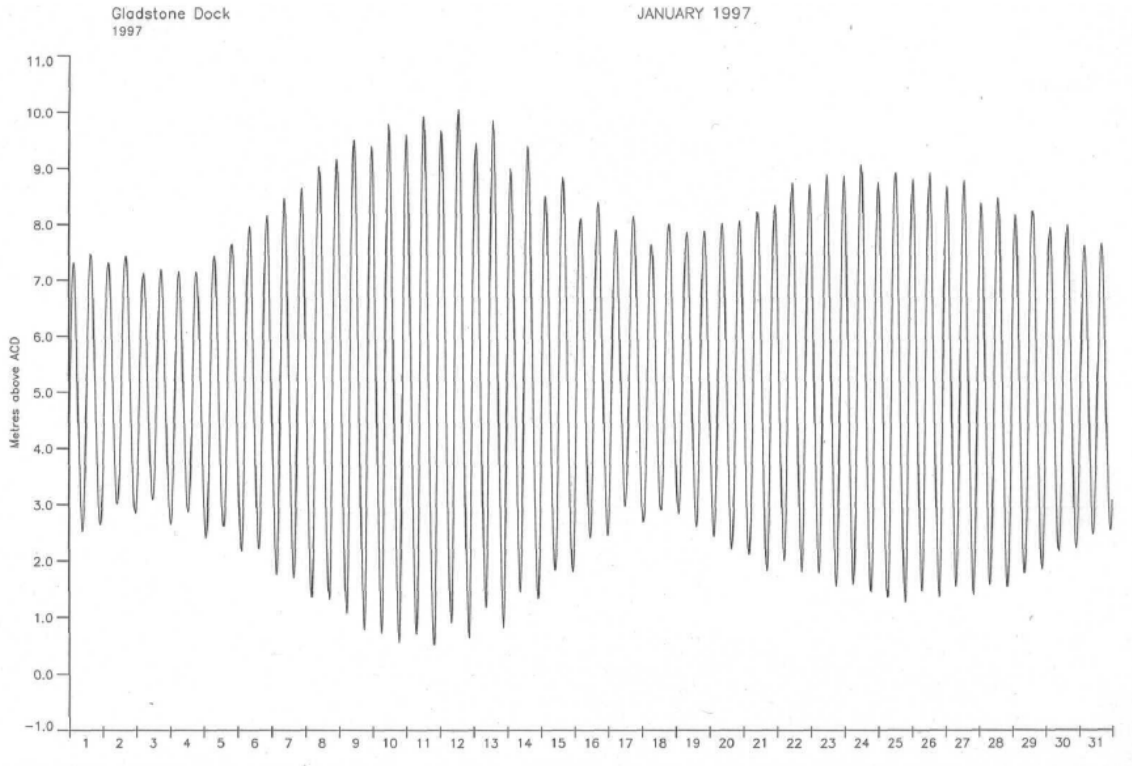

Figure B.1 Month long recording of tidal heights at the mouth of the Mersey Estuary (Prandle, 2009).

The moon's orbit is inclined (declination) at about 5º to the equator, which introduces a daily inequality producing a principal lunar diurnal constituent, O1. The equivalent solar declination is 27.3º, producing the principal solar diurnal constituent, P1 alongside the Principal Lunar and Solar diurnal constituent, K1. The lunar declination varies over a period of 18.6 years, changing the magnitude of the lunar constituents by up to +/- 4 per cent

The moon and sun's orbits show slight ellipticity, changing the distance, d. For the moon this produces a lunar ellipse constituent, N2, whilst for the sun constituents at annual, Sa, and semi-annual periods, Ssa, are produced.

Although the ratio of masses S/E = 3.3 x 10^5, overshadows that of M/E, the corresponding ratio of distances ds/dm ~ 390. Thus, the relative gravitational attraction of the moon to the sun is (S/M) / $(ds/dm)^3$ ~ 0.46.

In consequence of the above, equilibrium magnitudes of the Principal constituents relative to M2 are: S2 - 0.46; N2 - 0.19; O1- 0.42; P1 - 0.19 and K1- 0.58.

Appendix B.1.3 Tidal amphidromes

The integration of tidal potential over the spatial extent of the deep oceans means that direct attraction in adjacent shelf seas can be neglected compared with the propagation of energy from the oceans. In consequence tides in enclosed Seas and Lakes tend to be minimal. In practice, the world's oceans respond dynamically to the above tidal forces.

Tides propagate predominantly as Kelvin waves, and are dissipated by bottom friction in shallow water on continental shelves. Local enhancements can occur due to resonance producing very large tides. Responses in ocean basins and within Shelf Seas take the form of amphidromic systems. This is shown in Figure B.2 (overleaf) for

the M2 constituent in the North Sea. The amplitudes of such systems are a maximum along their coastal boundaries and the phases rotate (either clock-wise or anti-clockwise) such that high tidal levels on one side of the basin are balanced by low tidal levels on the opposite. While these surface displacements propagate around the system in a tidal period, the net ebb or flood excursions of individual particles seldom exceeds 20 kms.

These co-oscillating systems can accumulate energy over a number of cycles, resulting in Spring tides occurring several days after new or full moon. Basin morphology can selectively amplify the amphidromes for different constituents. In general, the observed amplitudes of semi-diurnal constituents, relative to diurnal, are significantly larger than indicated from their equilibrium ratios shown above.

Appendix B.1.4 Higher harmonics and residuals

The theories described in Section A.1 provide robust descriptions of the first-order estuarine responses for the primary tidal constituents. However, seemingly second-order effects can have longer-term importance on both mixing processes and sediment dynamics. While the first-order effects can be accurately modelled, numerical simulation of these second-order effects requires increasingly fine resolution in both space and time.

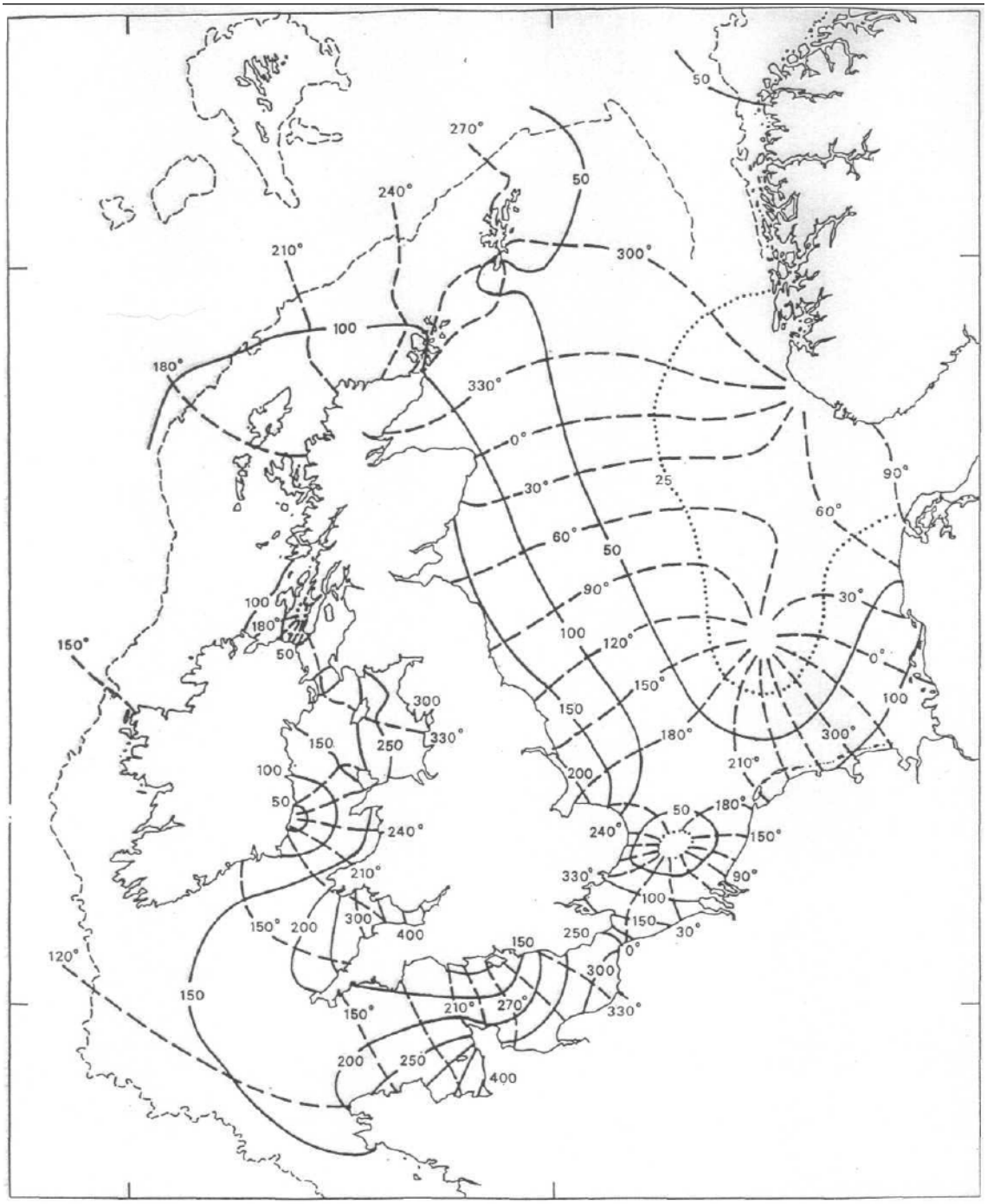

Figure B.2 M2 tidal amphidromes in the north west European continental shelf, after Flather (1976).

Appendix B.2 Surges

Detailed descriptions of the generation and propagation of storm surges are described by Heaps (1967, 1983). Surges propagate as shallow water waves, raising sea levels along coasts to the right of propagation. Flooding often involves not only large, but 'peculiar' surges. Rapid increases of sea level on time scales of hours can cause severe flooding in low lying coastal regions and dramatic loss of life. Rapid decreases in sea level can cause problems in the safe navigation of large vessels in shallow water.

Storm surge generation is represented by two forces, namely wind stress and the horizontal gradient of atmospheric pressure at the sea surface. The wind effect depends on water depth and increases in importance as the depth decreases, whereas the pressure effect is independent of depth. The most important mechanism for surge generation is wind stress acting over shallow water. Surges are therefore, large and dangerous, where storms impact on large areas of shallow continental shelves. In deep water, surge elevations are approximately hydrostatic as a 1 hPa decrease in atmospheric pressure gives ~ 1 cm increase in surge elevation.

Surges are superimposed on the normal astronomical tides. Where the tidal range is large, the relative timing of a surge peak and tidal high water is critical. A moderate surge at high tide may cause flooding, whereas a large surge may go unnoticed if its peak occurs at low water. In addition, non-linear processes become important in shallow water, modifying the storm surge and causing interaction between it and the tide.

Storm surges and extreme sea levels are expected to be experienced more frequently in the future, although the uncertainties on estimates are large. A large proportion of coastal areas in England and Wales have an elevation below the 1000 year return period level (Figure B.3). Consequently, a modest sea level rise of 50 cm will be of major importance to people living in coastal areas.

Three-dimensional (mid-latitude) storm surge forecasts provide detailed description of the circulation associated with surges (Figure B.4, overleaf). Surges generated north and west of Scotland can travel into the North Sea south along the east coast of England returning along the Dutch, German and Danish coasts. These are known as externally generated or 'external' surges.

Figure B.3 Coastal flood risk areas (Woodworth, pers. comm.).

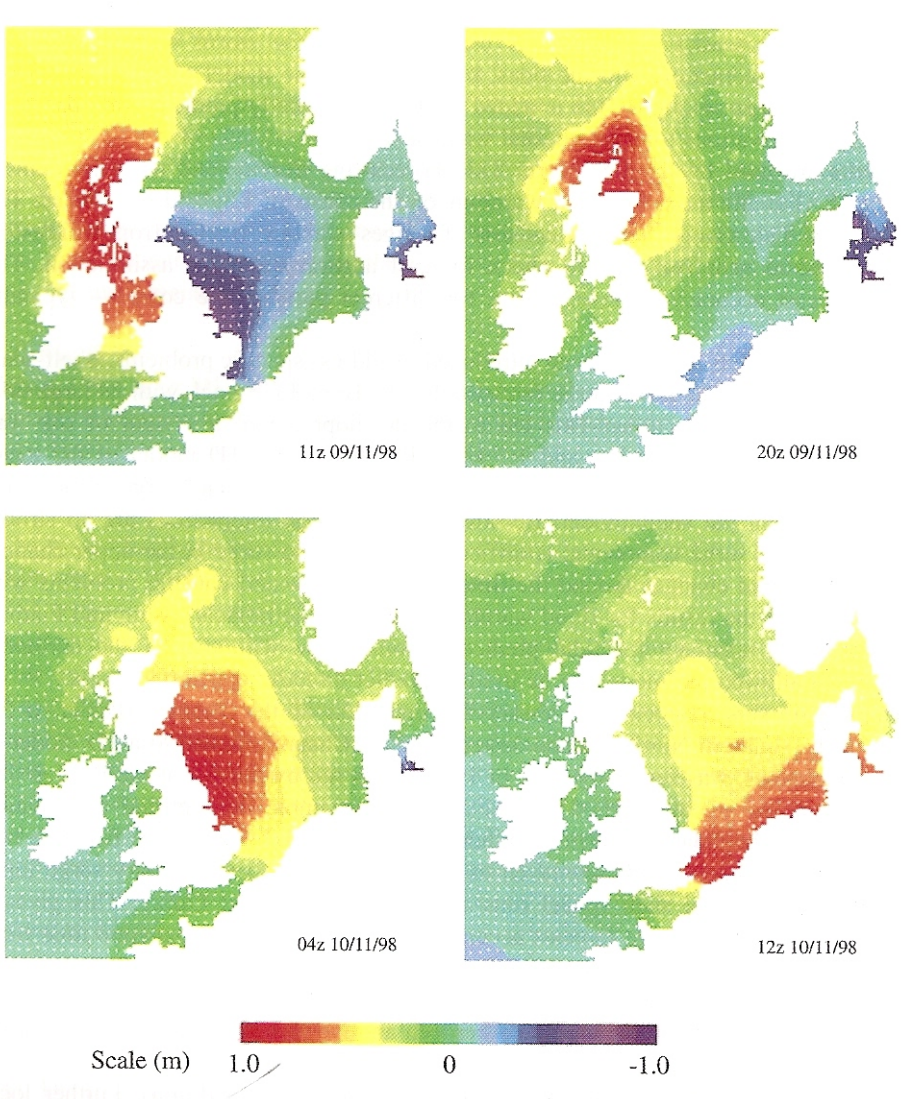

Figure B.4 Typical North Sea Storm Surge event (Woodworth, pers. comm.).

Appendix B.3 Surface waves

By contrast with tides and surges, surface wind waves have wavelengths which, except on beaches, are small in comparison with the water depth. They are generated by winds, which typically produce waves with a spectrum of frequencies (or wavelengths) and propagate in a spread of directions. The magnitude depends on the distance over which the wind acts, known as 'fetch'. Locally generated components, containing generally higher frequencies, are called ‘wind sea'. Non-linear interactions among wave components result in a transfer of energy from high to lower frequencies and the resulting longer period waves.

Ocean-generated waves travel very large distances, these are known as 'swell'. In shallowing water, the wave orbital velocities reach the seabed and their propagation slows, causing refraction and dissipation of energy by bottom friction. Wave energy is also dissipated in deep water by white capping and ultimately by breaking at the shore. Wave conditions at the coast therefore depend on fetch, wind duration, exposure to incoming swell and (local) bathymetry.

Around the UK, west and north-facing coasts are exposed to swell and have long fetch, thus they are characterized by large and long period waves. The Irish Sea is relatively enclosed, fetches are relatively short and so waves are not so large and have shorter period. Very shallow water dissipates wave energy and so reduces extreme wave heights.

Wave modelling is directly dependent on the prescription of wind-induced sea-surface stress provided by atmospheric models. To provide practical wave forecasts, there is a need for improvement of the quality of forecast winds in the medium range of up to five to ten days. Extended range (10 to 30 day) forecasts from Numerical Weather Prediction (NWP) models can provide ensemble forecasting techniques.

Ideally, a two-way coupling should be incorporated between the atmosphere and the waves. This should take into account the effects of density stratification caused by air/sea temperature difference. These stability effects also determine the level of gustiness of the winds, which has an effect on wave growth.

Operational forecasting for the open ocean is usually made using a global model domain with rather coarse horizontal resolution in order to capture the remote generation of wind waves and their great-circle propagation toward the coast as swell. Wave forecasting on regional scales requires finer spatial resolution and careful treatment of the local coastal boundary and bottom topography. A coastal version of the third-generation wave models, which allow for non-linear wave-wave interaction directly, has been developed to incorporate these effects.

Appendix B.4 Mean sea level

Tide gauges provide effective monitoring of mean sea level (msl). Sea level observations can be assimilated into shelf models to help define important quantities that are not observed directly such as open boundary and initial conditions. On time scales of decades and longer, measurements of sea level with respect to stable fixed points on land can provide an indirect measure of vertical crustal movement, global warming of the world's ocean, melting of Antarctic ice sheets, and deep-sea circulation (Woodworth *et al.,* 1999).

Over 80 per cent of British monthly msl variance can be related to seasonal changes, the static pressure effect and the influence of winds over the continental shelf (Woodworth *et al*., 1999). A smaller proportion of the variance can be related to the meteorological influences at stations bordering the southern North Sea. This is due to the cancelling effect of local pressure and wind at these stations. By modelling the influence of more distant and lagged pressure distributions, it is possible to account for typically 90 per cent of the monthly msl variance.

The seasonal variation of msl is approximated by the sum of an annual and semi-annual tide. The amplitude of the mean annual tide around the UK is 7 cm (Woodworth *et al.,* 1999). The joint contribution of the equilibrium tide, static pressure effect and local winds is shown to be too small to account for this mean amplitude. The large, unexplained component of the annual tide is probably due to the steric oscillation of the adjacent North Atlantic.

In order to compute changes in ocean steric heights, temperature, and salinity, measurements are required throughout the water column. However, very little such data exist from the Atlantic over long time scales. Sea surface temperatures, which have been routinely collected, show little inter-annual correlation with sea levels. Most areas of the eastern North Atlantic have warmed by between 0.2 – 1.0 ºC per decade since the 1980s (IACMST, 2005). Available surface salinity data show little secular trend in the area to the west of Britain, while almost nothing

is known of salinity trends at depth, over time scales of centuries. In addition, there are no large trends in the local meteorology that could force significant, sea level secular changes.

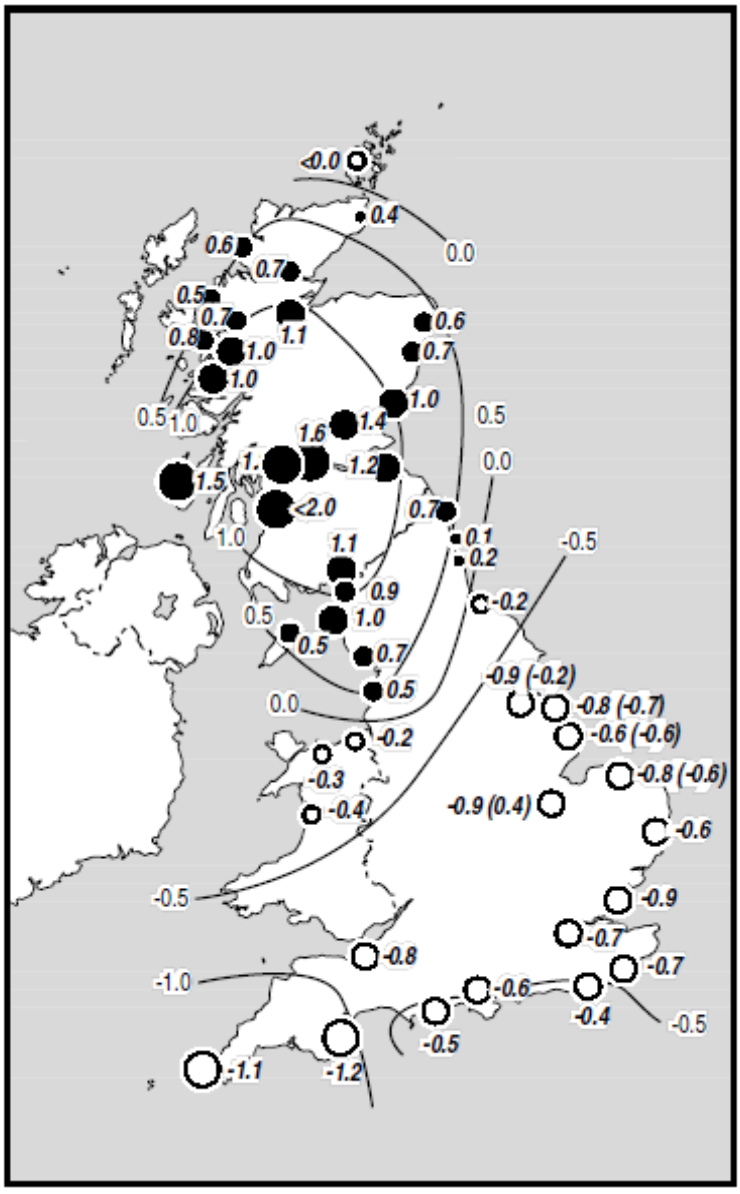

Figure B.5 Land movement in mm yr^{-1}, from Shennan and Horton (2002).

The likely scenario for the 21st century shown in Table B.1 (overleaf), will see rising sea levels as a result of the anticipated global air and ocean warming, leading to thermal expansion of the ocean and to glacier and polar ice melting. The result will be a real, long-term increase in ocean levels, considerably larger than any possible eustatic rise observed in the tide gauge data throughout the last two centuries. Sea level in the U.K. can also be expected to increase by the year 2100. There are obvious problems to be considered such as sea water intrusion into hitherto freshwater areas.

In the future, the expansion of the climate data set by means of remote sensing of oceans, atmosphere and ice caps, and by further in-situ measurements of the deep

ocean, will result in more sophisticated modelling of climatic trends, through which mechanisms responsible for sea-level secular variations of regional and global basis might be better understood.

Table B.1 Recent estimates of sea level rise from tide gauges from Church *et al.* (2001). The standard error for these estimates is also given along with the method used to correct for vertical land movement (VLM). See Church *et al.* (2001) for full details and references shown.

	Region	VLM	Rate ± s.e. (mm/yr)
Gornitz and Lebedeff (1987)	Global	Geological	1.2 ± 0.3
Peltier and Tushingham (1989, 1991)	Global	ICE-3G/M1	2.4 ± 0.9
Trupin and Wahr (1990)	Global	ICE-3G/M1	1.7 ± 0.13
Nakiboglu and Lambeck (1991)	Global	Spatial decomposition	1.2 ± 0.4
Douglas (1991)	Global	ICE-3G/M1	1.8 ± 0.1
Shennan and Woodworth (1992)	NW Europe	Geological	1.0 ± 0.15
Gornitz (1995)	N America E Coast	Geological	1.5 ± 0.7
Mitrovica and Davis (1995), Davis and Mitrovica (1996)	Global far field (far from former ice sheets)	PGR Model	1.4 ± 0.4
Davis and Mitrovica (1996)	N America E Coast	PGR Model	1.5 ± 0.3
Peltier (1996)	N America E Coast	ICE-4G/M2	1.9 ± 0.6
Peltier and Jiang (1997)	N America E Coast	Geological	2.0 ± 0.6
Peltier and Jiang	Global	ICE-4G/M2	1.8 ± 0.6
Douglas (1997)	Global	ICE-3G/M1	1.8 ± 0.1
Lambeck *et al.* (1998)	Fennoscandia	PGR Model	1.1 ± 0.2
Woodworth *et al*. (1999)	British Isles	Geological	1.0

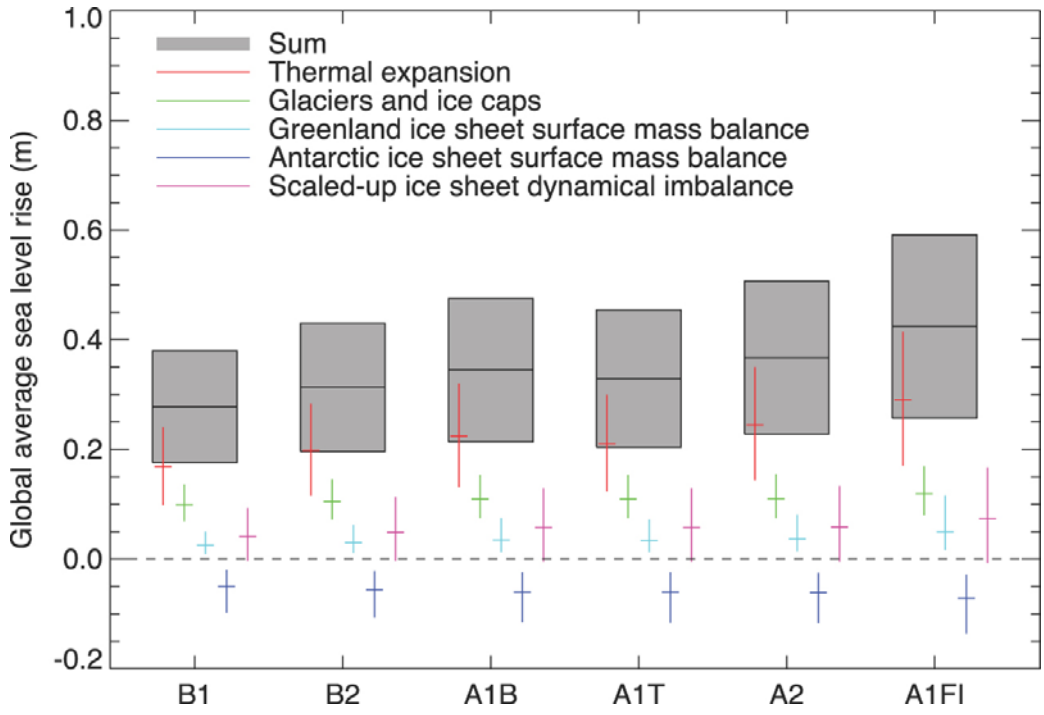

Figure B.6 Projections and uncertainties (5 to 95 per cent ranges) of global average sea level rise and its components in 2090 to 2099 (relative to 1980 to 1999) for the six SRES marker scenarios, from Meehl *et al.*, 2007, please see original for further explanation.

Appendix B.5 River flows

The mean discharge of the world's largest river, the Amazon, is 200,000 $m^3 s^{-1}$, representing 20 per cent of net global freshwater flow. Moreover, the cumulative discharge of the next nine largest rivers amounts to a similar total (Schubel and Hirschberg, 1982). Outside of these 10 largest rivers, discharge (Q) is less than 15,000 $m^3 s^{-1}$. From the theory in Section A.9, this corresponds to D_0 = 50 to 125 m. Thus, the range of values shown in Figure A.12 (page 57) clearly represents the vast majority of estuaries. Moreover, we note from the ratio of L_l/L shown in Figures A.7 (page 47) and A.4 (page 42) that the larger estuaries with D > 10 m will often involve freshwater plumes extending seawards.

Appendix B.5.1 Minimum flows for estuarine forcing

Prandle (2004) introduced the condition that estuarine lengths, L must be greater than 2.5 km (based on the requirement that depth, D_0 must be greater than tidal elevation amplitude, Z); where Z must be greater than 1 m for an estuary to be vertically mixed. These values of L and D_0 were regarded as effective minimum values for a 'mixed' estuary to 'function' over a complete tidal cycle. From the derivation that $D_0 = 12.8 (Q \tan \alpha)^{0.4}$ shown in Section A.9, substituting the value for transverse slope, tan α = 0.013, minimum values of river flow, Q, in $m^3 s^{-1}$ for Z = 1, 2 and 4 m are shown in Table B.2.

Table B.2 Minimum river flows ($m^3 s^{-1}$) for estuaries to function over a complete tidal cycle with tidal amplitude, Z.

	Z = 1 m	Z = 2 m	Z = 4 m
All estuaries	0.13	0.75	4.2
Rias	0.05	0.26	1.5
Coastal Plain	0.15	0.88	5.0
Bar built	0.12	0.69	3.9

Appendix B.5.2 Spacing between estuaries

Having postulated that estuarine bathymetry is determined by the tidal elevation amplitude (Z) and river flow (Q), the question arises as to how estuaries adjust over geological time scales to climate change. In particular, what are the consequences of changes in rainfall and catchment areas as coasts advance or retreat under falling or rising mean sea level?

For a long straight coastline with spacing, S (km), between estuaries and a rectangular catchment of landward extent, C (km), the river flow, Q, is given by:

$$Q = 0.032 S C R$$

where R is the annual rainfall reaching the river (m a^{-1}). Thus for typical UK values of S =10 km, C = 50 km and Q = 15 $m^3 s^{-1}$, this indicates R ~ 0.9 m a^{-1}, which is in broad agreement with observations (Prandle 2004).

By introducing the above relationship between estuarine depths and river flow, with side slope tan α = 0.013, we obtain the following expression for spacing between estuaries:

$$S = 41 D_0^{5/2} / C R$$

We note that few estuaries have values of D_0 > 20 m. Hence to avoid small values of S for continental land masses with large values of C, we anticipate the formation of deltas or multiple 'sub-estuaries' linked to the sea by tidal basins such as in Chesapeake Bay.

Where estuarine bathymetries were established under historical conditions with much larger (glacial melt) values of river flow, Q, we might expect saline mixing to start landwards of the mouth. Conversely, where saline mixing involves an offshore plume, we postulate either exceptionally large values of river flow or that bathymetric erosion to balance existing river flow is hindered.

Appendix B.6 Temperature

An important characteristic of temperatures in shelf seas is pronounced seasonality, particularly through its influence on density with thermal stratification developing readily in deeper water where tidal mixing is weak. Such stratification affects the biology and chemistry of the water column by limiting the vertical exchange of nutrients, suspended sediments and therefore, light.

In UK shelf seas, the sea surface temperature closely follows the air temperature, with a mean temperature 1-2 °C above the latter. Their seasonal amplitudes are closely similar in shallow water, but this is somewhat reduced in deeper water. Any increase in wind speed forces the sea-surface temperature to converge even more closely towards the ambient air temperature. Beneath the surface, increasing depths both delay and attenuate surface variability - a process reinforced by thermal stratification that exists between March and October in deeper waters. Anomalies in observed sea surface temperatures can generally be directly related to concurrent air temperature anomalies, with an indirect influence of anomalous wind conditions. However, Prandle (1998) found that air temperature anomalies are reduced in amplitude in their impact on depth-averaged sea temperatures because of the attenuating effect of water depth.

Model simulations emphasise the essentially localised nature of the air-sea thermal balance with only a secondary effect of horizontal advection and dispersion. Any changes in mean temperature along the Atlantic boundary will have little influence on the more enclosed regions of the North Sea. Moreover, the effect of corresponding changes in the annual cycle will be reduced even further.

Temperature and salinity data can be used together for water mass tracing and for water mass mixing estimates. Stratification, or a gradient in density in the vertical dimension, is one of the important parameters relevant to mixing. In particular, many chemical and biological processes are affected by and often correlated with temperature on time scales of a day, the annual cycle, and over longer periods associated with oceanic oscillations such as: El Niño, the North Atlantic Oscillation and Pacific Decadal Oscillation.

Coastal waters surrounding the UK became warmer during the 20th century and average annual seawater temperatures may rise a further 2 °C or more by the 2050s. This warming is part of a global rise in sea and air surface temperatures that will cause changes in the distribution and abundance of species. Initially, there will not be a wholesale movement northwards of southern species or a retreat northwards of northern species because many additional factors will influence the responses of the different organisms. Past changes provide a clue to more extensive changes expected in the future if global warming develops as predicted.

Appendix B.7 Salinity

Apart from an occasional surface scum line, the ebb and flood of saline intrusion in estuaries passes largely unnoticed. Yet the extent of saline intrusion was often the determining factor in the location of towns or industries reliant on fresh river water. Moreover, the extent and nature of intrusions determines net estuarine concentrations of both dissolved marine tracers and fluvial contaminants. At the interface with river water, salt water produces electrolytic attraction between fine suspended sediments resulting in rapidly settling 'flocs', which accumulate at the seaward (ebb) and landward (flood) limits of salinity intrusion (Dyer 1997).

In strongly tidal estuaries, saline intrusion has little impact on tidal propagation (Prandle 2009). Conversely, the nature of saline intrusion is overwhelmingly determined by the combination of tidal motions alongside the flow of river water. Pritchard (1955) introduced a generalised classification of estuaries according to their salinity intrusion, varying from fully-mixed (vertically) in strongly tidal, shallow estuaries with small river flows, through to 'arrested saline wedge' in deeper, micro-tidal estuaries with large river flows.

Abraham (1988) noted the significance of 'tidal straining', whereby, on the flood tide, larger near-surface tidal velocities advect denser more saline water over fresher lower layers, leading to mixing by convective overturning. Simpson *et al*. (1990) provided both theoretical and observational quantification of this phenomenon. The nature of saline intrusion in an estuary is governed by tidal amplitude, river flow and bathymetry. The pattern of intrusion may be altered by interventions such as dredging, barrier construction or flow regulation, together with impacts from changes in mean sea level or river flows linked to global climate change. Adjustments to the intrusion may have important implications for factors such as water quality, sedimentation and dispersion of pollutants. Dispersion of salt involves interacting three-dimensional variations in phase, amplitude and mean values of both currents and the saline distribution. These variations are sensitive to the level of density stratification which may vary appreciably temporally and both axially and transversally. The spectrum of such spatial and temporal variations include:

i. the tidal cycle, with pronounced vertical mixing occurring on one or both of peak flood and ebb currents due to bottom friction, or at slack tides due to internal friction;

ii. the neap-spring cycle, with mixing occurring more readily on spring than neap tides;

iii. the hydrological cycle, with variations in both river flow and salinity of sea water at the mouth;

iv. storm events including storm surges generated both internally and externally and surface wave mixing; and

v. variations in water density due to other parameters, in particular temperature and suspended sediment load.

Close to shore, salinity often predominates over temperature in determining coastal stratification levels. Seasonal variations at the coast (due to river flow variations) generally decrease offshore, with little variability found at distances greater than 50 km offshore.

Appendix B.8 Sediment supply

The predominant influences on sediment regimes in estuaries are tidal and storm currents, enhanced in exposed shallow water by wave stirring. Figure B.7 (overleaf) describes the processes determining sediment erosion, transport and deposition. Detailed accounts of the mechanics of sediment motion associated with tidal currents and waves can be found in Van Rijn (1993) and Soulsby (1997). Postma (1967) describes general features of the erosion, deposition and intervening transport of suspended particulate matter (SPM) in tidal regimes. For all but the coarsest grain sediment, several cycles of ebb and flood movement may occur between erosion and subsequent deposition. Hence, deposition can occur over a wide region beyond the source. Since time in suspension increases for finer, slower settling material, such mechanisms may contribute to a residue of fine materials on tidal flats and to trapping of coarser material in deeper channels.

Understanding and predicting concentrations of SPM in estuaries is important because of their impact on:

i. light occlusion and therefore primary production

ii. pathways for adsorbed contaminants

iii. rates of accretion, erosion and associated bathymetric evolution.

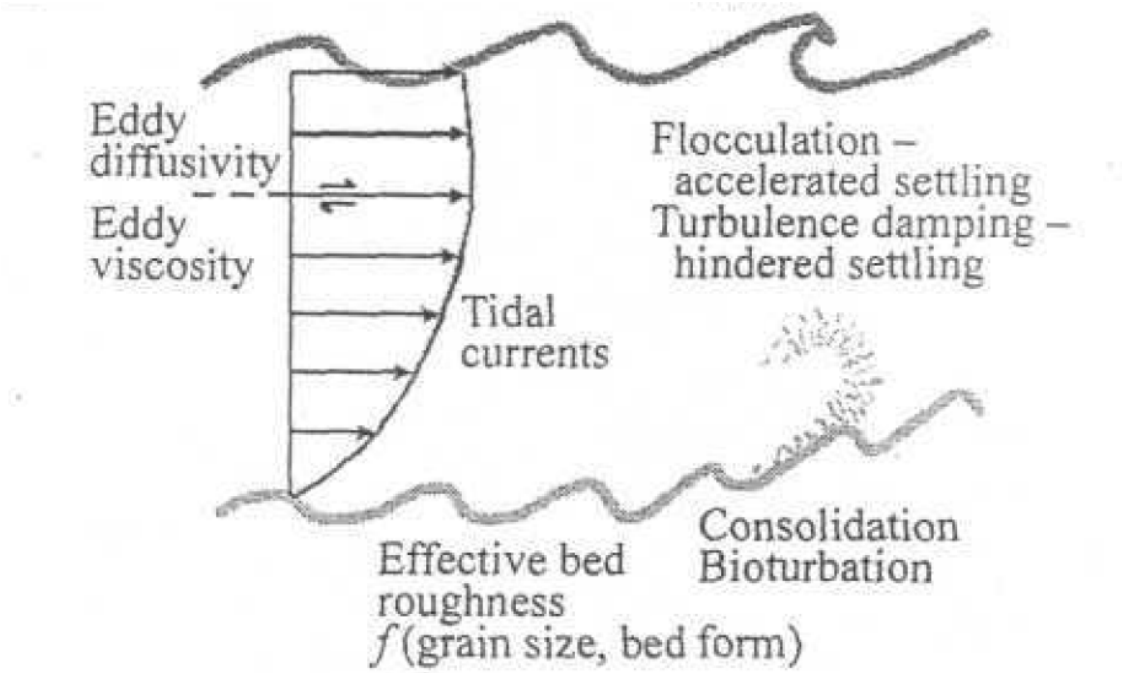

Figure B.7 Processes determining sediment erosion, transport and deposition, after Prandle (2009).

Appendix B.8.1 Spring-neap cycle

In the absence of significant residual currents, the erosional time series for an M2 - S2 dominated tidal regime will show pronounced components at M4, MS4, MSf, and Z0 frequencies (please refer to the Glossary for full explanation of these different tidal constituents). The latter components are generated by nonlinear combinations of M2 and S2 currents and not by any (usually small) tidal current amplitudes at these

emergent frequencies. The similarity in amplitudes of the M4 and MS4 constituents may reduce the quarter-diurnal signal at neap tides (when their phases are opposed) and thereby suggests an enhanced semi-diurnal sediment signal that might be wrongly interpreted as indicating horizontal advection or a large diurnal current component. When residual currents increase to an of order 10 per cent of the M2 amplitude (as in strongly-tidal shallow waters), the suspended sediment time series will include M2 and S2 constituents of comparable magnitude to those described for M4, MS4 and MSf constituents. Over a spring-neap tidal, for finer sediments, the peak in suspended sediment concentration will generally occur 2-3 days after the occurrence of maximum tidal currents (Prandle 1997).

Appendix B.8.2 Observed time-series

Figure B.8 shows three examples of simultaneous time series recordings of suspended sediment and tidal velocity as shown by Prandle (1997). These examples were selected as illustrative of tidally dominated conditions and correspond to tranquil weather conditions. The Dover Strait is a highly (tidally) energetic zone, 30 km wide and up to 60 m deep, linking the North Sea to the English Channel, with currents exceeding speeds of 1 m s^{-1}. The Mersey Estuary is a shallow (< 20 m deep) estuary with tidal range up to 10 m and the measurements shown were taken in the narrow entrance channel, which is 1 km wide and 10 km long. The Holderness measurements were taken some 4 km offshore of a long, rapidly eroding coastline comprising glacial till. The Dover Strait and Mersey sediment recordings used transmissometers, whereas the Holderness recordings were obtained from an optical backscatter sensor.

In all three cases the fortnightly, MSf, constituent is largest. The spectral peak in the sediment distribution in the Dover Strait corresponds to a sediment settling velocity of 10^{-4} m s^{-1}. The Mersey and Holderness are likely to contain more coarse grained components. In all three cases the M2 or M4 constituent is next largest. Likewise the phase values for all constituents (relative to the associated current values) are generally in the range of 0-90º.

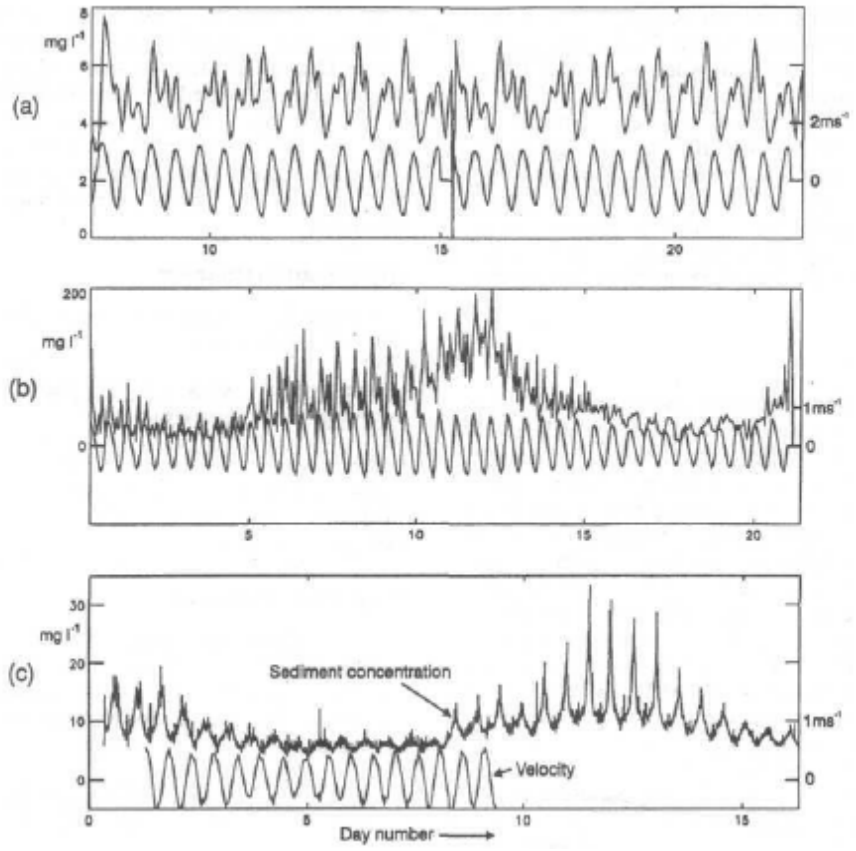

Figure B.8 Observed suspended particulate matter (SPM) and current time-series in (a) Dover Straits; (b) Mersey Estuary, and (c) Holderness Coast, after Prandle (2009).

Appendix B.8.3 Sediment modelling

The mean suspended sediment concentration in the Mersey is an order of magnitude higher than in the Dover Strait (Figure B.8), concentrations at Holderness lie between these two. Thus, there is a suggestion of limited supply in the Dover Strait; moreover, the phase relationship for the M2 constituent is indicative of a significant advective component.

Accurate simulation of sediment fluxes requires an initial prescription of the distribution of surface sediments. Simulations over larger and longer space and time scales need to incorporate sequential changes in these surface sediments as they adjust to variations in tidal and wave conditions resulting from trends and cycles in the inter-related evolving bathymetry. On even longer time scales, likely changes in both mean sea level and sources of marine and fluvial sediments need to be incorporated.

Reproducing these characteristics in models remains sensitive to the largely empirical formulae used in prescribing erosion and deposition rates. Bed roughness strongly influences these rates and is largely determined by the composition (fine to coarse) and form (ripples, waves) of the bed. Sediment processes are complicated by the continuous dynamical feedback between this roughness and the overlying vertical structure of tidal currents and waves and their associated turbulence regimes. Bed roughness can change significantly over both the ebb to flood and neap to spring tidal cycles. Associated erosion and deposition rates may then vary considerably over these cycles and dramatically over seasons or in the course of a major event.

Conventionally, erosion is assumed to occur when the bed shear forces exceed the resistance of the bed sediment, characterised by a 'critical shear stress for erosion'. Subsequent settlement of particles depends on their size and density, and the regime of turbulence and chemical forces in the surrounding water. Sedimentation is usually assumed to occur when quiescent dynamical conditions are below some threshold for erosion.

Appendix B.8.4 Observed suspended particulate matter (SPM) time-series

Observations are crucial to developing and assessing SPM models (Prandle, 2009). In-situ concentrations are routinely monitored acoustically, optically and mechanically. Acoustic backscatter probes (ABS) provide vertical profiles of concentration whilst multi-frequency probes provide information on grain size, usually at a single point. Pumped samples, bottles and traps are used in mechanical devices. Recent developments of in-situ laser particle sizers provide valuable information on particle spectra non-invasively (mechanical samplers can corrupt these spectra).

Available observations suffer from fundamental shortcomings, namely:

i. calibration from sensor units to concentration involving complex sensitivity to particle size spectra in optical and acoustic instruments and to atmospheric corrections and sun angle effects in remote sensing

ii. unresolved particle-size spectra

iii. limited spatial and temporal coverage relative to the in-homogeneity of sediment distributions.

The spatial resolution of in-situ concentration measurements is generally limited to single points (or limited profiles) in Optical Back Scatter (OBS) and ABS sensors, and to surface values from satellite or aircraft sensors.

Each instrument has its own calibration peculiarities. Moreover, all of these calibrations vary as the mean particle size changes. Optical devices rely on occlusion of light either by transmittance or reflectance. Since this is dependent on the surface area of the particle, recordings are more sensitive to finer scale particles. Hence, observed concentrations need to be calibrated by reference to some representative particle radius. The plate-like character of flocs complicates such calibrations.

Conversely, acoustic backscatter (in the range of frequencies used in ABS instruments) increases with particle volume and, therefore, these instruments are more sensitive to coarse particles. The optical instruments also experience fouling and all of the instruments can be swamped above certain concentrations.

Satellite images of near-surface SPM concentrations can be used in conjunction with model simulations to infer the magnitude of discrete sediment sources. Aircraft surveillance using multi-wavelength imagery can differentiate between the reflectance from SPM associated with chlorophyll and that from various sediment fractions. However, the need for atmospheric corrections introduces some reliance on in-situ calibrations.

On the longer time scale, information in sediment cores (judicious choice of location is crucial) may be dated using seasonal striations, specific contaminants (radio nuclides, Pb-210, etc.) and various natural chemical signals or biological fossils. The range of such techniques is expanding rapidly providing multiple opportunities to derive both geographic provenance and associated age. Both Light Detection and Ranging (LIDAR) and Synthetic Aperture Radar (SAR) can be used to determine sequences of bathymetric evolution (Prandle, 2009).

Appendix C UK morphological data-sets

Appendix C.1 Joint Nature Conservation Committee (JNCC) data

Table C.1 Joint Nature Conservation Committee (JNCC) data after Davidson and Buck (1997).

Estuary No.[1]	Estuary No.[2]	Estuary name	Type	SAHW (ha)	INTA (ha)	SAMSH (ha)	SHL (km)	L (km)	TIDE (m)
1	121	Stour-Pegwell	9	863	709	99	79.9	35.1	4.5
2	122	Rother Estuary	5	376	344	54	23	6.6	5.3
3	123	Cuckmere Estuary	4	47	15	10	16.7	8.4	6.5
4	124	Ouse Estuary	4	124	6	0	49.2	20.3	6.1
5	125	Adur Estuary	4	153	46	9	46.5	20.6	5.5
6	126	Arun Estuary	4	171	3	0	80.3	37.1	5.3
7	127	Pagham Harbour	5	266	245	33	9.8	2.6	4.9
8	128	Chichester Harbour	5	2946	2342	1077	80.6	8.1	4.2
9	129	Langstone Harbour	5	1925	1513	100	43	7.7	4.2
10	130	Portsmouth Harbour	5	1593	964	181	55.2	10.8	4.1
11	131	Southampton Water	4	3975	1376	355	109.8	20.2	4
12	132	Beaulieu River	5	546	417	185	31.3	10.4	3.2
13	134	Bembridge Harbour	4	158	130	0	7.7	20.3	3.1
14	135	Wootton Creek	4	475	466	14	18.5	1.8	3.8
15	136	Medina Estuary	4	219	101	13	19.6	7.4	4.2
16	137	Newtown Estuary	5	332	296	120	30	3.3	2.9
17	138	Yar Estuary	4	110	97	66	7.9	3.2	2.5
18	139	Lymington Estuary	4	1367	589	506	18.1	4.2	2.5
19	139	Christchurch Harbour	5	239	122	50	21.4	6.6	1.2
20	140	Poole Harbour	5	3805	2050	697	102.9	16.3	1.4
21	141	Weymouth	5	1617	278	51	47.5	16.7	1.9
22		WestBay		0	0	0	0	0	0.5
23	142	Axe Estuary	5	79	62	34	8.1	3.8	3.7
24	143	Otter Estuary	5	36	19	19	6.1	1.1	4.1
25	144	Exe Estuary	5	1874	1201	66	47.8	16.7	4.1
26	145	Teign Estuary	3	370	219	13	20.4	9.1	4.2
27	146	Dart Estuary	3	863	313	25	60.5	19.8	4
28	147	Kingsbridge Estuary	3	674	446	4	48.6	8.3	4.6
29	148	Avon Estuary	3	214	146	26	19.8	7.8	4.7
30	149	Erme Estuary	3	145	72	21	17.1	6	4.7
31	150	Yealm Estuary	3	446	154	2	28.1	7.7	4.7
32	151	Plymouth Sound	3	3962	1809	359	208.6	34.1	4.7
33	152	Looe Estuary	3	56	43	6	12.6	4.1	4.8
34	153	Fowey Estuary	3	305	146	3	39.2	11.1	4.8
35	154	Falmouth	3	2482	746	93	126.8	18.1	5.3
36	155	Helford Estuary	3	568	186	5	44.3	9.2	4.7
37	1	Hayle Estuary	5	358	321	19	19.5	2.4	5
38	2	Gannel Estuary	3	122	85	20	9.2	3.7	6.9
39	3	Camel Estuary	3	839	610	50	43	15.3	5.9
40	4	Taw-Torridge Estuary	5	2463	2018	240	87.9	20.8	7.3
41	6	Parrett	9	6529	5147	487	109.4	46.3	9.7
42	7	Severn Estuary	4	55684	890	933	353	111.2	12.3
43	9	Ogmore Estuary	4	187	173	15	8	1.6	8.9
44	10	Afan Estuary	5	38	18	0	4.9	2.5	8.6

Estuary No.[1]	Estuary No.[2]	Estuary name	Type	SAHW (ha)	INTA (ha)	SAMSH (ha)	SHL (km)	L (km)	TIDE (m)
45	11	Neath Estuary	3	1129	1079	159	26.9	10.6	8.6
46	12	Tawe Estuary	9	785	748	0	22.8	6.5	8.6
47	13	Loughor Estuary	4	9524	6553	2187	84.7	30.2	7.1
48	14	Carmarthen Bay	9	8295	5360	910	115.7	30.7	7.5
49	15	Milford Haven	3	5448	1710	385	170.7	35.4	6.3
50	16	Nyfer Estuary	5	100	75	10	6.1	3.1	4
51	17	Teifi Estuary	5	302	181	46	21	10	4.1
52	18	Aberystwyth	5	18	5	1	7.1	2.4	4.3
53	19	Dyfi Estuary	5	1954	1524	546	52.2	19.6	4.3
54	20	Dysynni Estuary	5	117	69	22	9.9	4.4	4.3
55	21	Mawddach Estuary	5	1159	976	219	37.7	13.8	4.3
56	22	Artro Estuary	5	120	11	10	7.4	1.7	4.4
57	23	Glaslyn	5	2050	1750	348	54	15.7	4.4
58	24	Pwllheli Harbour	5	85	60	3	4.6	2.4	4.5
59	25	Foryd Bay	5	343	285	123	9.4	4.5	4.7
60	26	Traeth Melynog	5	365	314	66	10.9	5.4	4.7
61	27	Cefni Estuary	5	744	618	111	26.1	12.7	4.7
62	28	Alaw Estuary	2	1085	721	63	38.2	10.4	5
63	29	Traeth Dulas	5	103	103	21	5.2	2.9	6.4
64	32	Conwy Estuary	4	1494	1081	105	55.8	24.7	7.1
65	33	Clwyd Estuary	4	422	386	43	19.1	8.1	6.7
66	34	Dee Estuary	4	16101	12981	2108	108.5	37	7.6
67	35	Mersey Estuary	4	8914	5606	847	102.9	45.6	8.9
68	37	Ribble Estuary	4	11924	10674	2184	107.5	28.4	7.9
69	38	Morecambe Bay	9	45462	34339	3253	254	40.3	8.4
70	39	Duddon Estuary	4	6092	5056	540	65.5	22.6	8.1
71	40	Esk Estuary	5	1134	1049	158	42	11.4	7.7
72	41	Solway Firth	6	42056	27550	2925	213.6	46.3	8.4
73	90	Tweed Estuary	6	199	68	0	27.7	9.9	4.1
74	92	Alnmouth	5	135	111	24	12.7	4.4	3.3
75	93	Coquet	5	75	45	15	12.9	5	3.3
76	94	Wansbeck Estuary	4	102	37	0	12.3	5.8	4.2
77	95	Blyth Estuary	5	168	90	0	21.5	6.6	4.2
78	96	Tyne Estuary	6	792	60	3	83.1	32.7	4.3
79	97	Wear Estuary	6	200	29	6	37.5	17	4.4
80	98	Tees Estuary	4	1347	471	34	121.4	38.3	4.8
81	99	Esk Estuary	6	30	9	0	8.5	3.8	4.6
82	100	Humber Estuary	4	30357	1354	1419	675.5	144.7	6
83	101	The Wash	9	66654	29770	4228	359	90.2	6.5
84	103	Yare	5	1534	769	0	317	46.8	1.9
85	104	Waveney - Oulton	5	129	30	0	6.8	20.1	1.9
86	105	Blyth Estuary	5	311	235	79	25.4	10.8	2.1
87	106	Ore-Alde	5	1821	1332	562	73.2	28	2.2
88	107	Deben Estuary	4	1007	687	461	49.8	19.7	3.2
89	108	Harwich	4	1786	576	119	50.7	20.1	3.6
90	110	Hamford Water	9	2377	1570	863	54	18.3	3.8
91	111	Colne Estuary	4	2335	2002	671	89.6	16.2	4.6
92	112	Blackwater Estuary	4	5184	3315	1103	107.5	21.2	4.6
93	114	Crouch-Roach	4	2754	1536	8382	158.5	29.6	5
94	117	Thames Estuary	4	4745	1126	0	232	82.5	6.5
95	119	Medway Estuary	4	6441	4008	754	143.4	40.9	5.1
96	120	Swale Estuary	4	3283	2696	414	79.3	18.4	4.9

Notes: [1]Estuary numbers from Futurecoast dataset
[2]Estuary numbers from JNCC dataset
SAHW – surface area at high water; INTA – between high water and mean low water; SAM – saltmarsh extent; SHL – shoreline length (including islands); L – Tidal length from mouth to upstream normal tide length, and TIDE – tidal range on mean spring tide (note: range is double amplitude)

Appendix C.2 Futurecoast data

Table C.2 Futurecoast data.

Estuary No.[1]	Estuary name	VOLHW (ha m)	VOLW (ha m)	QMAX ($m^3 s^{-1}$)	CAHW (m^2)	WIDTH (m)
1	Stour-Pegwell	2153	87	21.3	2353	400
2	Rother Estuary	947	9	37.4	706	100
3	Cuckmere Estuary	889	665	31.5	98	10
4	Ouse Estuary	7816	7078	62.5	28	55
5	Adur Estuary	1541	850	30.6	284	125
6	Arun Estuary	25829	24931	83	171	40
7	Pagham Harbour	627	5	0	0	100
8	Chichester Harbour	5798	605	3.4	7995	2430
9	Langstone Harbour	4949	252	7.7	4703	160
10	Portsmouth Harbour	5219	1036	14	6228	220
11	Southampton Water	25669	13231	34.9	19654	1980
12	Beaulieu River	898	114	0	6433	1000
13	Bembridge Harbour	410	12	5.8	5268	200
14	Wootton Creek	197	1	0	1008	300
15	Medina Estuary	1012	332	5.4	2621	420
16	Newtown Estuary	370	11	0	1876	107
17	Yar Estuary	78	7	0	1408	60
18	Lymington Estuary	374	15	15	2875	450
19	Christchurch Harbour	297	114	113.8	118	61
20	Poole Harbour	4997	1593	20	3266	300
21	Weymouth	221	191	1.9	788	140
22	West Bay	6	3	12.6	125	25
23	Axe Estuary	134	19	107.9	90	30
24	Otter Estuary	370	296	60.4	30	10
25	Exe Estuary	6119	1131	370.6	1669	380
26	Teign Estuary	1299	232	141.6	534	135
27	Dart Estuary	4876	2100	229.5	9988	220
28	Kingsbridge Estuary	2335	270	0	11043	520
29	Avon Estuary	692	90	56.5	940	625
30	Erme Estuary	708	245	42.3	6591	1100
31	Yealm Estuary	3047	1318	21.5	1275	450
32	Plymouth Sound	21039	7512	456.1	28043	1220
33	Looe Estuary	162	11	0	225	50
34	Fowey Estuary	1530	424	55.6	6159	290
35	Falmouth	23161	12230	26.4	25630	1920
36	Helford Estuary	4115	1894	0	2821	620
37	Hayle Estuary	364	4	5.7	7	150
38	Gannel Estuary	512	67	14.6	7750	630
39	Camel Estuary	3279	276	60.5	10801	1100
40	Taw-Torridge Estuary	7851	697	523	6440	1000
41	Parrett	1760	149	243.3	7312	500
42	Severn Estuary	1155335	580033	2000.7	280000	13000
43	Ogmore Estuary	179	37	150.1	150	50
44	Afan Estuary	344	95	93.2	14	150
45	Neath Estuary	2762	1257	192.2	562	1000
46	Tawe Estuary	942	0	229.2	25	220
47	Loughor Estuary	30912	6424	74.6	20250	3000
48	Carmarthen Bay	11871	171	533.5	16800	3800
49	Milford Haven	60941	33217	142.2	13000	2200
50	Nyfer Estuary	249	19	16.7	675	450
51	Teifi Estuary	363	6	197.3	250	100
52	Aberystwyth	155	91	98.4	750	350
53	Dyfi Estuary	4328	2305	321.6	3291	1250
54	Dysynni Estuary	412	105	65.7	2	30

Estuary No.[1]	Estuary name	VOLHW (ha m)	VOLW (ha m)	QMAX ($m^3 s^{-1}$)	CAHW (m^2)	WIDTH (m)
55	Mawddach Estuary	1827	756	156.5	4181	400
56	Artro Estuary	255	1	0	10	5
57	Glaslyn	4457	702	85.5	6236	1500
58	Pwllheli Harbour	265	25	12	0	125
59	Foryd Bay	702	49	22.3	0	540
60	Traeth Melynog	847	25	0	0	1730
61	Cefni Estuary	1872	79	0	2650	830
62	Alaw Estuary	3968	503	0	7000	7400
63	Traeth Dulas	262	0	0	1250	50
64	Conwy Estuary	2947	125	374.8	2461	200
65	Clwyd Estuary	577	5	132.4	360	400
66	Dee Estuary	129789	72135	203.9	76313	8000
67	Mersey Estuary	127930	18714	717.8	35918	1525
68	Ribble Estuary	44122	727	836.3	36050	8500
69	Morecambe Bay	151408	1270	1197.5	160000	16500
70	Duddon Estuary	18355	292	122.3	24300	5000
71	Esk Estuary	1690	112	55	4500	730
72	Solway Firth	261165	35889	2589	104000	13000
73	Tweed Estuary	284	57	1065.6	2797	500
74	Alnmouth	114	0	67.3	514	60
75	Coquet	198	49	25.5	360	60
76	Wansbeck Estuary	830	521	106.4	168	60
77	Blyth Estuary	1004	13	64.7	1111	120
78	Tyne Estuary	4948	764	1020.6	9684	360
79	Wear Estuary	1027	11	247.8	1412	200
80	Tees Estuary	5617	35	348.5	1976	1240
81	Esk Estuary	95	13	117.6	1025	50
82	Humber Estuary	273393	25350	1683.6	103529	7500
83	The Wash	495860	173103	406.1	299500	19150
84	Yare	2907	723	57.1	390	65
85	Waveney - Oulton	526	310	32	288	48
86	Blyth Estuary	866	0	13.9	105	35
87	Ore-Alde	3982	389	11.8	1623	122
88	Deben Estuary	1439	5	3	2013	168
89	Harwich	18769	1108	53.1	14165	1813
90	Hamford Water	4724	128	0	6024	1650
91	Colne Estuary	2681	62	23.2	4466	1440
92	Blackwater Estuary	19050	5763	49.9	20419	2850
93	Crouch-Roach	7999	687	18.4	6384	1234
94	Thames Estuary	96225	10132	572.7	58062	2100
95	Medway Estuary	25479	2590	152.8	22495	1430
96	Swale Estuary	9327	566	0	9918	4900

Notes: VOLHW – volume at high water; VOLW – volume at low water; QMAX – maximum annual daily mean river flow; CAHW – Cross-sectional area at the mouth; WIDTH – width at the mouth

Appendix C.3 Estuarine Research Programme (ERP) dataset

Table C.3 Data from the Estuarine Research Programme.

Estuary No.	Estuary name	Volume, ha m			Surface area, ha			Cross sectional area, m^2		
		LW	MW	HW	LW	MW	HW	LW	MW	HW
1	Stour-Pegwell	60	292	1610	53	250	953	284	900	2353
2	Rother Estuary	0	0	128	0	0	110	0	0	706
3	Cuckmere Estuary	0	0	224	0	0	214	0	0	98
4	Ouse Estuary	0	0	129	0	0	133	0	0	28
5	Adur Estuary	0	0	247	0	0	329	0	0	284
6	Arun Estuary	0	0	49	0	0	122	0	0	171
7	Pagham Harbour	0	0	9	0	0	16	0	0	0
8	Chichester Harbour	2350	5140	9500	1210	1660	3410	3461	5446	7995
9	Langstone Harbour	1360	3250	6190	836	1100	2680	2933	3738	4703
10	Portsmouth Harbour	2630	4790	7210	907	1150	1950	3278	4790	6228
11	Southampton Water	7830	13300	18900	2000	2670	6280	10174	15529	19654
12	Beaulieu River	347	716	1380	184	260	841	1902	4344	6433
13	Bembridge Harbour	57	187	555	38	166	219	1418	3261	5268
14	Wootton Creek	5	21	63	6	11	95	117	488	1008
15	Medina Estuary	142	294	472	72	94	243	918	1806	2621
16	Newtown Estuary	279	432	601	80	111	157	437	1137	1876
17	Yar Estuary	9	28	53	11	18	37	247	838	1408
18	Lymington Estuary	60	141	245	49	74	238	699	1787	2875
19	Christchurch Harbour	54	104	195	79	96	462	17	42	118
20	Poole Harbour	2200	4320	5650	1820	2440	2940	2639	3051	3266
21	Weymouth	1660	2220	3850	484	1060	1840	26632	29489	33184
22	West Bay	0	0	0	0	0	0	0	0	0
23	Axe Estuary	0	1	11	0	2	18	4	78	258
24	Otter Estuary	0	3	7	0	2	4	0	40	178
25	Exe Estuary	523	2250	4690	746	1060	1810	1059	1669	2807
26	Teign Estuary	248	469	513	103	146	191	331	452	534
27	Dart Estuary	2000	3470	4900	574	670	1020	6168	8237	9988
28	Kingsbridge Estuary	191	685	1680	145	277	1200	5305	8214	11043
29	Avon Estuary	0	4	84	0	6	260	0	364	1566
30	Erme Estuary	19	115	260	29	45	123	751	3768	6591
31	Yealm Estuary	154	366	671	76	101	381	3158	5099	7041
32	Plymouth Sound	9060	13400	18900	1500	2050	5380	14467	21633	28043
33	Looe Estuary	0	0	119	0	0	192	0	0	9
34	Fowey Estuary	297	560	1100	84	154	404	2763	4404	6159
35	Falmouth	9100	13300	18100	1550	1870	25700	16357	21092	25630
36	Helford Estuary	630	1160	1840	212	240	551	3202	4756	6453
37	Hayle Estuary	232	272	386	14	15	149	0	0	7
38	Gannel Estuary	72	158	308	25	31	118	3671	5617	7749
39	Camel Estuary	823	1867	3609	181	409	777	3018	6341	10801
40	Taw-Torridge Estuary	0	0	0	0	0	0	0	0	0
41	Parrett	26	1010	3210	75	294	744	344	3482	7312
42	Severn Estuary	200000	419000	714000	36000	44200	61700	136286	206336	280998
43	Ogmore Estuary	0	0	0	0	0	0	0	0	0
44	Afan Estuary	0	0	9	0	0	39	0	0	14
45	Neath Estuary	0	0	94	0	0	51	0	0	562
46	Tawe Estuary	0	0	8	0	0	217	0	0	25
47	Loughor Estuary	0	0	0	0	0	0	0	0	0
48	Carmarthen Bay	0	0	0	0	0	0	0	0	0
49	Milford Haven	0	0	0	0	0	0	0	0	0
50	Nyfer Estuary	0	0	0	0	0	0	0	0	0
51	Teifi Estuary	4020	4880	6210	491	530	836	33814	38754	45510
52	Aberystwyth	0	0	0	0	0	0	0	0	0
53	Dyfi Estuary	79	515	2030	117	397	1090	335	1276	3291
54	Dysynni Estuary	0	0	0	0	0	0	0	0	0
55	Mawddach Estuary	77	314	919	82	195	522	1029	2204	4181
56	Artro Estuary	0	0	0	0	0	0	0	0	0

Estuary No.	Estuary name	Volume, ha m			Surface area, ha			Cross sectional area, m^2		
		LW	MW	HW	LW	MW	HW	LW	MW	HW
57	Glaslyn	149	1050	2680	347	495	1570	279	2611	6236
58	Pwllheli Harbour	0	0	0	0	0	0	0	0	0
59	Foryd Bay	0	0	0	0	0	0	0	0	0
60	Traeth Melynog	0	0	0	0	0	0	0	0	0
61	Cefni Estuary	0	0	0	0	0	0	0	0	0
62	Alaw Estuary	0	0	0	0	0	0	0	0	0
63	Traeth Dulas	0	0	0	0	0	0	0	0	0
64	Conwy Estuary	64	291	1450	34	136	764	143	1192	2461
65	Clwyd Estuary	0	0	0	0	0	0	0	0	0
66	Dee Estuary	10700	36600	70400	5580	7520	10800	29529	52369	76313
67	Mersey Estuary	16400	39200	88100	3590	6790	18600	16805	26057	35918
68	Ribble Estuary	0	0	0	0	0	0	0	0	0
69	Morecambe Bay	0	0	0	0	0	0	0	0	0
70	Duddon Estuary	0	0	0	0	0	0	0	0	0
71	Esk Estuary	0	0	0	0	0	0	0	0	0
72	Solway Firth	0	0	0	0	0	0	0	0	0
73	Tweed Estuary	29	106	230	34	49	76	278	1291	2797
74	Alnmouth	2	20	72	4	13	89	10	159	514
75	Coquet	0	0	0	0	0	0	0	0	0
76	Wansbeck Estuary	0	0	0	0	0	0	0	0	0
77	Blyth Estuary	310	456	851	68	85	425	740	916	1111
78	Tyne Estuary	2050	3380	5190	549	651	1400	5193	7537	9684
79	Wear Estuary	108	226	585	44	70	424	591	924	1412
80	Tees Estuary	1310	1700	3230	170	182	2190	0	234	1976
81	Esk Estuary	18	44	572	9	12	26	239	644	1025
82	Humber Estuary	116000	193000	290000	19300	35500	64800	61091	87052	103529
83	The Wash	0	0	0	0	0	0	0	0	0
84	Yare	0	0	0	0	0	0	0	0	0
85	Waveney - Oulton	0	0	0	0	0	0	0	0	0
86	Blyth Estuary	13	25	112	9	15	895	230	433	609
87	Ore-Alde	1140	2440	4420	778	1030	3050	521	1081	1623
88	Deben Estuary	639	1430	2580	417	578	1310	734	1317	2013
89	Harwich	1450	2760	5790	708	922	3800	3820	4974	6698
90	Hamford Water	379	1160	3100	342	554	2940	1244	3215	6024
91	Colne Estuary	91	619	1980	150	296	1660	666	2367	4466
92	Blackwater Estuary	5280	11000	19500	2050	2850	4830	8778	13933	20419
93	Crouch-Roach Estuary	2070	3940	8670	663	1050	3100	2557	4437	6384
94	Thames Estuary	41700	61100	96700	6490	8190	20000	23148	38521	58062
95	Medway Estuary	7960	13600	24400	2170	2750	7560	15235	184320	22495
96	Swale Estuary	0	0		0	0	0	0	0	0

Notes: [1]Estuary numbers from Futurecoast dataset
[2]Estuary numbers from JNCC dataset
SAHW – surface area at high water; INTA – between high water and mean low water; SAM – saltmarsh extent; SHL – shoreline length (including islands); L – Tidal length from mouth to upstream normal tide length, and TIDE – tidal range on mean spring tide (note: range is double amplitude)

Appendix C.4 Data derived in this report

Table C.4 Data derived in this report.

Estuary No.	Estuary name	DEPTH (m)	BREADTH (m)	SLOPE (x1000)	D2B/DB	HS (m)	msl (mm/dec)
1	Stour-Pegwell	3.2	344	18.8	0.56	1.2	34
2	Rother Estuary	3.1	92	68.2	0	1.5	31
3	Cuckmere Estuary	0	0	0	0	1.7	29
4	Ouse Estuary	0	0	0	0	1.7	28
5	Adur Estuary	17.4	14	0	0	1.6	28
6	Arun Estuary	0	0	0	0	1.5	27
7	Pagham Harbour	2.9	0	0	0	1.5	27
8	Chichester Harbour	3.2	1230	5.2	0.59	1.5	27
9	Langstone Harbour	3.2	719	9	0.71	1.3	26
10	Portsmouth Harbour	4.7	822	11.5	0.53	1.3	26
11	Southampton Water	10.9	1534	14.2	0.69	1.2	26
12	Beaulieu River	2.6	1269	4.1	0.77	1.3	26
13	Bembridge Harbour	2.4	1089	4.4	-0.41	1.5	26
14	Wootton Creek	0	0	0	0	1.5	26
15	Medina Estuary	7.1	270	52.7	0.74	1.5	26
16	Newtown Estuary	1.8	442	8.1	0.19	1.5	26
17	Yar Estuary	1.6	383	8.3	0.46	1.5	25
18	Lymington Estuary	1.3	817	3.2	0.74	1.5	25
19	Christchurch Harbour	1.9	44	84.1	0.91	1	25
20	Poole Harbour	1.9	1149	3.4	-0.11	0.9	24
21	Weymouth	1.2	280	8.8	0.15	2.2	24
22	West Bay	0	0	0	0	1.8	24
23	Axe Estuary	2.9	15	367.1	0	1.5	24
24	Otter Estuary	0	0	0	0	0.5	24
25	Exe Estuary	4.5	226	39.6	0.41	0.3	24
26	T eign Estuary	5	67	147.4	0.02	0.2	24
27	Dart Estuary	9.3	877	21.2	0.57	0.3	24
28	Kingsbridge Estuary	4.7	1384	6.7	0.75	2	24
29	Avon Estuary	4.5	117	77.1	0	2	24
30	Erme Estuary	7.4	637	23.3	0.66	1.8	23
31	Yealm Estuary	11.3	92	243.4	0.84	1.7	23
32	Plymouth Sound	8.3	2533	6.5	0.72	1.5	23
33	Looe Estuary	3.9	29	259.3	0	1.5	23
34	Fowey Estuary	7.6	580	26.3	0.56	1.4	23
35	Falmouth	16	1397	22.9	0.97	1.4	23
36	Helford Estuary	12.1	195	124.3	0.83	1.5	23
37	Hayle Estuary	2.7	0	0	0.99	2.5	23
38	Gannel Estuary	6	722	16.6	0.87	2.5	23
39	Camel Estuary	5.2	1122	9.2	0.23	2.5	23
40	Taw-Torridge Estuary	5.3	579	18.2	0	1.5	23
41	Parrett	5.1	534	18.9	0.35	1	23
42	Severn Estuary	35.3	6836	10.3	0.36	1.5	24
43	Ogmore Estuary	0	0	0	0	2	23
44	Afan Estuary	13.8	0	0	0	2.1	23
45	Neath Estuary	4.7	46	204.3	0	2.1	23
46	Tawe Estuary	4.3	2	0	0	2.2	23
47	Loughor Estuary	6.8	1688	8	0	2.5	22
48	Carmarthen Bay	3.9	1592	4.9	0	2.5	22
49	Milford Haven	19.2	591	65	0	2.5	21
50	Nyfer Estuary	3.3	105	63.2	0	1.7	21
51	Teifi Estuary	2.1	43	99.4	0.77	1.7	21
52	Aberystwyth	15.1	44	672.4	0	1.6	21
53	Dyfi Estuary	3.4	489	13.7	0.42	1.5	21
54	Dysynni Estuary	5.1	0	0	0	1.6	21

Estuary No.	Estuary name	DEPTH (m)	BREADTH (m)	SLOPE (x1000)	D2B/DB	HS (m)	msl (mm/dec)
55	Mawddach Estuary	3	647	9.1	0.49	1.5	21
56	Artro Estuary	0	0	0	0	1.5	21
57	Glaslyn	3	950	6.2	0.76	1.2	20
58	Pwllheli Harbour	4.1	0	0	0	1.4	20
59	Foryd Bay	3.3	0	0	0	1.4	19
60	Traeth Melynog	3.1	0	0	0	1.4	19
61	Cefni Estuary	3.3	373	17.7	0	1.4	18
62	Alaw Estuary	5	809	12.4	0	1.7	17
63	Traeth Dulas	3.5	129	53.3	0	1.5	18
64	Conwy Estuary	4.2	240	34.5	0.72	1.4	19
65	Clwyd Estuary	3.6	37	191.5	0	1.4	20
66	Dee Estuary	12.3	4490	5.5	0.26	1.1	20
67	Mersey Estuary	15.8	1706	18.5	0.57	1.1	21
68	Ribble Estuary	4.9	3129	3.1	0	1.3	19
69	Morecambe Bay	4.4	13493	0.7	0	1.2	17
70	Duddon Estuary	4.6	2094	4.4	0	1.5	16
71	Esk Estuary	4.5	406	22	0	1.6	16
72	Solway Firth	8.6	7091	2.4	0	0.8	13
73	Tweed Estuary	2.9	449	13	0.29	1.6	15
74	Alnmouth	1.6	111	29.7	0.79	1.7	16
75	Coquet	3.9	58	131.1	0	1.7	17
76	Wansbeck Estuary	14.2	10	0	0	1.7	17
77	Blyth Estuary	5.7	130	87.7	0.9	1.7	18
78	Tyne Estuary	10.3	772	26.8	0.76	1.7	18
79	Wear Estuary	8.1	132	121.7	0.86	1.7	19
80	Tees Estuary	5.9	214	55.3	0.99	1.5	20
81	Esk Estuary	4	136	59.1	0.65	1.7	20
82	Humber Estuary	10.5	7366	2.8	0.29	1	26
83	The Wash	11.6	19360	1.2	0	1	30
84	Yare	2.8	96	58.9	0	1.4	33
85	Waveney - Oulton	7.2	36	394.9	0	1.4	31
86	Blyth Estuary	1.7	31	110.2	0.99	1.2	35
87	Ore-Alde	2.7	387	13.9	0.78	1.2	37
88	Deben Estuary	1.6	448	7.3	0.64	0.9	38
89	Harwich	9.4	1273	14.7	0.86	0.5	39
90	Hamford Water	2.2	1101	4	0.84	0.5	39
91	Colne Estuary	2.7	675	7.9	0.81	0.5	39
92	Blackwater Estuary	5	2463	4.1	0.42	0.3	39
93	Crouch-Roach	3.6	837	8.7	0.68	0.4	15
94	Thames Estuary	24.1	2191	22	0.75	0.1	38
95	Medway Estuary	5.4	2498	4.3	0.78	0.2	37
96	Swale Estuary	3.5	1331	5.3	0	0.5	35

Appendix C.5 Environment Agency data

Table C.5 Environment Agency data.

EA_Area_CD	Name	FID_1	SM_Area	Est_Area	Typol	F-C	JNCC
Northern AN	WELLAND	65	3.66	1.77	3		
Devon SW	KINGSBRIDGE	48	0.03	4.81	4	28	3
Dales NE	TEES	7	0.71	11.43	2	81	6
Thames SE	THAMES MERGE	69	5.23	247.78	3	95	4
Hampshire IoW	MEDINA	41	0.10	1.63	4	15	4
Northern CY	FFRAW	58	0.01	0.09	4		
Devon SW	EXE	13	0.51	17.93	2	25	5
Central NW	LUNE	85	3.77	3.02	3		
Cornwall SW	FOWEY	18	0.07	2.65	2	34	3
South West CY	OGMORE	101	0.09	0.41	1	44	5
Northumbria NE	BLYTH (N)	2	0.13	1.68	2		
Northern CY	CEFNI	59	0.80	7.78	4	62	2
North NW	DUDDON	90	4.62	12.72	3	71	5
Kent SO	ROTHER	92	1.01	0.38	1	2	5
Hampshire IoW	WALLINGTON	39	0.10	0.38	4		
Northern CY	FORYD BAY	56	1.35	2.43	4	60	5
Northern CY	DYSYNNI	24	0.39	0.95	2	55	5
Sussex SO	OUSE	94	0.03	1.33	1	4	4
South Wessex SW	WEY	0	0.00	0.31	2		
Northumbria NE	WEAR	6	0.01	2.08	2	80	4
North NW	KENT	88	5.38	98.10	3		
Hampshire IoW	NEWTOWN RIVER	42	0.79	1.92	4	16	5
South East CY	WYE	77	0.14	2.59	3		
Cornwall SW	CAMEL	72	0.41	10.91	3	39	3
Northern AN	WITHAM	63	0.59	0.91	3		
Northern CY	DYFI & LERI	22	6.09	14.33	2	54	5
North NW	LEVEN	87	3.62	29.22	3		
Eastern AN	BURE & W &Y& L	9	0.44	8.88	2	85/86	5
Eastern AN	CROUCH	32	7.93	23.75	4	94	4
Northern CY	CONWY	103	1.71	15.57	1	65	4
Sussex SO	ADUR	96	0.09	1.37	1	5	4
Kent SO	STOUR (KENT)	35	1.08	5.46	4		
Eastern AN	ALDE & ORE	28	5.33	10.88	4	88	4
Cornwall SW	HELFORD	52	0.02	7.62	4	36	5
Northern AN	HUMBER Merge	62	9.68	326.47	3	83	9
Northern CY	MAWDDACH	23	3.07	9.52	2	56	5
Sussex SO	ARUN	95	0.26	1.37	1	6	4
Eastern AN	BLACKWATER & C	34	13.79	52.27	4	93	4
Central AN	GREAT OUSE	67	2.02	11.89	3		
Northumbria NE	TYNE	5	0.07	8.10	2	79	6
Northern CY	GLASLYN	25	5.44	15.65	2	58	5
South West CY	YSTWYTH / RHEIDOL	21	0.00	0.25	2	53	5
South East CY	BRISTOL AVON	76	0.39	2.02	3		
Cornwall SW	CARRICK ROADS I	53	0.81	12.59	4		
Cornwall SW	LOOE	51	0.04	0.48	4	33	3
Northern CY	CLYWD	102	0.35	0.64	1	66	4
Sussex SO	CUCKMERE	93	0.05	0.36	1	3	4
Hampshire IoW	EASTERN YAR	45	0.16	0.81	4	17	4
Devon SW	AXE	11	0.11	0.33	2	23	5
Central NW	RIBBLE	84	20.67	45.28	3	69	9
Hampshire IoW	LYMINGTON	38	2.21	2.45	4	18	4
Hampshire IoW	WOOTTON CREEK	44	0.00	0.23	4		
South East CY	SEVERN MERGE	74	8.63	536.45	3	42	4
Cornwall SW	HAYLE	73	0.06	1.87	3	37	5

EA_Area_CD	Name	FID_1	SM_Area	Est_Area	Typol	F-C	JNCC
Hampshire IoW	BEAULIEU RIVER	37	1.59	3.07	4	12	5
Northumbria NE	ALN	3	0.13	0.49	2	75	5
Devon SW	DART	15	0.24	8.31	2	27	3
South East CY	USK	75	0.55	4.36	3		
Cornwall SW	PLYMOUTH SOUND	50	3.36	30.21	4	32	3
Northern CY	ATRO	54	0.75	0.71	4	57	5
Eastern AN	STOUR (ESSEX)	31	1.35	25.53	4		
South West CY	SOLFACH	0	0.00	0.12	4		
Northern CY	DWYFOR	26	0.01	0.09	2		
Eastern AN	HAMFORD WATER	33	4.26	11.20	4	91	4
Eastern AN	DEBEN	29	2.25	7.82	4	89	4
South West CY	NYFER	19	0.11	1.03	2	51	5
Northern AN	STEEPING	64	0.96	0.12	3		
South Wessex SW	CHRISTCHURCH H	46	0.43	2.76	4	19	5
Cornwall SW	GANNEL	97	0.13	1.08	1	38	3
Northern CY	DEE (N. WALES)	81	24.36	109.28	3	67	4
Cornwall SW	YEALM	49	0.06	2.03	4	31	3
Northern AN	NENE	66	0.10	2.03	3		
South West CY	NEATH	100	1.66	1.36	1	46	9
North NW	DERWENT	91	0.01	0.27	3		
Hampshire IoW	WESTERN YAR	43	0.67	0.51	4		
South West CY	TEIFI	20	0.28	6.16	2	52	5
Northern CY	ALAW	60	0.17	0.58	4	63	5
South West CY	LOUGHOR	78	8.24	11.18	3	48	9
Devon SW	AVON	16	0.11	1.83	2	29	3
Kent SO	SWALE	71	4.65	29.06	3		
Eastern AN	ORWELL	30	0.64	12.49	4		
Kent SO	MEDWAY	70	14.03	56.57	3	96	4
South West CY	TAWE	0	0.00	0.93	1	47	4
North NW	ESK (W)	89	0.91	3.59	3	72	6
South West CY	GWAUN	0	0.00	0.18	4		
South NW	MERSEY	82	9.70	80.19	3	68	4
Devon SW	ERME	17	0.10	1.35	2	30	3
North NW	SOLWAY	61	33.89	305.59	3	73	6
Central AN	WASH INNER	68	18.36	133.61	3	84	5
South West CY	AFAN	0	0.00	0.79	1	45	3
South Wessex SW	PARRETT	99	1.48	70.84	1	41	9
Devon SW	TAW / TORRIDGE	98	1.58	14.61	1	40	5
Central NW	WYRE	86	2.91	6.37	3		
Devon SW	TEIGN	14	0.05	3.54	2	26	3
Northern CY	BRAINT	57	0.05	0.25	4		
Sussex SO	CHICHESTER H EAST	36	0.48	1.70	4	8	5

Notes: EA_AREA_CD – Environment Agency region;
FID-1 – identification number;
SM Area – saltmarsh area in units of $100m^2$;
Est Area – estuarine area in units of $100m^2$;
Typol – Environment Agency Typology,
F-C Futurecoast Estuary Number;
JNCC – Joint Nature Conservation Committee Typology: 3 – Ria; 4 – Coastal Plain; 5 – Bar Built; 6 – Complex; 9 – Embayment.

Would you like to find out more about us, or about your environment?

Then call us on

08708 506 506* (Mon-Fri 8-6)

email

enquiries@environment-agency.gov.uk

or visit our website

www.environment-agency.gov.uk

incident hotline 0800 80 70 60 (24hrs)
floodline 0845 988 1188

* Approximate call costs: 8p plus 6p per minute (standard landline).
Please note charges will vary across telephone providers

Environment first: This publication is printed on recycled paper.